HIGH FREQUENCY ELECTROCHEMICAL NANOPOLISHING OF ALPHA TITANIUM

A Thesis

by

ABBAS MOIZ BHAI KANCHWALA

Submitted to the Office of Graduate Studies of
Texas A&M University
in partial fulfillment of the requirements for the degree of

MASTER OF SCIENCE

Chair of Committee,	V. Jorge Leon
Co-Chair of Committee,	Wayne N.P. Hung
Committee Member,	Amarnath Banerjee
Head of Department,	César O. Malavé

August 2013

Major Subject: Industrial Engineering

ABSTRACT

Product miniaturization is an ever increasing customer demand in aerospace, bio-medical, defense and electronics industries. These microparts play a vital role and are required to abide by stringent norms set forth by various quality control agencies. To maintain their functionality over a period of time, they are made of special engineering materials rather than silicon as commonly used in microelectronics. Lithography, etching, embossing, electroplating, laser machining and other micro manufacturing techniques have been employed traditionally to manufacture microcomponents; however, these techniques would be expensive, cause surface damage, or produce a very rough surface.

Electrochemical polishing is capable of machining/polishing any conducting material while holding close dimensional tolerances. This research develops a high frequency electrochemical nanopolishing technique for commercially pure alpha titanium.

An alcohol and salt based electrolyte was used with direct current as well as alternating current on alpha titanium plate. For both current types, optimal surface roughness R_a ~ 300 nm was obtained on poly grained surface using interferometry and ~ 2 nm within a single grain by atomic force microscopy. Comparable results were obtained by other researchers with 30-120 nm R_a for titanium and titanium alloys.

Linear regression models were developed to predict the surface roughness. The surface roughness predicted by the models was found to be within 26% of the measured values.

DEDICATION

I dedicate this work to my parents Mr. Moiz T. Kanchwala and Mrs. Sugra M. Kanchwala, my beloved sisters Mrs. Farida J. Badami and Mrs. Tasneem M. Ahmedali, my fiancée Ms. Anisa Y. Laxmidhar and my close friend Ms. Chhaya S. Chavan. They are the pillars of my life and I have always turned towards them whenever I needed support. I thank them for their constant support and encouragement without which I would never have been able to accomplish this. I am indebted to my family for the numerous sacrifices that they have made and the hard work they have put in to make the best things available for me. I thank them for constantly encouraging me throughout my masters journey even though they were far from me.

ACKNOWLEDGMENTS

I would like to thank Dr. Wayne Hung for providing the opportunity to work on this project. I am thankful to him for his constant support, encouragement and guidance during the course of this research. I am also thankful to Dr. V. Jorge Leon and Dr. Amarnath Banerjee for their inputs and guidance during the research.

I thank Ms. Marie Genna, Mr. Dakota Brock, Mr. Adam Farmer, Mr. Joseph Sargeant, Mr. Dmytro Berestovskyi, and Mr. Srideep Waghela at Texas A&M University for their help in carrying out the experiments and providing vital inputs whenever needed.

I would also like to thank our sponsor, Agilent Technologies for providing the equipment and materials needed to carry out the research. I extend my gratitude towards the ETID department at Texas A&M University for making me financially secure and facilitating me in carrying out the research.

Finally, thanks to all my friends here at Texas A&M University for their patience and help, my mother and father for their encouragement and to my fiancee for her patience and love.

NOMENCLATURE

A	Area of electrode (mm^2)
C	Material constant (cm^3/A-s) for workpiece
d	Mass density of workpiece material (g/mm^3)
D	Duty cycle of pulsed waveform (%)
E	Voltage (volts) applied across the electrodes
F	Faraday's constant = 96,487 (coulomb/mol)
f	Flow rate of electrolyte (ml/min)
g	Inter electrode gap or effective inter electrode gap as stated (µm)
I	Current (A) flowing through the circuit
M	Molecular mass of anode (g/mol)
n	The number of valence electrons of the workpiece material
N	Frequency of alternating current (Hz)
R	Resistance of electrolyte and system (ohm)
r	Resistivity of electrolyte (ohm.mm)
R_a	Average surface roughness (nm)
R_z	Average of first five maximum peak-to-valley surface roughness (nm)
t	Time (s) for which current flows through the circuit
V	Volume of material (mm^3)
V_p	Volume of material removed during pulse on time (mm^3)

y	Predicted surface roughness (R_z nm)
β_i	Coefficient of respective i^{th} variable used in regression analysis
τ	Pulse on time (sec)
ε	Error term in prediction equation (nm)

TABLE OF CONTENTS

Page

Page

Page

LIST OF FIGURES

Page

Page

Page

LIST OF TABLES

Page

Page

1. INTRODUCTION

Product miniaturization has been triggered by the progress of the modern electronics technology that was constantly incorporating newer, smaller and more intricate parts into its products. Along with semiconductors, the demand for producing metallic micro parts also increased. The mass production of these parts required the fabrication of molds from hard alloys, mostly alloyed steels, which required metal removal to form the final shape of a component (1). Alloys of nickel, iron, or cobalt are difficult to be machined using the traditional processes. A cutting tool has to be harder than the workpiece, it moves relative to a workpiece to shear the material as chips, leading to residual stresses and plastically deformed burrs after machining. Significant tool wear and tool shape also limit the application of traditional techniques. Titanium being a bio-compatible material started finding applications in the medical industry and micro titanium parts became the need of the day. Traditional methods like milling were developed and non traditional methods like electrical discharge machining (EDM), chemical etching and laser machining were tried. Although these were steadily improved, only a few methods were useful in the lower micrometer to nanometer range (2). Surface residual stresses and rough surface finish may be caused by EDM that works on the principle of melting or vaporizing the material by means of discrete sparks. Chemical etching requires intricate masking and is commonly isotropic in nature, therefore, is limited to simple part shapes. Toxic chemicals are used in wet etching and extreme care has to be taken to dispose them. Dry-etching techniques require high cost equipment and it is difficult to machine

selectively using this technique. Laser machining causes thermal stresses in the surface of the workpiece and can change its microstructure, thus causing unwanted damage. Also, it is difficult to use laser machining on highly reflective surfaces which greatly increases the cost. Micromachining processes like milling can be used to remove the majority of material and define the part geometry; however, these processes leave behind lethal burrs and a rough surface that can interfere with the part function. The burrs, if present on a medical implant, can damage the live tissues in the vicinity of the implant and cause complications eventually. A detached burr can spread into the body and cause further infection. Also, if a component is made up of multiple aligning parts, then burrs can lead to misalignment and hamper the functioning of the product. A rough surface finish can severely affect the flow property of fluid in a micromachined channel in microfluidic devices, or may even damage biological species flowing through a channel. Removing burrs and polishing a machined surface is, therefore, required for many microcomponents.

Electrochemical machining is one of the non-traditional machining techniques that has the potential to overcome these issues. In electrochemical machining, material is removed by controlled electrochemical dissolution of an anodic workpiece in an electrochemical cell. Electrochemical technique can be used to machine (ECM) or polish (ECP) materials. Unwanted burr can be removed while surrounding surface can be polished simultaneously by this technique.

Although the electrochemical polishing process has been investigated, there is limited research using pulsed current in the polishing of CP alpha titanium and the investigation of the polishing effects at the microstructure level. In this research, the polished microstructure has been studied using atomic force microscopy. An analysis of the effect of parameters on the surface finish is carried out and effect of AC and DC current types has been studied. This research is part of a larger project to machine and polish complex and deep microchannels for medical applications.

The objectives of this study are to:

- Design an electrochemical system for deburring and polishing and compare the effect of current types.
- Determine the local optimal machining parameters for the best surface finish.

The scopes of this research are to:

- Limit the study to commercially pure alpha titanium plates.
- Utilize an alcohol based electrolyte developed from another project and available power supplies.

2. LITERATURE REVIEW

2.1 Microfluidic devices

Microfluidic devices find many applications in the biomedical industry and are also used for clinical diagnostics (3; 4). Traditionally; peroral, topical, transmucosal and inhalation methods have been used as the most common means for drug delivery. These methods do not enable accurate dose control and hence require repeated dosage. With the advancement in the micromanufacturing technologies, microfluidic devices have been developed which can help overcome these problems. In these devices, the drug is placed in a reservoir and it is delivered to the required area through microchannel openings. The dosage amounts can be controlled precisely by determining the number, geometry and dimensions of the microchannels (5). In addition to this, some medical implants require microchannels that have to be made in biocompatible materials. These microchannels can be manufactured using chemical etching, lithography, laser machining and micromilling. Chemical etching and laser machining have various difficulties associated with them as discussed earlier. Micromilling can be used to make high aspect ratio microchannels, but it produces a bad surface finish and leaves burrs that can disrupt the flow of the fluid in a microchannel. Micromilling the channels followed by electropolishing to improve the surface texture can help manufacture these devices with high productivity and close dimensional control while maintaining the required surface finish. A microfluidic device is shown in Figure 1:

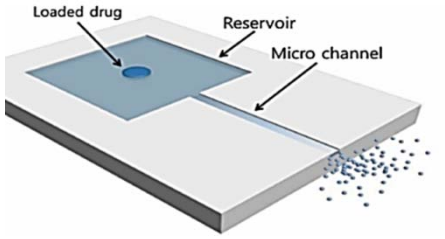

Fig. 1: Microfluidic device (5)

2.2 Biomedical materials

Various metals, ceramics and polymers are commonly used for manufacturing biomedical implants. These are required to exhibit specific properties like biocompatibility and corrosion resistance.

Electrochemical polishing requires a conducting workpiece material and hence, can only be used to polish metals. Stainless steels like SS316L, cobalt alloys, CP titanium and its alloys like Ti-6Al-4V and shape memory alloys like Nitinol alloys are most commonly used to manufacture biomedical devices (6). In the early days, stainless steel was used successfully as an implant, followed by cobalt based alloys. In recent times titanium and its alloys have gained importance in manufacturing biomedical devices due to its light weight, excellent mechanical properties and biocompatibility. Titanium exhibits its excellent biocompatibility due to its oxides that make it extremely resistant to corrosion from most chemicals. Ti-6Al-4V has been the favorite titanium alloy for medical implants but in the long run it can cause harm in permanent implants due to the toxic effect of released aluminium and vanadium. Thus, vanadium and aluminium free titanium alloys are being introduced for implants (6). Commercially pure titanium (CP

Ti) is one of the best biocompatible material since its surface properties help build a stable and inert oxide layer instantaneously. Many other properties unique to titanium like low level of electronic conductivity, high corrosion resistance, thermodynamic state at physiological pH values, low ion formation in acqueous solutions, etc. make it the most suited biocompatible material (6). For some of its biomedical applications like microfluidic devices, implants, etc. a smooth and bright surface finish on the workpiece is required to maintain their functionality. Mechanical polishing and chemical polishing methods have been tried with limited success in polishing titanium due to the existence of reaction layer, its high chemical activity and low thermal conductivity. Mechanical polishing is a tedious process for titanium and can cause contamination of the polished surfaces. On the other hand, electrochemical polishing can give a bright, clean and smooth surface on a titanium workpiece under suitable process parameters (7). The effect of the polishing at the grain level of the workpiece material needs to be studied to obtain a uniform polishing effect. Hence, this research focuses on studying the effect of ECM/ECP parameters on surface quality of pure alpha Ti and the polishing effect at the microstructure level is studied using Atomic Force Microscopy (AFM).

2.3 Overview of deburring and polishing techniques

The secondary operation to remove unwanted burr, or deburring, is necessary to ensure the part integrity. Figure 2 shows excessive burrs generated after micromilling of a microchannel. Common techniques like tumbling, grinding, abrasive blasting, thermal energy methods or high pressure water jet have been used as deburring methods (8).

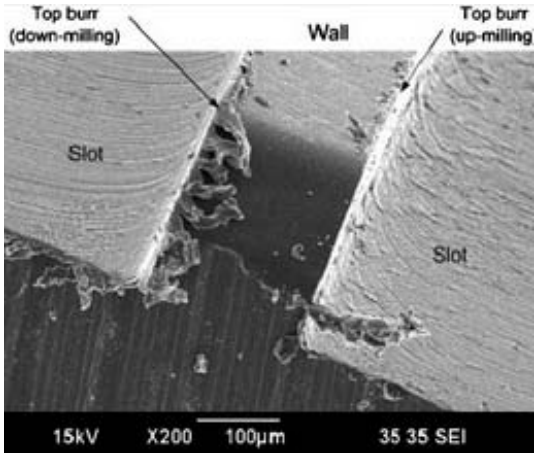

Fig. 2: Burrs generated after micromilling of a microchannel (9)

Tumbling (8) is a very crude method of burr removal and there is not much control over the surface being treated. A workpiece to be deburred is kept in a tumbler along with some abrasives and deburring action is carried out due to the friction and shearing force generated between the workpiece and the abrasives while tumbling. This technique can only be used for deburring macro parts.

Grinding and abrasive blasting make use of abrasives for material removal. Grinding is done by using an abrasive wheel that is held against the workpiece as the wheel rotates whereas in abrasive blasting a stream of abrasive material is propelled under high pressure against the workpiece to be deburred. Both processes make use of mechanical forces that can damage the surface texture of the workpiece and leave impurities on the surface which is undesirable in many critical applications. These methods also induce residual surface stresses into the workpiece material.

Sometimes cryogenic deburring is carried out in which the workpiece to be deburred is cooled to cryogenic temperatures (-195^0 C). Subsequent blasting of the workpiece

surface using abrasives or tumbling would remove the brittle and fragile burrs on the workpiece (8).

In thermal energy method, an explosive gas mixture is used. The workpieces are kept in an explosion proof gas chamber and the mixture is ignited. Burrs are burned away at a very high temperature. The entire process hardly takes a few milliseconds (10).

Honing, lapping and buffing processes have been used for polishing a workpiece surface to improve its surface quality. Honing makes use of an abrasive stone which is scrubbed against the workpiece along a controlled path to give it a good surface finish. It is used to improve the geometric form and surface texture of the workpiece. Lapping relies on rubbing two surfaces against each other with an abrasive between them while buffing is carried out by using a loose, fine grit abrasive on a rotating wheel which is rubbed against the workpiece. By progressively polishing in steps with finer abrasive grits, a good surface finish can be achieved. All these processes are contact type and rely on friction to remove material plastically that might lead to residual surface stresses and contamination.

Recently, ECM that is based on Faraday's principles of electrolysis has been gaining popularity as a deburring technique. It is a non contact process and does not leave behind residual stresses in the workpiece. It can also be used for deburring complex shapes and contours of macro/micro parts (11). By adjusting the process parameters, the technique can also be used for polishing the workpiece surface with good control over the polishing area.

2.4 Electrolysis

Electrolysis is a method in which an electric current is used to drive an otherwise non-spontaneous chemical reaction.

Electrolysis is the passage of an electric current through an ionic substance that is either molten or dissolved in a suitable solvent, resulting in chemical reactions at the electrodes and separation of materials.

The main components required to achieve electrolysis are:

- Electrolyte: An electrolyte is a substance containing free and mobile ions which can carry the electric current in the electrolyte. In the absence of mobile ions electrolysis cannot occur.
- Power source: Energy is required to create or discharge the ions in the electrolyte; the power source provides this energy. The electric current in the external circuit is carried by electrons.
- Two electrodes : The cathode and anode are electrical conductors which provide the physical interface between the electrical circuit providing the energy, and the electrolyte

Metal, graphite and semiconductors are commonly used as electrodes. Choice of suitable electrode material depends on the chemical reactivity between the electrode and electrolyte and the cost of manufacture.

The reactions are not spontaneous and require a potential difference in order to occur (12; 13). The power source provides this potential difference.

2.5 Electrochemical machining/polishing

Electrochemical machining or electrochemical polishing is the material removal process developing from Faraday's principles. In this process the workpiece to be machined is the anode and the tool is the cathode, immersed in a suitable electrolyte. The shape of the tool is made the inverse of the feature to be machined on the workpiece and the tool is held very close to the workpiece. When an electric potential difference is applied between the two electrodes, the following reactions take place during the electrolysis of titanium in an alcohol based electrolyte (7):

At the Anode:

Metal ions are transferred into solution:

$$Ti \longrightarrow Ti^{4+} + 4e^{-} \quad (1)$$

Passive oxide layers are formed:

$$Ti + 2OH^{-} \longrightarrow TiO + H_2O + 2e^{-} \quad (2)$$

Oxygen is evolved:

$$4OH^{-} \longrightarrow O_2 + 2H_2O + 2e^{-} \quad (3)$$

The electrolyte in the gap between the two electrodes needs to be flushed continuously in order to remove the ions and keep the workpiece surface exposed to fresh electrolyte. If the ions are not flushed then instead of machining the workpiece material, machining would be carried out on the debris and hence machining would not progress. Also after enough deposition has taken place, the cathode dimension increases while the inter electrode gap decreases which may create a short circuit between the two electrodes. A good electrolyte flow rate also helps in maintaining the temperature of the workpiece

and flushes the gases generated. The tool is advanced into the workpiece to aid material removal (11).

The phenomenon of ECM/ECP can be embodied in Faraday's two laws of electrolysis as follows (12):

1. The amount of any substance dissolved or deposited is directly proportional to the current flowing in the electrolyte.
2. The amount of different substances deposited or dissolved by the same quantity of current is proportional to the material constant.

Let, V = Volume of material removed by ECM (mm^3)

C = Material constant (mm^3/A-s)

I = current (A)

t = time for which current flows (s)

M = molecular mass of anode (g/mol)

n = valence electrons of workpiece (anode) material

F = Faraday's constant = 96,487 (Coulomb/mol)

d = mass density of workpiece material (g/mm^3)

E = Voltage (volt)

R = Resistance of electrolyte and system (ohm)

g = inter electrode gap (mm)

r = resistivity of electrolyte (ohm.mm)

A = area of electrode (mm^2)

Faraday's laws of electrolysis gives:

$$V = CIt \tag{4}$$

The material constant depends on the workpiece material and is given by (14):

$$C = \frac{M}{nFd} \tag{5}$$

Since the electrolyte serves as the conductor of electric current, Ohm's law can be applied to this type of conductor which gives:

$$I = \frac{E}{R} \tag{6}$$

The resistance of the electrolyte depends upon the interelectrode gap, area of the electrode and resistivity of the electrolyte (14). It is given as follows:

$$R = \frac{gr}{A} \tag{7}$$

Substituting in above equation and re-arranging the terms we get:

$$Material\ removal\ rate\ = MRR\ = \frac{V}{t} = \frac{CEA}{gr} \tag{8}$$

The above equations are derived assuming 100% efficiency (15).

Thus, we see that the *MRR* depends on the voltage, current and the inter electrode gap (IEG). The above equations are for direct voltage and current (DC). When a DC current is flowing through the circuit, machining takes place continuously and a lot of ions from the workpiece get deposited on the tool due to improper flushing. It is expected that the use of alternating current (AC) current would provide much better flushing. Since no machining takes place during the off time of each cycle when the current in the circuit goes to zero, it provides a better opportunity for the electrolyte to flush away the ions.

Since the electrolyte must be neutral, there must be a balance between the total positive charge and the negative charge. At the end of the reaction, the amount of material lost by one of the electrodes is equal to the amount of material gained by the other. Hence, this process can be used for both material removal and addition. The major applications of electrolysis are electroplating and electropolishing (11).

In the case of pulsed ECM, the theoretical volume of material removed over pulse-on duration can be modified from equation (8) to give:

$$V_P = \int_0^{\tau} \frac{CEAdt}{gr} \tag{9}$$

where, τ = pulse ON time (sec).

V_p= Volume of material removed during pulse ON time (mm^3).

It is observed that when metals dissolve anodically in an acqueous or non-acqueous medium, the weight of metal dissolved is sometimes greater than that calculated from Faraday's law by assuming expected metal valence, thus implying that they dissolve with ionic valence less than normal. The electrochemical process parameters like the electrolyte used, mechanical disintegration, gas bubble blocking, hydrogen embrittlement, passive layer cracking are considered as some of the possible reasons for such behavior (16; 17). Ion dissolution valence is required in describing the dissolution during the electrochemical process and calculating material removal according to Faraday's law. Table 1 shows the possible dissolution valence of some metals in different electrolytes.

Table 1: Metal dissolution valence in different metal electrolyte systems (18)

Metal	Electrolyte	Dissolution Valence
Ni	NaCl	2
Fe	NaCl	2 and 3
Ni	$NaNO_3$	2*
Fe	$NaNO_3$	2*
Ni	$NaClO_3$	2*
Fe	$NaClO_3$	2*
Cr	$NaCl$	6
Cr	$NaNO_3$	6
Cu	KCl	1 and 2
Cu	KNO_3	2 and 1
Cu	K_2SO_4	2 and 1
Ti	NaCl	4
Ti	NaBr	4
Mo	KOH	6
Mo	K_2CO_3	6

* Accompanied by oxygen evolution.

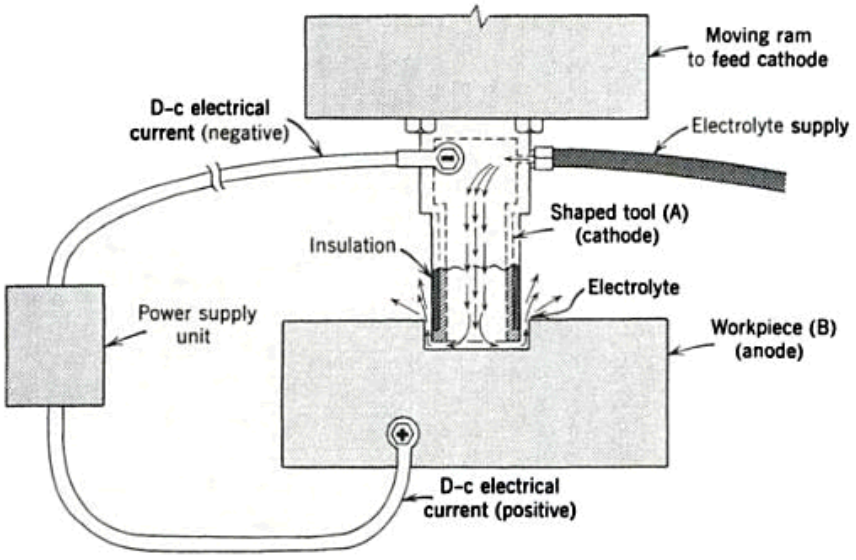

Fig. 3: Principle of electrochemical machining/polishing (19)

A schematic of an electrochemical machining/polishing cell is shown in Figure 3. The positive terminal of the power supply is connected to the workpiece while the negative terminal is connected to the tool. Electrolyte is pumped through the internal opening in the electrode which flushes the debris generated during machining. The electrode is mounted on a moving ram in order to maintain the inter electrode gap as machining takes place. Some portion near the tip of the electrode is insulated in order to reduce the effect of conicity in machining.

In ECM there are several process configurations that can be selected based on the requirements and capabilities of the machine. The various configurations are:

1. Tool and the workpiece are stationary.
2. The tool moves linearly while rotating and the workpiece is held stationary.
3. Tool and the workpiece, both move.

In ECM, material removal takes place below the electrode, leading to machining of the opposite profile on the workpiece. Different shaped profiles can be machined using ECM as shown in Figure 4:

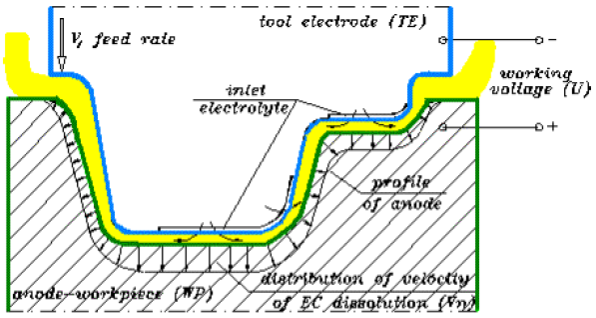

Fig. 4: Profile forming using ECM (20)

2.6 Pulse electrochemical machining/polishing

As ECM is a non-contact process, the dimensional accuracy and control of the process depend on the IEG distribution. The IEG also governs the tool design in order to compensate for the inaccuracies, thus making its design complex. The IEG distribution is influenced by the uneven distributions of the electrical field, the electrolyte flow field and the anodic chemical reactions on the local anodic material (21). The influences of these factors on the ECM process are significant and often random in nature that complicates the IEG distribution prediction. Uniform electrolyte flow over the entire gap region is extremely important to get a uniform surface finish in ECM. A stagnant flow zone or distorted electrolyte flow can cause poor dimensional accuracy, surface defects, short circuit and tool damage (21). Overcuts or wildcuts are caused by stray currents wherever a conducting path between the electrodes is formed by the electrolyte. In an effort to overcome these issues, new techniques were tried to achieve a better control over the IEG distribution. Maintaining shorter IEG can help reduce the variation in gap distribution thus reducing the dimensional control errors. Overcut depends on the electrolyte current efficiency and the anodic polarization. By restricting the anodic dissolution in the regions of high current density, i.e. shorter gaps, this problem can be overcome. Heat and bubbles are generated with anodic dissolution and hence, high electrolyte flow rates are required to reduce the defects caused by them, thus requiring more rigid and larger pumping system. A technique in which machining can be done at short IEG gaps while maintaining control over the anodic polarization and dissolution with proper flushing of the heat and gases can overcome these issues.

Pulsed electrochemical machining (PECM) is believed to possess the potential to address these issues. In pulse electrochemical machining PECM a pulsed voltage or current replaces the constant voltage and current in ECM/ECP (22). In this, due to the planned interruption, the current is turned off before the normal anodic dissolution ends which helps in the gap state recovery by thorough electrolyte flushing. The voltage is resumed as soon as the gap state has recovered and a new cycle repeats. The relatively short IEG and pulse on and off-times help in reducing the variation of the electrolyte conductivity due to better flushing of the gases and heat generated. In a PECM setup, the output of the pulse generator is given to the positive workpiece and negative tool through the voltage amplifier which helps in adjusting the voltage across the terminals. The process can be monitored by a computer with the help of an input/output interface and analog/digital converters. A schematic of PECM is shown in Figure 5:

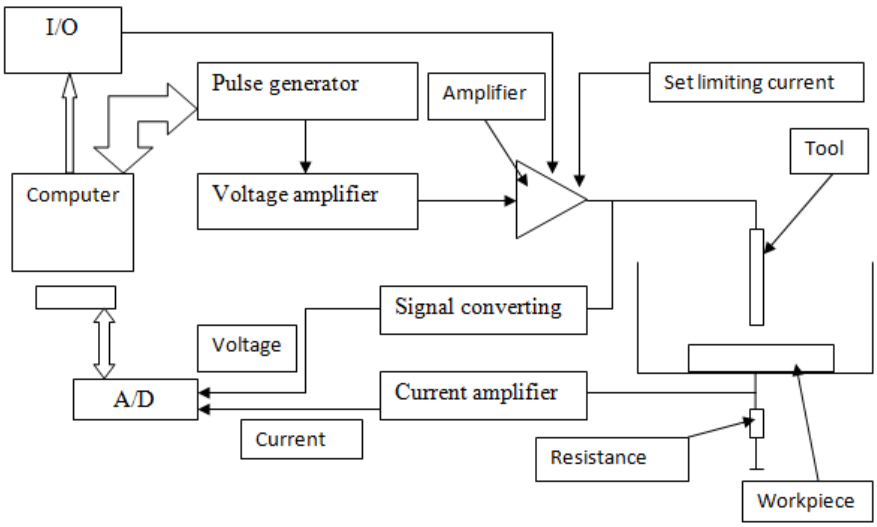

Fig. 5: A schematic of the PECM set-up (23)

2.6.1 Comparative study of ECM and PECM

Studies have shown that, compared with ECM, PECM results in more stable inter electrode gap state resulting in better anodic dissolution efficiency, dimensional accuracy and surface finish (24).

2.6.1.1 Dimensional accuracy and control

Better dimensional control and accuracy is obtained by using PECM than ECM. Using PECM in the batch production of dies and blades in industry, an accuracy of 0.05 mm – 0.10 mm has been achieved (25; 26), whereas for less complicated shapes, accuracies as high as 0.02-0.05 mm has been reported (25). Precision components have been manufactured within 0.01 mm deviation by using PECM (27) whereas the precision using ECM is expected to be 0.2 mm (28). Shorter on-time in PECM helps confine the active anodic dissolution to the area of high current density and thereby increase the machining accuracy (21). Plot of shaping error vs pulse on-time is shown in Figure 6:

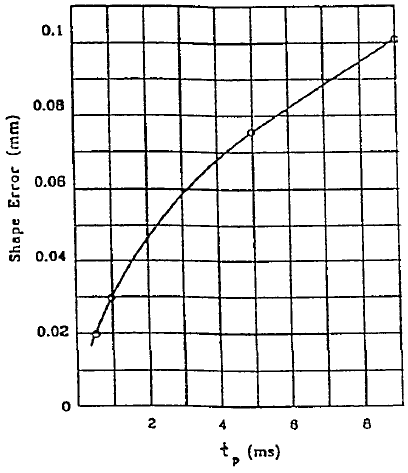

Fig. 6: Shape error vs pulse on-time (21)

2.6.1.2 Surface finish

An increase in current density is reported during pulse on time in PECM due to decrease in ohmic resistance when the pulse interval is set properly (21; 25). A current density of 50 A/cm^2 can be achieved with PECM when the mean value of the pulsed voltage is set at 10V with pulse duration of 10 ms and pulse interval of 50 ms, whereas, a current density of only 30 A/cm^2 is achieved in ECM under equivalent conditions (25). This higher density provides a condition for higher material removal rate and better surface finish due to the reduced possibility of selective dissolutions (21). Figure 7 shows the effect of pulse on-time and off-time on surface roughness when polishing Ti alloy.

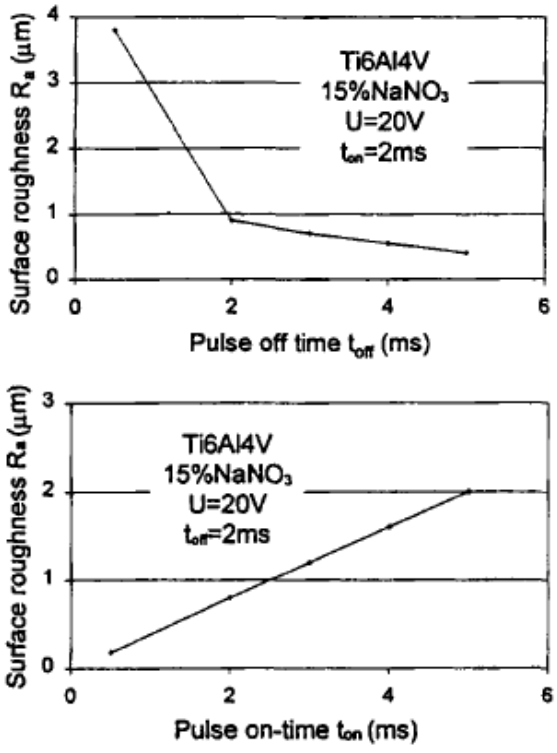

Fig. 7: Effect of pulse on-time and off-time on surface roughness of Ti alloy (29)

Blades and dies for various industrial applications have been PECM'ed to obtain a surface finish of 0.16-0.63 µm (R_a) (26). With recent developments, techniques have been patented that can give surface finish R_{max} < 1 µm with a mirror finish (21). However; in the machining of titanium and its alloys, surface pitting is observed due to the partial breakage of the surface oxidation film. This can be avoided by the proper selection of PECM process parameters. A plot showing the effect of temperature and current density on the surface roughness during the electropolishing of SS304 using EP4000 electrolyte is shown in Figure 8 (30):

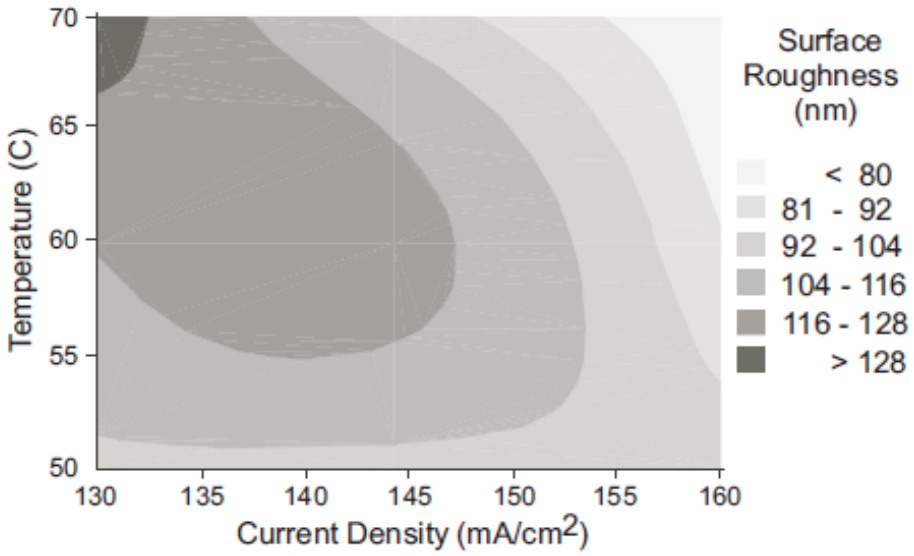

Fig. 8: Plot showing the effect of temperature and current density on surface roughness in the electropolishing of SS304 using EP4000 (30)

2.6.1.3 Cost and productivity

Cost of the power source for PECM increases due to its increased complexity, but savings can be achieved on the pumping system required and the machine tool rigidity due to lower electrolyte flow requirements. The productivity of PECM is lower than continuous ECM because of the off time during which no machining takes place. However, a reduction in the overall production time can be achieved due to the higher accuracy and control in PECM. The secondary finishing operations required in continuous ECM are reduced in PECM which can save a lot of time and effort and give almost twice the productivity (31). It is reported that in a die sinking operation, the fitter's finishing time reduced from 20 hours required with ECM, to 3 hours with PECM although the shaping time increased from 12 minutes to 55 minutes (21).

2.7 System parameters

The ECM process depends upon various inherent parameter settings. Some of these parameters are fixed and others are dynamic.

2.7.1 Static parameters

Static parameters in ECM/ECP include the electrolyte, tool electrode and workpiece material.

2.7.1.1 Electrolyte

The primary function of the electrolyte is to provide the optimal conditions for machining to take place. The electrolyte acts as the conducting medium between the electrodes and provides the favorable conditions required for the dissolution of the workpiece material. It also provides for flushing the machining debris that is accumulated in the IEG and reduces the temperature that is generated during machining. The electrolyte used during machining must have a high conductivity, low viscosity, should be non corrosive, it should not vaporize and it should be cheap. The electrolyte must be able to flush away the debris that are generated and also maintain its properties for a long period of time. The electrolyte can be used over and over again until it has reacted with some other material during machining, but care must be taken to filter the machined products from the electrolyte.

The electrolytes used in ECM/ECP are mainly classified as (20):

1. Passive and non-passive electrolytes.
2. Acqueous or non-acqueous electrolytes.
3. Organic or non-organic based on solvent types acid, alkaline or neutral.

Passive electrolytes are those that contain oxidizing anions such as sodium nitrate. These are environmentally friendlier and can be used without a ventilating hood. Passive electrolytes are known to produce more precise parts due to the formation of oxide films and oxygen evolution in the stray current regions (32).

Non passive electrolytes contain aggressive anions like sodium chloride and hence require special equipment while working with it. The material removal rate is higher with non passive electrolytes but at the cost of precision (33).

Electrolyte can be supplied to the machining gap in different ways depending upon the process configuration in use (34).

1. The electrolyte is pumped continuously over a solid electrode and flows through the machining gap onto the workpiece (external flow).
2. The electrolyte is pumped through an electrode which is in the form of a tube. The electrolyte flows through the internal opening of the tube, into the gap and over the workpiece (internal flow).
3. The electrolyte is directed into the gap between the electrodes through a nozzle. It flushes the debris and flows over the workpiece (side flow).

Internal flow helps remove the dissolved material right outside where the two electrode cross sections coincide, but it can cause stagnation outside this area. External flow can turn turbulent at high flow rates but it provides much more fluid flow at lower pressures. Side flow is easy to setup but it gives an irregular cleaning zone compared to others (35). The following Scanning electron microscopy images in Figure 9 show the effect of different electrolytes.

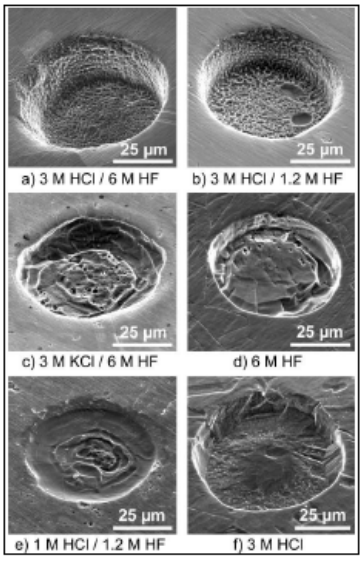

Fig. 9: Holes drilled into stainless steel using different electrolyte solutions (36)

The electrolyte concentration also affects the hole size (37; 38). Higher conductivity of electrolyte facilitates higher current flow, thus increasing the amount of material removed. The mass of material machined, increases with the electrolyte concentration as shown in Figure 10.

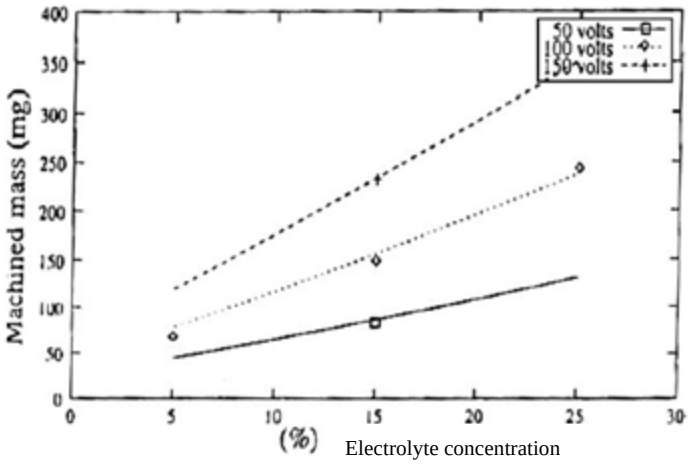

Fig. 10: Effect of electrolyte concentration on material removed for different voltages. (Machining duration = 30 min, electrolyte used = HCl, work material = HSS) (38)

The temperature of the electrolyte is also critical since it affects the conductivity of the electrolyte. A temperature increase of the electrolyte results in overcut as more heat and gases are generated in the machining gap while machining. The temperature of the electrolyte must be maintained so as to minimize this problem (35; 39).

2.7.1.2 Tool electrode

The shape of the tool electrode is determined by the shape that is to be machined/polished on the workpiece. As mentioned earlier, the inversed profile of the shape of the tool is machined/polished into the workpiece. The basic properties required of the tool electrode are that the electrode should have good electrical conductivity, resistance to chemical erosion, ease of machinability into different shapes and resistance to chemical reaction with the electrolyte. Commonly used electrode materials are copper,

brass, stainless steel, titanium, etc. (40). The tool electrode is machined using other micromachining techniques like EDM.

As the ECM/ECP progresses, material removal takes place not only at the bottom of the electrode but also at the side walls, thus accurate dimensional control is difficult. In the case of drilling, the dissolution time at the entrance to the hole is much longer than that at the exit (41), thus giving a tapered hole, this is called conicity. Another reason of conicity is the variations in the gap resistivity (35; 39). The following figure shows a linear relationship between the current flowing between the base of the hole and the tip of the tool, and the conicity of the holes produced. As shown in Figure 11, as the current increases the effect of conicity decreases, this is attributed to the increased precipitation of removed metal ions on hole inner surface that prevents excessive side machining (37).

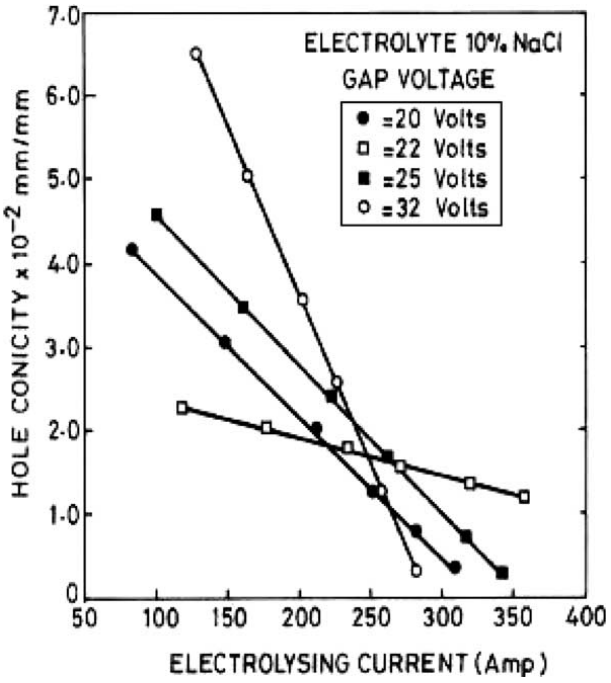

Fig. 11: Effect of current on the hole conicity at different gap voltages (39)

In order to avoid this problem the side walls of the tool are coated with an insulating material which prevents the machining in that region, thus giving much more accurate dimensions. Different methods like spin coating have been developed to coat the electrodes with insulating materials as shown in Figure 12. Alternatively, different electrode designs as shown in Figure 13 have also been suggested which help reduce the effect of the side wall machining (41).

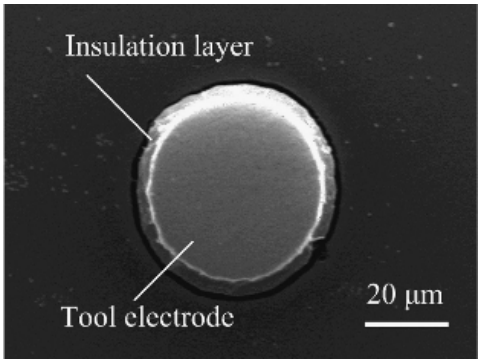

Fig. 12: Sectional image of an insulated tool electrode (41)

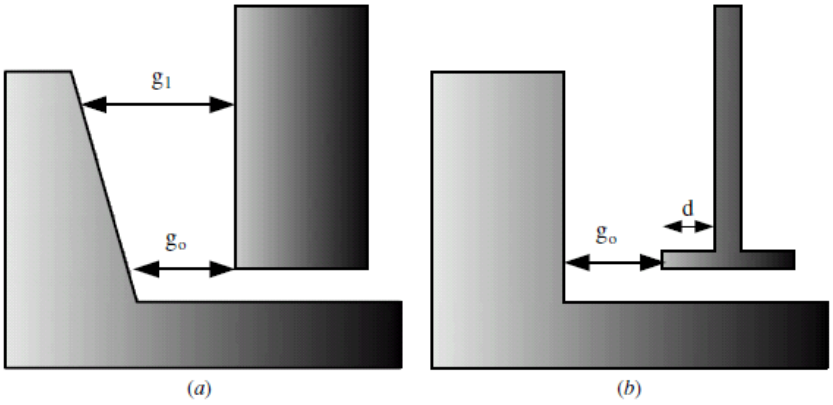

Fig. 13: The effect of electrode shape on the side wall profile
(a) Cylindrical (b) Disc shaped (42)

2.7.1.3 Workpiece material

This can be considered as an independent parameter and is decided by the designer based on the type of application for which the material may be used. The only constraint for it to be ECM/ECP'ed is that it should be conductive. Very hard to machine materials can also be machined using ECM/ECP. The material removal rate is independent of hardness, but it depends on the molecular weight of the dissolved workpiece material and its dissolution valence state.

All the other variables in ECM/ECP have to be decided such that they give good machining results for the chosen workpiece material. The proper electrolyte and tool electrode material selection is critical to achieve such results since some materials react with particular electrolytes. Table 2 enlists the electrolytes for good results.

Table 2: Electrolytes for different materials (34)

Alloy	Electrolyte
Iron based	Chloride solutions in water
Ni based	HCl or mixture of Brine and H_2SO_4
Ti based	30% isopropyl alcohol + 70% ethanol+ $ZnCl_2$ + $AlCl_3$ in a 1:5 concentration solution. Or 10% HF + 10% HCl + 10% HNO_3
Co-Cr-W based	NaCl
WC based	Strong alkaline solutions

2.7.2 Dynamic parameters

Dynamic parameters in ECM/ECP are the inter-electrode gap, current and voltage, pulse frequency and machining time.

2.7.2.1 Interelectrode gap

Interelectrode gap is the distance between the cathode (tool electrode) and the anode (workpiece). The electrolyte bridges this gap while machining and allows for the ions to move between the two electrodes. In order to bring about localized material removal by dissolution, the tool electrode has to be brought as close to the workpiece as possible. At larger gaps, higher voltage is required to maintain the current density required while at shorter gaps a lower voltage is sufficient. Larger IEG gives wider profiles of machined holes due to larger activation area and can increase the inaccuracies while smaller IEG gives a narrower profile. However, smaller IEG restricts the flow of the electrolyte. Material removal rate also depends on the IEG. Thus, the IEG has to be set so as to best suite the application. Theoretical and actual effect of the IEG on the material removal is shown in Figure 14:

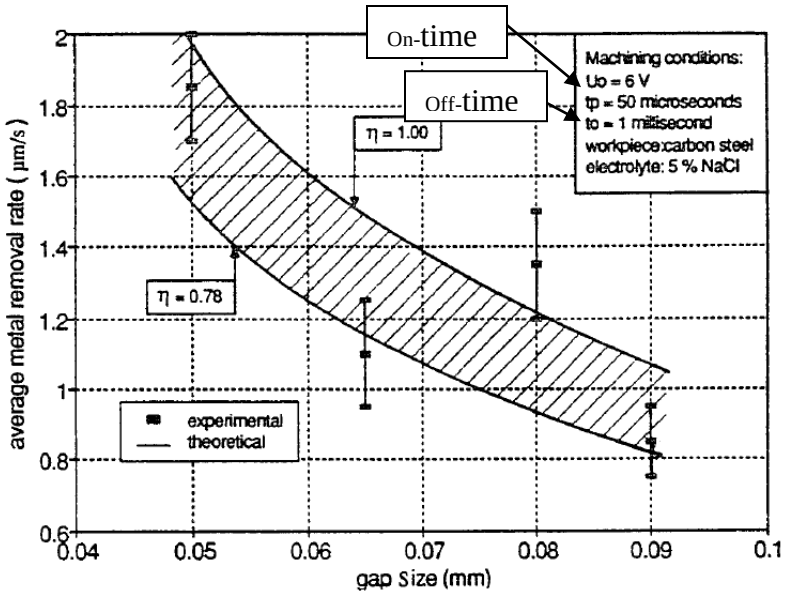

Fig. 14: Theoretical and actual material removal rate vs interelectrode gap (21)

2.7.2.2 Electrolyte flow rate

The electrolyte acts as a bridge between the two electrodes and facilitates chemical reactions which help carry out the machining. The MRR is determined not only by the rate at which the reactions are facilitated by the electrolyte but also by the efficiency with which the machined products are flushed away by it. The selection of the flow patterns and velocity plays a critical role in obtaining good results. Effect of electrolyte flow rate on overcut is shown in Figure 15 (b). The surface finish and the depth of cut are greatly affected by the gradient in the flow path (43). Figure 15 (a) shows the distinct regions of electrolyte flow that have been identified.

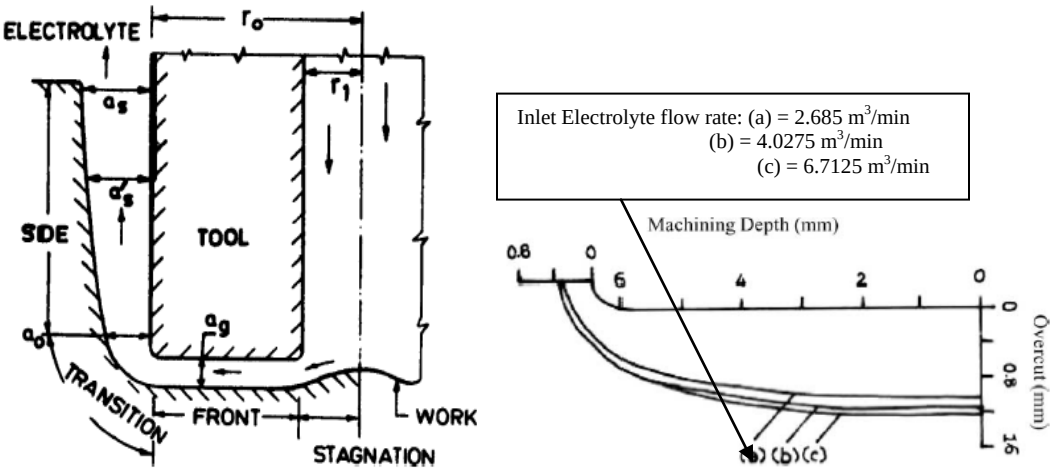

Fig. 15: (a) Distinct regions of electrolyte flow (39) (b) Effect of electrolyte flow rate on overcut (38)

2.7.2.3 Current and voltage

A double layer forms at the interface between the electrodes when the tool electrode and workpiece are immersed in the electrolyte. When potential difference is applied, the cell

can be considered as equivalent to a circuit consisting of capacitors and resistors (42). The applied voltage and current can be of two types, DC full wave rectified and pulsed DC. Current density (i.e. the ratio of current and effective electrode surface area) is determined by the rate at which ions arrive at the electrodes and this depends on the applied voltage, concentration of electrolyte, IEG and tool feed rates. The relationship is shown in Figure 16:

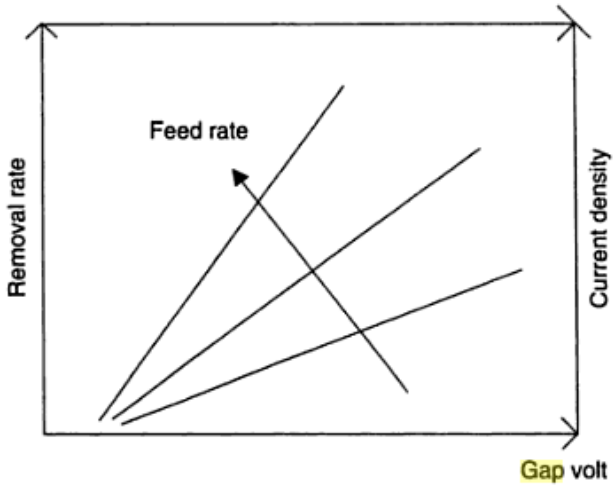

Fig. 16: Effect of tool feed rate and gap voltage on the current density and material removal rate (44)

It has been found that there exists a plateau region in the plot of current density against the applied voltage for given tool, workpiece and electrolyte combination and the optimal current density for electropolishing is expected to be at the end of the plateau region (30). Figure 17 shows such a region in the electropolishing of CP Ti using a mixed acid solution as electrolyte (45).

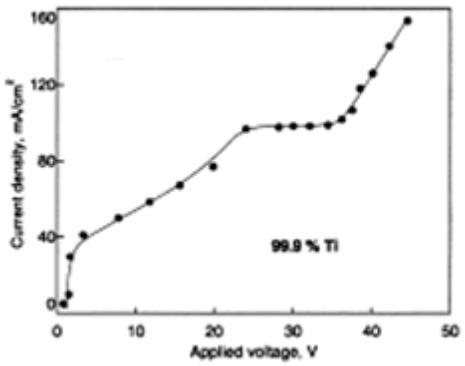

Fig. 17: Current density vs voltage in electropolishing of CP Ti using mixed acid solution as electrolyte (45)

The magnitude of current & hence current density is also determined by the gap between the two electrodes. The closer the tool is to the workpiece, the length of the conductive path is decreased which increases the current in the circuit. As current density increases, the material removal rate also increases and theoretically there exists a linear relationship between them. Figure 18 shows a comparison between the theoretical MRR and measured MRR in PECM of Ni-Ti alloy at applied current density.

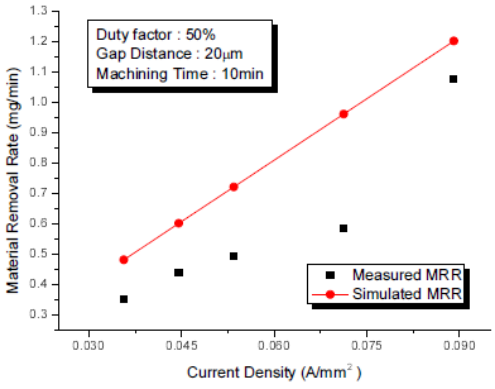

Fig. 18: Measured and simulated MRR for given current density on Ni-Ti (Ni-56%, Ti-44%) alloy using $NaNO_2$ (1.5M), $Na_2C_4H_4O_6$ (0.1M) electrolyte (46)

2.7.2.4 Pulse frequency

Conventionally electrochemical machining has been carried out using a DC current. However, high frequency pulsed voltage would provide better resolution of the machined area. The type of waveform used while machining plays an important role in determining the quality of the profile and surface finish of the machined part. The main advantage of using ultrahigh frequency pulsed current waveform is that the electrochemical reactions get restricted close to the electrode region (47; 48; 49; 50). In the case of DC current this region exceeds much farther than the 0.1 mm spatial resolution (47). Although the accuracy increases, the machining efficiency decreases as machining is only performed during the pulse on-time. The off-time is utilized to flush out all the debris that are generated during machining and dissipate all the heat and gases generated during machining. Figure 19 shows the effect of frequency in PECM on MRR. In some PECM systems, the inter electrode gap is increased by retracting the tool to assist the electrolyte flushing. Electron motion is highly confined in pulsed ECM and this leads to the low machining rates (13; 51).

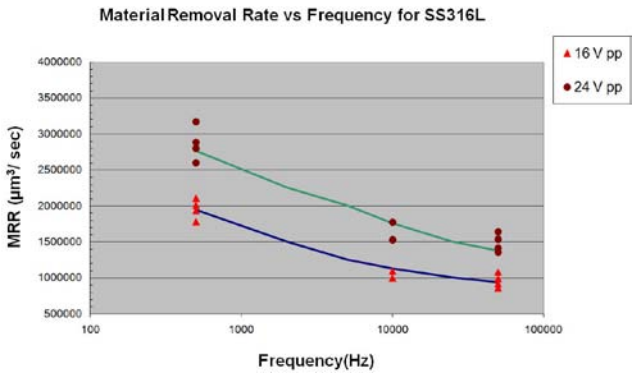

Fig. 19: Effect of frequency on MRR in machining of SS316L using 3% $NaNO_3$ (34)

Shorter pulse on-time duration decreases the concentration polarization effect which increases the peak current. This decreases the selective dissolution and improves the surface roughness. Thus, though shorter on-times are desired, it has to be kept long enough for the anodic surface that is charged or polarized to gain enough energy to start the dissolution process (29; 52). Figure 20 shows the effect of pulse frequency on the surface roughness at different pulse durations in the electropolishing of SS304 using EPS4000 electrolyte that is based on a mixture of phosphoric and sulphuric acids.

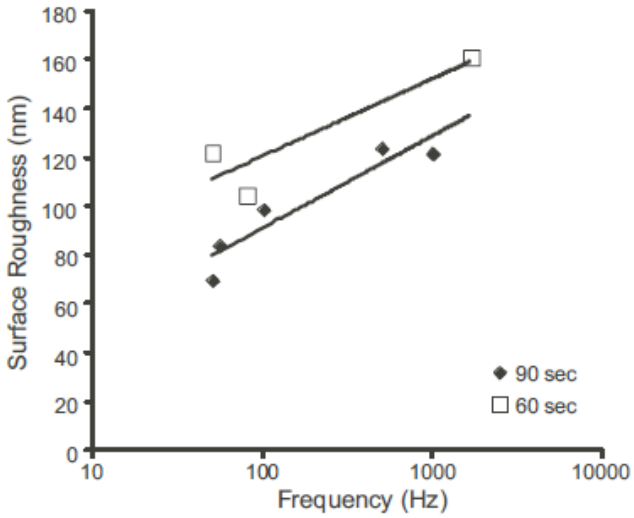

Fig. 20: Effect of pulse frequency on surface roughness at different on-times (Workpiece = SS304, electrolyte solution = EPS4000) (30)

During the drilling of holes, as the pulse duration increases the hole size increases and the voltage also has a similar effect. This is shown in Figure 21:

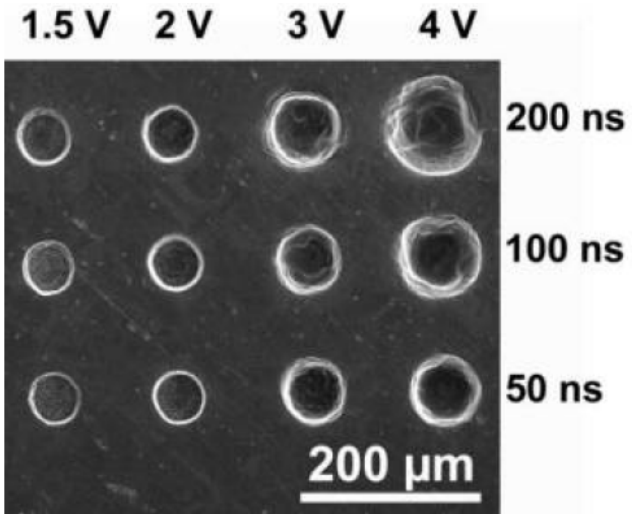

Fig. 21: Array of holes drilled into stainless steel at different pulse duration and voltage. (Tool: Cylindrical Pt wire of 50 µm diameter, Electrolyte: 3M HCl/6M HF) (53)

The pulse parameters such as pulse on/off time affect the current density, the anodic overpotential and the current efficiency significantly. As a result, the local anodic dissolution rate is more sensitive to the changes in the local current density, leading to higher dissolution localization and more uniform gap distribution than in the ECM with continuous current (54). Variation in the current efficiency with current density is shown in Figure 22.

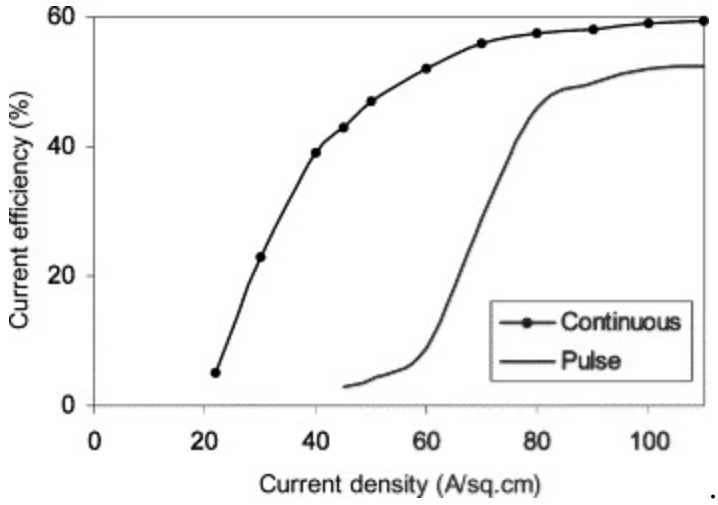

Fig. 22: Current efficiency against current density for continuous and pulsed voltage for an interval of 10 ms with pulse duration of 1 ms (55)

A relatively small inverse polarity is sometimes made use of on pulsed systems to promote the possible dissolution of metal plating on the tool cathode during the inverse polarity (56; 57).

2.8 Advantages of electrochemical machining/polishing

Electrochemical machining has several advantages on offer over other machining processes and is ideally suited for some of the applications, making it the best option for many applications.

Its main advantages over the other processes are as follows (22; 44; 58; 59):

1. It can polish difficult to cut (hard) materials even with a soft tool, since it is a non contact type process.
2. No tool wear as it operates in a non contact working mode avoiding problems such as elastic deformation, vibration and breakage.
3. Improved surface finish gives an attractive appearance.
4. Surface is easier to clean due to decreased surface adhesion.
5. A very good surface finish in the nanometer range can be obtained.
6. Does not affect the microstructure or surface properties.
7. Complex features can be machined/polished.
8. Surface stresses are not generated during polishing.
9. It can be used for micro as well as macro polishing.
10. It is an environmentally friendly process
11. Labor requirements are low.

2.9 Disadvantages of electrochemical machining/polishing

Some of the disadvantages of electrochemical polishing are listed (22; 44; 58; 59):

1. The energy requirements for ECP are much higher as compared to turning or drilling.
2. Only electrically conducting materials can be machined using this technique.
3. High current must be applied in some cases which increases the risk of the process
4. Explosive hydrogen gas is generated in machining with some electrolytes and has to be disposed carefully.
5. Workpiece has to be cleaned and oiled directly after machining as electrolyte can corrode the tool, workpiece and equipment if not cleaned properly.
6. Electrolyte has to be stored and handled with utmost care.

2.10 Applications of electrochemical machining

Electrochemical machining is used in a number of applications like de-burring, hole drilling, shaping, etc. These are elaborated in the following sections:

2.10.1 Hole drilling

ECM can also be used for drilling holes (11) as shown in Figure 23. Using a cathode which is either tubular or solid in form, holes can be machined into the conducting anode material. The debris that are formed in the gap between the cathode and anode needs to be flushed out continuously otherwise we would end up machining on the debris and hence would not be able to drill deeper into the workpiece. The pile up of the debris may also cause a short circuit and hence needs to be prevented. An electrolyte that is pumped through the cathode flushes the material gathered in the inter electrode gap and also creates the path for the current to flow. It also prevents the accumulation of ions at the electrodes.

Machining is very aggressive in the gap between the extreme end of the tool and the base of the hole being drilled in the workpiece. Some machining also occurs at the sidewalls as the entire electrode is electrically charged though at a lower rate. Due to this lateral machining, the diameter of the hole is slightly larger than that required. This can be avoided by insulating the sidewalls of the cathode or by designing the cathode in such a way that the current density at the sidewalls is lower than at the base of the tool. The electrolyte if chosen carefully can also help prevent this problem as hole drilling depends

on the current densities between the workpiece and tool. Some electrolytes are better suited for purposes of hole drilling due to their current efficiency – current density characteristics. Sodium chloride if used for hole drilling produces much less accurate components than sodium nitrate.

Different shaped holes can also be drilled using ECM, since the shape of the hole depends on the shape of the cathode. Holes with very high aspect ratios, 0.5 mm to 1mm diameter holes of depth upto 110 mm have been drilled accurately by this method (11).

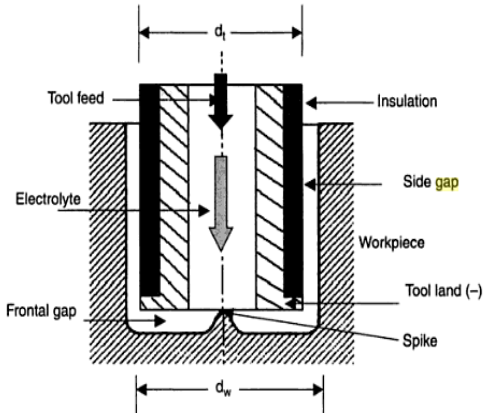

Fig. 23: Electrochemical hole drilling by ECM (44).

2.10.2 Full form shaping

In full-form shaping a constant gap between the entire workpiece and tool is maintained as the tool progresses towards the workpiece at a fixed rate. Compressor and turbine blades shown in Figure 24 can be easily formed using this method as they can be placed

close to each other, thus increasing the efficiency. Very high current densities are used to form the required shapes and the entire area between the electrodes has to be supplied with the electrolyte as it flows between them, thus requiring high pumping pressures and volume flow.

Fig. 24: Turbine blades machined using ECM (44).

2.10.3 Electrochemical grinding

In electrochemical grinding, insulating abrasive particles embedded in a grinding wheel made up of a conducting material are used. The interelectrode gap is created due to the abrasives projecting from the grinding wheel and an electrolyte flushes the debris that are formed during grinding, this is shown in Figure 25. The grinding wheel is used as the cathode and the anode is the workpiece.

Electrochemical grinding has the ability to produce highly accurate parts and can be used to grind hard materials like tungsten carbide as well as fragile parts like hypodermic

needles, making it a very versatile process. The only drawback being the loss of accuracy while grinding inside corners on the workpiece.

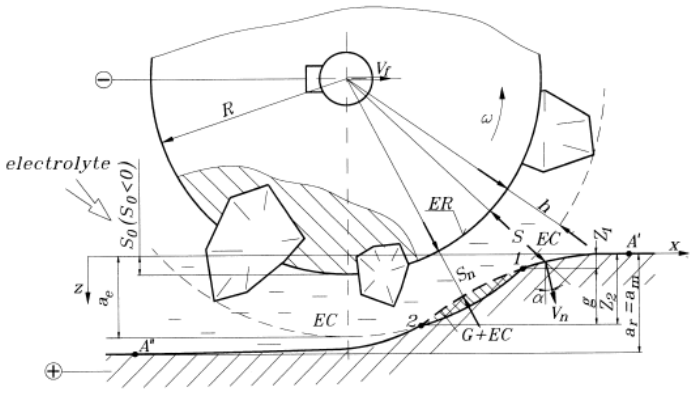

Fig. 25: Schematic diagram for abrasive electrochemical grinding (60).

2.10.4 Electrochemical arc machining

This process makes use of the electrical discharges in the electrolyte between the electrodes. Metal removal takes place due to both metal erosion as well as ECM. An arc is defined as a stable thermionic phenomenon while a spark is a sudden and noisy discharge between electrodes. This process makes use of arcs instead of sparks and hence is named accordingly.

This process can be used for all the purposes that ECM could be used. Very fast metal removal rates can be achieved due to the combined effects of arcing and ECM. Any surface damage caused by the ECAM action can be removed by carrying out ECM of the part after machining.

2.11 Applications of electrochemical polishing

Electrochemical polishing works on the same principles as electrochemical machining, the difference lies in the amount of material removed in the process. The amount of material removed in machining is much higher as compared to polishing. Polishing is used to improve the surface texture thus removing little material. Its main applications are listed below (61):

2.11.1 Ultracleaning

Electrochemical polishing is known to give a good, bright surface finish. As the polishing takes place due to the removal of material from the surface, surface impurities are also removed as the polishing takes place. Scales, rust, foreign debris, oils and grinding compounds are removed as the base material is polished. Thus, electrochemical polishing gives us a chemically clean, non-coated, non-distorted and a corrosion resistant part. Figure 26 shows a part that has been ultracleaned by electropolishing.

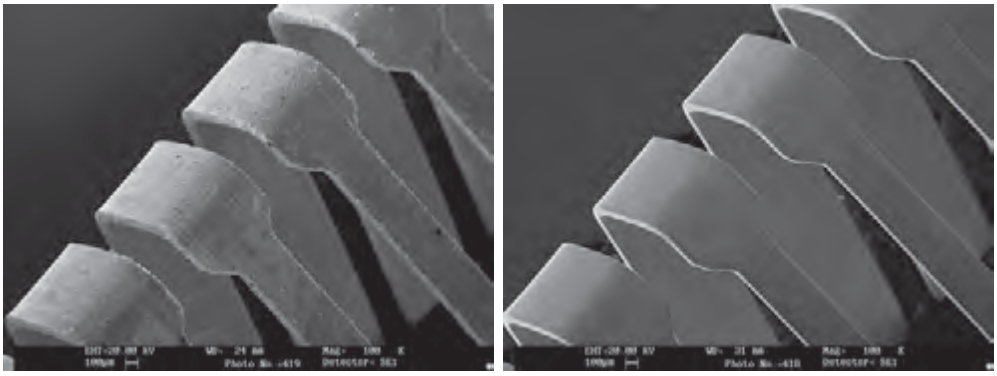

(a) (b)

Fig. 26: Image of beryllium/nickel alloy (a) before (b) after ultracleaning (61)

2.11.2 Passivating

Passivation is a chemical process that helps restore the contaminated surface properties. Due to the many sources of contamination, passivation is recommended most the time by engineers. In stainless steel it helps develop a chromium rich surface that is resistant to corrosion. Passivation is usually preceded by pickling. Pickling solution made of hazardous hydrofluoric acid is initially used to dissolve the imbedded steel flecks and other impurities followed by passivation which helps develop a corrosion resistant film. The chemicals used for these processes are not eco friendly and are being banned from industry. Figure 27 shows the end of a tube with a laser cut through hole that has been passivated using ECM.

Electropolishing process is a potential candidate that has helped replace these processes. As the surface material is removed all the impurities are removed along with it. It can also be used to improve the corrosion resistance of other alloys without causing any distortion, flash attack or hydrogen embrittlement problems.

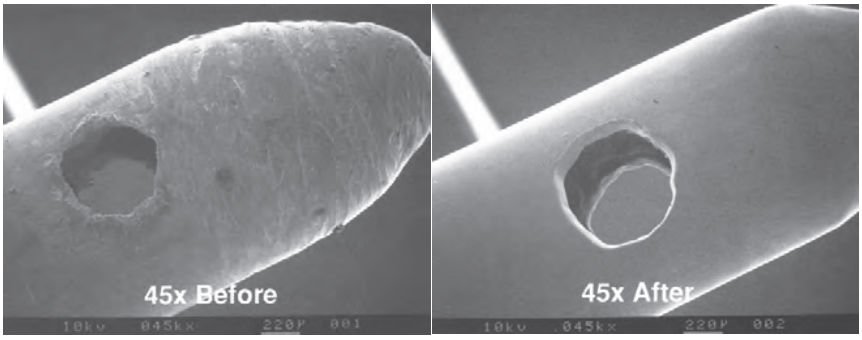

(a) (b)

Fig. 27: End of a tube with laser cut through hole (a) before (b) after passivation (61)

2.11.3 Sizing

Electropolishing allows us to remove material in a controlled fashion, in the range of 3 µm (0.0001”) (61). This accurate control over the material being removed and the ability to machine complex shapes and parts has enabled its use in part sizing. Electropolishing can be an economical method to recover material that has been scrapped due to non conformance of dimensions. Also, it can be used in production sizing, as shown in Figure 28, when many fragile parts cannot be sized by the traditional operations due to potential damage to the workpiece and the induction of surface stresses or contaminants.

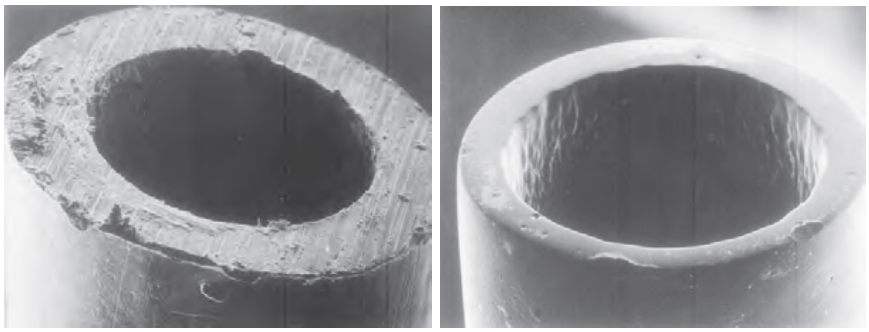

(a) (b)

Fig. 28: Tube wall (a) before sizing (b) after sizing (61)

2.11.4 Destressing

Surface stresses can be removed from components subject to high stress and cycle duties by electropolishing. Surface stresses usually exist within the outermost 30 µm (0.001”) of a component’s surface (61). By removing surface material in that range electrochemical polishing can help remove the various tensile, compressive and other

stresses present on the workpiece surface. Electropolishing does not introduce new surface stresses unlike shot peening, vibra-finishing and other processes. It also reduces or eliminates stress risers caused by heat treating, decarburization and microscopic scratches, tool and grinding marks, thus, helping us enhance metal fatigue.

2.11.5 Deburring and microfinishing

Burrs are generated in machining processes and are undesirable in most applications. Manual deburring should be minimized since it is time consuming and ineffective. Also, many a times, the complex structure of the workpiece makes it impossible to deburr using the conventional processes available. Electrochemical machining with its known advantages is a suitable choice for deburring of complex shaped workpieces and can also be used for selective deburring.

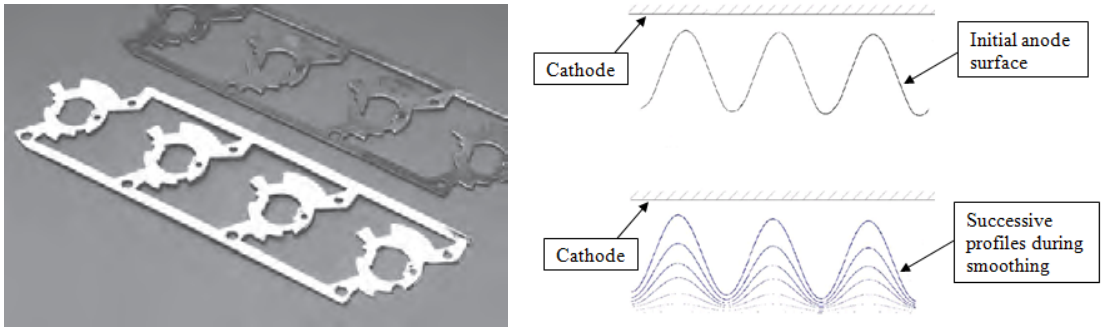

Fig. 29: (a) ECM deburring of parts (61) (b) Current density at cathode & burrs (11)

Figure 29 (a) shows a picture of a component before deburring and after it has been deburred using ECM. For deburring of components a plane, flat-faced cathode tool is

generally placed opposite a workpiece that has an irregular surface as shown in Figure 29 (b). The current density at the peaks of the surface irregularities is higher than those at the valleys due to its proximity to the cathode and its small surface area as shown in Figure 29 (b). The former encounter the high currents first and are removed preferentially making the workpiece surface smooth. Electrochemical smoothing is the only type of ECM which is capable of precisely replicating the shape of the cathode tool on the anode workpiece (11).

Researchers have investigated the effect of different parameters in ECM and PECM to obtain good surface results. Tajima (7) has reported mirror like surfaces with an average surface roughness (R_a) of 0.03 to 0.12 µm using DC current and an alcohol based electrolyte on wrought Ti and Ti-6Al-4V but cast Ti gave a dull and rougher surface (Ra = 0.67 to 0.80 µm) (7). In a study by Maurer (62), he investigates the effect of pulse duration on the hole diameter micromachined in Ni-Ti SMA using ultrashort pulses. Holes upto a depth of 3 µm were machined with good control over its diameter by varying the pulse on-time (62). A model for machining of Ti alloys using PECM with good dimensional control and accuracy has been developed by Wei (21). Effect of tool shapes and various activation methods on the surface quality of titanium have also been studied. Disc shaped electrodes and electrodes with an insulated tip helped reduce conicity and obtain a better accuracy over the machined area (41; 42). Rotating tool electrodes in ECM were also tried and they were found to give a better surface finish on the workpiece as compared to a stationery tool (63). However; the effects depend on the tool, workpiece and electrolyte combination used and hence should be selected carefully.

Chen (64) has reported a polished surface on pure titanium (99.995% pure) with a mean roughness (R_z) of the polished surface as 1.966 nm when measured by atomic force microscopy (AFM) over a 2 ×2 μm^2scan area.

Discrepancy in surface finish values due to different measuring techniques, processing methods and process parameters were seen in published literature. This research develops an ECP technique for CP Ti, compares measured value of polished Ti surface using AFM and interferometry and highlights differences in polishing due to AC or DC currents.

3. EXPERIMENTS

Numerous experiments were carried out with DC as well as AC current to determine the initial feasible starting point for further exploration. Further experimentation using design of experiments techniques was carried out in the neighborhood of the feasible point to get better results.

The results of the experiments depend upon the robustness and stability of the system. The system was selected to fulfill these requirements and suitable fixtures as required were designed for this purpose. Most of the system components used for our experiments were already designed in a previous project with the idea to keep the system robust, free from vibrations and as compact as possible while fulfilling its purpose so that errors due to system inconsistencies are minimized. A detailed design description of the system components is given in Appendix A.

3.1 Equipment

The system designed for de-burring and polishing the Ti plates and for measuring data consisted of many components. The instruments used are listed as follows:

1. Velmex Bi-Slide and VXM-2 stepper motor controller.
2. Keyence LK-G157 laser head and LK-GD500 controller.
3. Agilent 33250A function generator.
4. LEADER LPS-151 DC Tracking power supply.
5. Tektronix TDS 1002B oscilloscope.

6. Fluke 45 multimeter.
7. Manostat Vera 72-315-000 electrolyte pump.
8. Agilent 33502A 50 V_{p-p} / 100 kHz 2 channel Isolated Amplifier.
9. National Instruments PCI-8432/4 interface board.
10. STM6 Olympus optical measuring microscope.
11. ZygoNewView 100 Interferometer.
12. JEOL6400 Scanning Electron Microscope.
13. Bruker Dimension Icon Atomic Force Microscope.

A detailed description of these instruments is provided in Appendix C.

3.2 Procedure

3.2.1 Electrode setup

A hollow stainless steel (SS) tube was used as the tool for all the experiments unless otherwise mentioned. The tool was press fit into a teflon adapter coupling designed to streamline the flow of the electrolyte. Design details of this coupling are given in Appendix B. This coupling sits on the small cylindrical portion at the top of the electrode holder as shown. The tool was secured in the electrode holder using the screws in the electrode holder designed for this purpose. Using these, the electrode was aligned at the center and held firmly in position. The assembly was then mounted on an arm screwed to the bi-slide and held in position. This setup is shown in Figure 30:

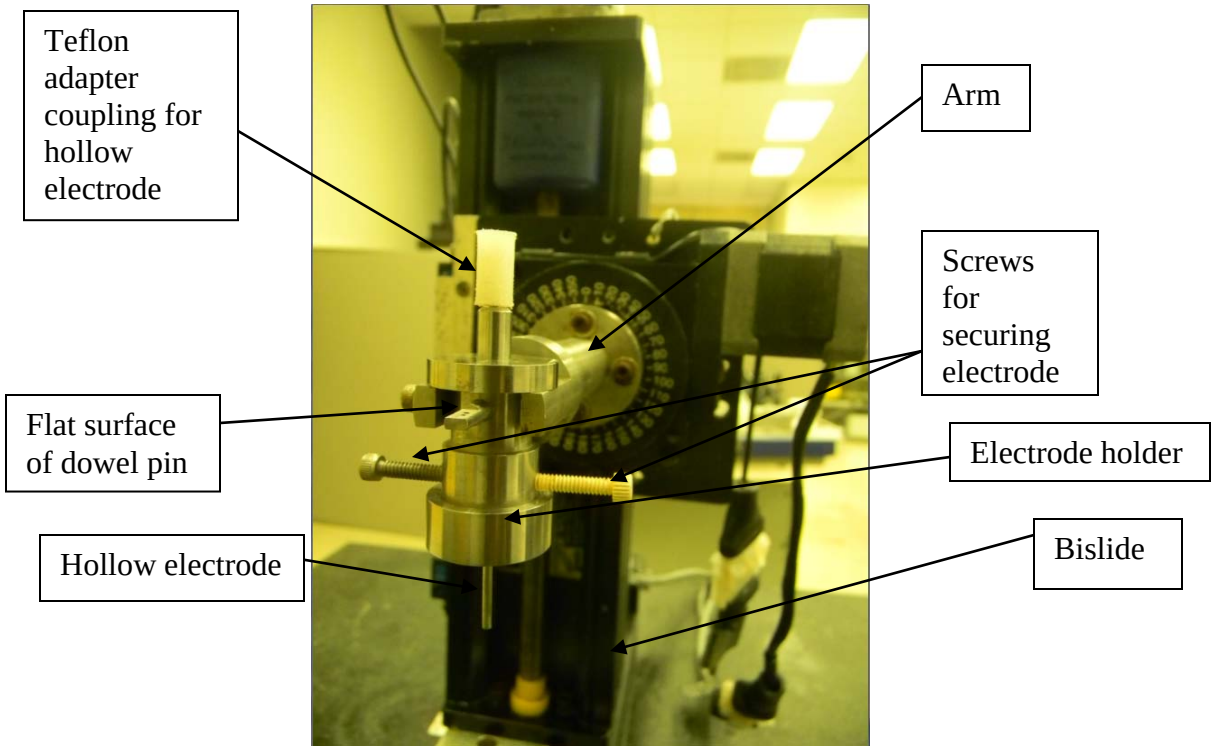

Fig. 30: Electrode setup mounted on arm fixed on bislide

3.2.2 Workpiece setup

The workpieces for the experiments were 50mm X 40mm X 0.5 mm Ti plates. They were cleaned ultrasonically before machining to remove any unwanted dirt from the surface. After cleaning the workpiece, it was clamped onto the workpiece fixture using teflon washer and screw. The workpiece fixture was mounted onto the electrolyte bath which was kept in the ice bath and the whole assembly was in turn mounted onto a flat plate. The workpiece was clamped rigidly in position by using aluminum clamps screwed in the flat plate. The assembly was then leveled using the flat plate fixture to ensure a constant interelectrode gap. The setup is shown in Figure 31:

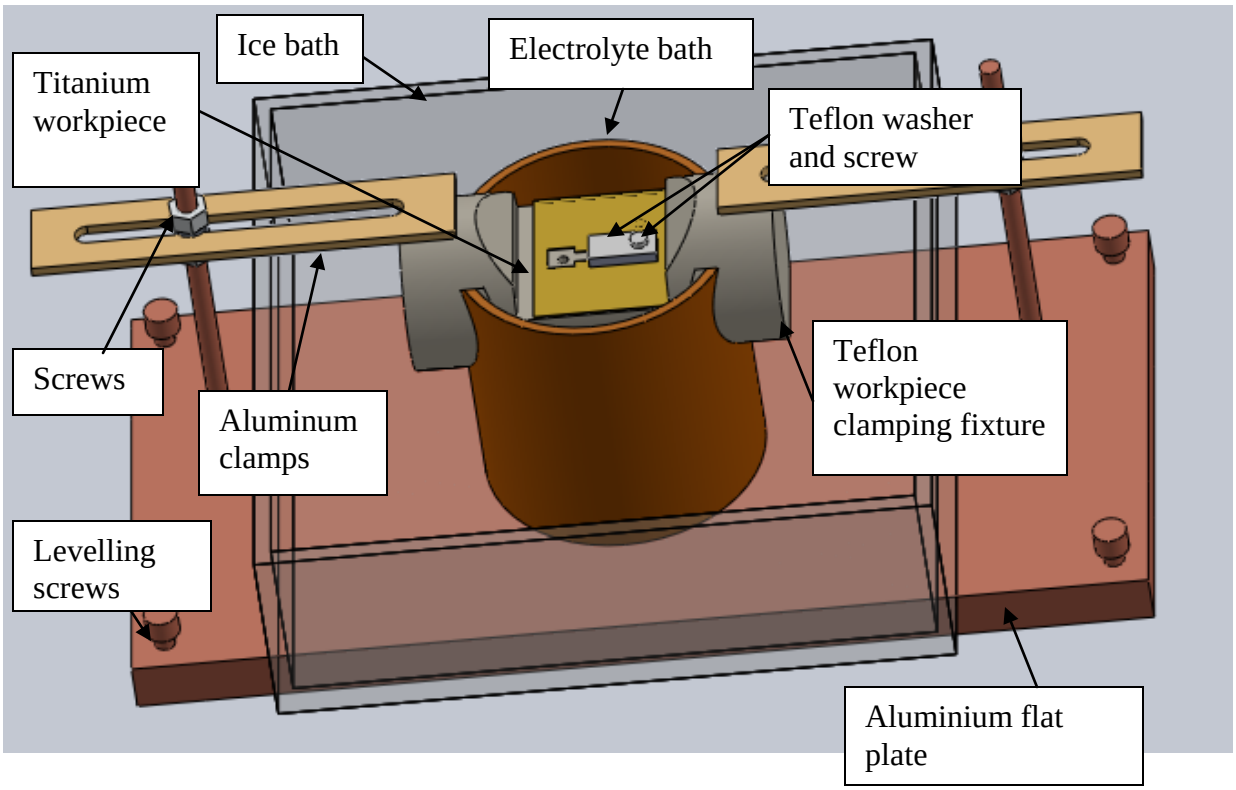

Fig. 31: Workpiece setup for machining

3.2.3 Tool positioning

Two methods, contact type and non-contact type, could be used for positioning the tool relative to the workpiece. The contact type method was used for positioning the workpieces unless otherwise mentioned.

3.2.3.1 Method 1 – Contact type

The FLUKE 45 dual display multimeter makes a beeping sound when its positive and negative terminals make contact. The proper connections were made for this purpose. The procedure to position the tool using this method is as follows:

Step 1: Connect the tool to the negative and the workpiece to the positive terminal of the multimeter.

Step 2: Shine the laser displacement sensor on the top i.e. flat surface of the dowel pin in the electrode holder shown in figure 30.

Step 3: Lower the tool until it makes contact with the workpiece, thus making a continuous beeping sound from the multimeter and zero the laser sensor at this position.

Step 4: Raise the tool by the required amount and set the gap.

This method can be used as long as the tool is not very fragile, and it is secured firmly in the tool holder.

3.2.3.2 Method 2 – Non - Contact type

Step 1: Measure the distance ‘X’ on the optical microscope, which is the projection of the electrode from the tool holder as shown in Figure 32.

Step 2: Note the distance ‘Y = 29 mm’ from the design of the tool holder, which is the distance from the end of the tool holder to the flat surface of the dowel pin.

Step 3: Shine the laser displacement sensor on the workpiece surface. The reading shown by it is Z. Zero the displacement sensor at that position.

Step 4: Shine the laser sensor on flat surface of the dowel pin. It will give (g + X + Y).

Step 5: Offset the laser sensor by the value (X + Y), the controller will display the value of the gap between the electrode and workpiece. This method is based on the following equation:

$$g = Z - (X + Y + Z') \quad (10)$$

Z’ is the reading given by the displacement sensor when it was shining on the flat surface of the dowel pin, without being zeroed on the workpiece.

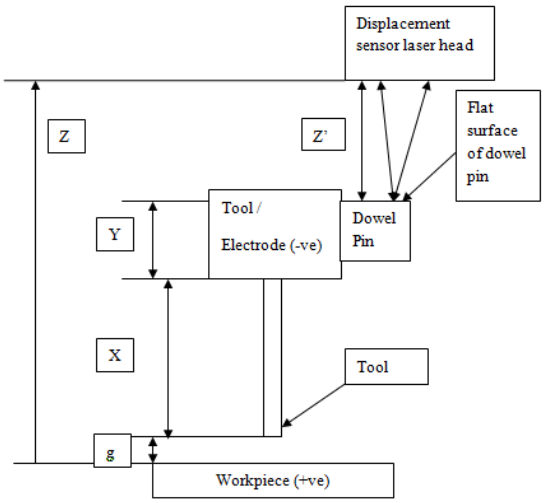

Fig. 32: Schematic explaining non-contact type gap measuring technique

3.2.4 Electrolyte

An alcohol and salt based electrolyte developed in another project was used for our experiments. Fresh electrolyte was prepared before the start of each experiment to reduce the effect due to electrolyte composition variation. A detailed procedure to prepare this electrolyte is provided in Appendix D. The system was setup for the internal flow configuration for all the experiments unless otherwise mentioned.

3.2.5 Circuit connections

Figure 33 is the wiring diagram showing the connections to be made for PECM.

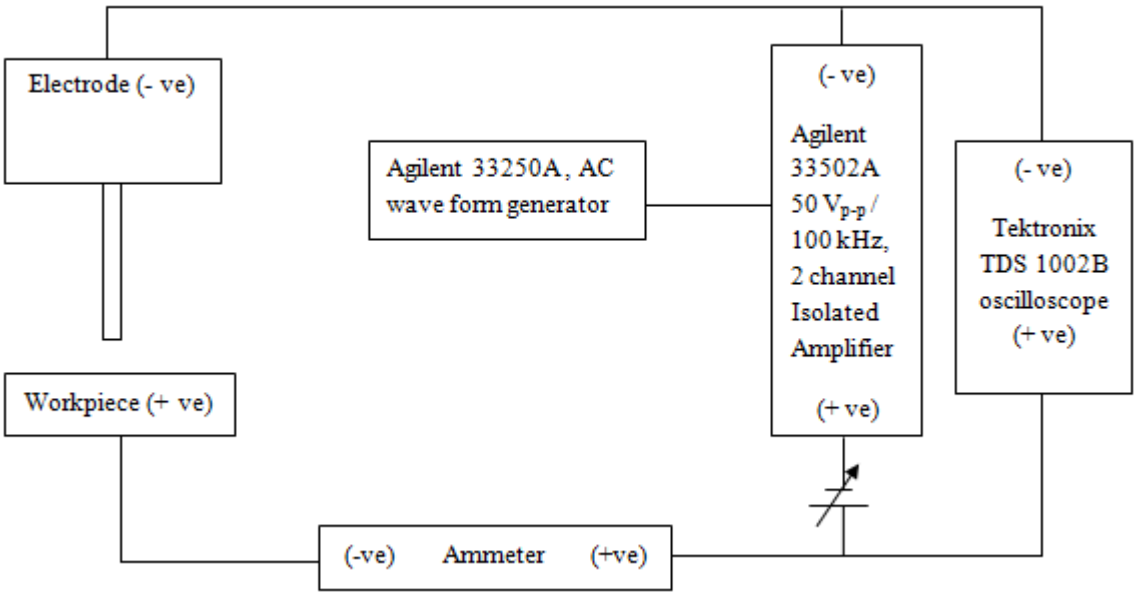

Fig. 33: Wiring diagram

3.2.6 Temperature and electrode surface control

The temperature of the electrolyte was maintained as low as possible ~5-10 ^{0} C by keeping the apparatus surrounded by an ice-water bath to minimize the change in the electrolyte composition during machining, thus reducing the effect due to changes in electrolyte.

The electrode surface was cleaned after each run by using cotton swabs. While cleaning, the electrolyte was kept running in order to flush out the ions accumulated in the inside surface of the electrode. Once the inside surface of the electrode was clean, electrolyte flow was stopped and the polarities of the electrode and workpiece were inverted while cleaning the outside surface, this facilitated easy cleaning and reduced the effect due to change in electrode surface condition.

3.2.7 Experiment design

The aim of these experiments was to study the effect of the different ECP parameters that would result in a polished surface on the workpiece and would establish a baseline for comparison. The electrode used for these experiments was a stainless steel hollow tube. The electrode was cut to the required length on a wire EDM machine, its end was polished using 15 μm diamond polishing compound. The workpieces were pure alpha titanium plate of size 50 mm X 40 mm X 0.5 mm. The alcohol based electrolyte mentioned earlier was used for these experiments.

Determining the levels of the parameters in factorial design is crucial to determining the optimal results. These levels are determined through experimentation and the

experimental region is further explored using a 2^k full factorial experimental design to understand the effects of different parameters on the surface quality. The surface quality is determined by the resulting surface roughness (R_a and R_z).

3.2.8 Measurement of surface finish

In order to measure the quality of the polished area, surface finish of the electrochemically polished titanium plate was assessed by interferometry and atomic force microscopy (AFM).

The surface roughness (R_z) measurements for analyzing the data were carried out using the white light interferometer. It can generate three dimensional surface profiles by scanning the surface of the workpiece through interference of the light reflected from its surface. The workpiece was set on the stage of the instrument and made horizontal by adjusting the stage using tilting knobs and water-bubble level. The bipolar scanning length of the instrument was set to 40 µm and the polished surface of the workpiece was brought in focus. The working distance was further adjusted by using fine movements until fringes were seen on the polished surface. The light intensity on the workpiece surface was adjusted to obtain a good plot of the surface profile with minimum black spots. A circular section was used to measure the surface roughness of the polished spot. Measurements were taken along a circular section at two different radii 130 µm and 380µm, and the average of these values was considered as the roughness value of the polished area.

3.3 Electrochemical polishing of titanium using direct current

These experiments were carried out using fresh electrolyte. In these experiments, the ECP process factors that were considered for analyzing the effect on surface finish were the electrolyte flow rate (ml/min), voltage (volts), the polishing time (s) and the effective IEG (µm) which is the average of the distance between the tip of the electrode and the two circular sections along which R_z was measured. A hollow SS electrode with (outside diameter (o.d) – Ø 2.74 mm, inside diameter (i.d) – Ø 2.44 mm) was used for these experiments. The response data (i.e surface roughness) will be analyzed using a regression model for the full factorial design to find the best parameters. The levels of factors that were decided through experimentation are shown in Table 3:

Table 3: Factor-and-level table for experiments using DC current

		High level (+)	Low level (-)
g =	Effective IEG (µm)	2370	2340
t =	polishing time (s)	45	5
V=	voltage applied (V)	55	20
F=	Flow rate (ml/min)	420	190

The reported effective interelectrode gap is shown in Figure 34:

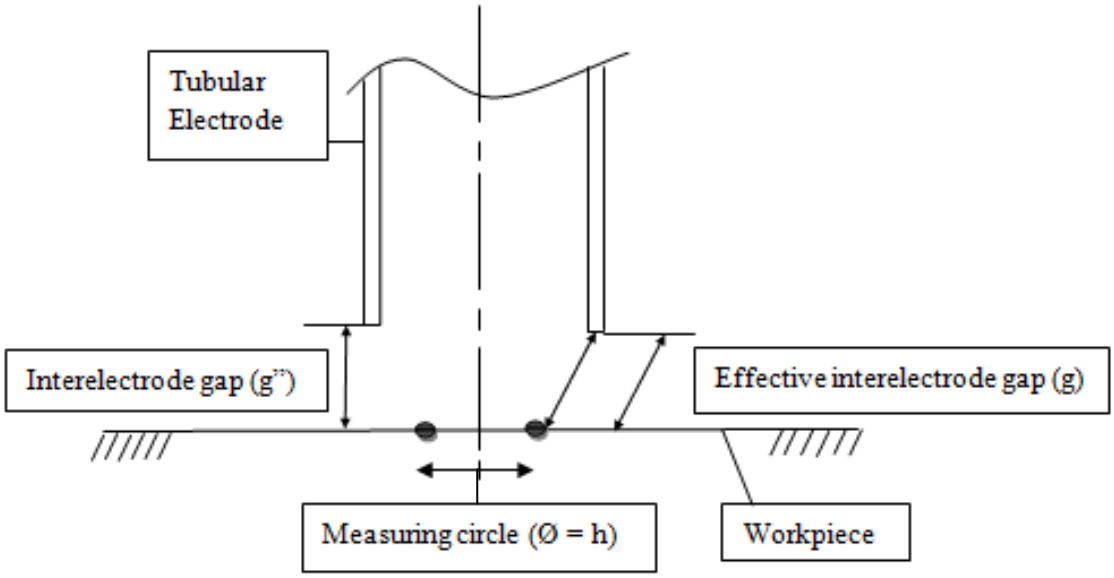

Fig. 34: Schematic showing effective interelectrode gap.

The effective interelectrode gap is calculated as follows:

Let, g = effective interelectrode gap.

$g"$ = Interelectrode gap.

h = diameter of circular section along which surface finish is measured.

r = inside radius of tubular electrode.

The effective interelectrode gap is found using Pythagoras theorem as follows:

$$g^2 = g"^2 + \left(r - \frac{h}{2}\right)^2 \quad (11)$$

The reported effective interelectrode gap is the average of the effective interelectrode gaps calculated at the two measuring circles of radius 130 µm and 380 µm.

In the next table, the (+) represents high level setting corresponding to the respective factor while the (–) represents its low level setting. Spots were polished at each of the factor level combinations shown in the table below. The electrode was held stationery while the polishing was being carried out. The sequence of the design matrix was followed while carrying out the experiments and each run was repeated twice to check for repeatability of the process. The current (A) in the circuit was recorded using a multimeter and surface roughness (R_a & R_z) at the different runs was measured using the methodology explained earlier. The workpiece surface finish obtained was also observed under the optical microscope to check for pitting and surface contamination.

Experiments were carried out at each factor and level combination as shown in Table 4:

Table 4: Design matrix for full factorial experiments using DC current

	Factor			
Run No.	Flow rate (F)	Voltage (V)	Effective IEG (g)	Polishing time (t)
1	+	+	+	+
2	+	+	+	-
3	+	+	-	+
4	+	+	-	-
5	+	-	+	+
6	+	-	+	-
7	+	-	-	+
8	+	-	-	-
9	-	+	+	+
10	-	+	+	-
11	-	+	-	+
12	-	+	-	-
13	-	-	+	+
14	-	-	+	-
15	-	-	-	+
16	-	-	-	-

3.4 Electrochemical polishing of titanium using alternating current

These experiments were carried out using fresh electrolyte. In these experiments, the ECP process factors that were considered for analyzing the effect on surface finish were the peak to peak voltage (volts), frequency of alternating current (Hz), duty factor (%), effective interelectrode gap (µm) as defined earlier and the polishing time (s). A hollow SS electrode with (o.d – Ø 1.64 mm, i.d – Ø 1.20 mm) was used for these experiments. Levels of the factors that were decided through experimentation are shown in Table 5:

Table 5: Factor-and-level table for experiments using AC current

		High level (+)	Low level (-)
g =	Effective IEG (µm)	1360	1180
t =	polishing time (sec)	150	40
V=	voltage applied (V_{p-p})	Max = 28V, Min = 0V	Max = 20V, Min = 0V
N=	Frequency (Hz)	1000	50
D=	Duty cycle (%)	80	40

The flow rate of the electrolyte was maintained at 135 ml/min. In the Table 6 below, the (+) represents high level setting for the respective factor while the (–) represents its low level setting. Spots were polished at each of the factor level combinations shown in the table below. The electrode was held stationery while the polishing was being carried out. The sequence of the design matrix was followed while carrying out the experiments and each run was repeated twice to check for repeatability. The current (A) in the circuit was recorded using a multimeter and surface roughness (R_a & R_z) at the different runs was measured using the methodology explained earlier. The workpiece surface finish was also observed under optical microscope to check for pitting and surface contamination.

Table 6: Design matrix for full factorial experiments using AC current

	Factor				
Run No.	V	N	D	g	t
	Voltage	Frequency	Duty cycle	Effective IEG	Polishing time
1	+	+	+	+	+
2	+	+	+	+	-
3	+	+	+	-	+
4	+	+	+	-	-
5	+	+	-	+	+
6	+	+	-	+	-
7	+	+	-	-	+
8	+	+	-	-	-
9	+	-	+	+	+
10	+	-	+	+	-
11	+	-	+	-	+
12	+	-	+	-	-
13	+	-	-	+	+
14	+	-	-	+	-
15	+	-	-	-	+
16	+	-	-	-	-
17	-	+	+	+	+
18	-	+	+	+	-
19	-	+	+	-	+
20	-	+	+	-	-
21	-	+	-	+	+
22	-	+	-	+	-
23	-	+	-	-	+
24	-	+	-	-	-
25	-	-	+	+	+
26	-	-	+	+	-
27	-	-	+	-	+
28	-	-	+	-	-
29	-	-	-	+	+
30	-	-	-	+	-
31	-	-	-	-	+
32	-	-	-	-	-

3.5 Comparison of AC and DC current types

Experiments were carried out to compare the current types for surface finish. Fresh electrolyte was prepared and a hollow SS electrode with outside diameter – Ø 1.64 mm, inside diameter – Ø 1.20 mm was used for these experiments. Five spots were polished using each of the current types. For AC current type, the spots were polished at electrolyte flow rate = 135 ml/min, frequency of square waveform = 50 Hz, duty cycle = 80%, effective IEG = 1235 µm, polishing time = 150 sec. Current in the circuit for AC experiments varied between 5.9 to 39.2 mA. Equivalent experimental conditions for DC current were determined as electrolyte flow rate = 135 ml/min, effective IEG = 1235 µm, polishing time = 120 sec. The current was kept in the same range as AC experiments by varying the voltage.

3.6 Verification experiments

Additional experiments were carried out to confirm the repeatability of the process and to validate the regression equation developed from the regression analysis for predicting the surface roughness at given parameter values in the experimental region. These experiments were run for DC as well as AC current at the midpoint levels of each parameter and were repeated 10 times to estimate the variability in the process. Fresh electrolyte was used for these experiments.

3.6.1 Verification experiments for DC current

These experiments were carried out using fresh electrolyte. A hollow SS electrode with o.d – Ø 2.74 mm and i.d – Ø 2.44 mm was used for these experiments. The parameters were set at their midpoint levels i.e 0 in coded form. In the uncoded form, the electrolyte flow rate was 305 ml/min, voltage across the electrodes was 38 V, effective IEG was kept at 2355 µm and the polishing was carried out for 25 sec.

3.6.2 Verification experiments for AC current

These experiments were carried out using fresh electrolyte. A hollow SS electrode with (o.d – Ø 1.64 mm, i.d – Ø 1.20 mm) was used for these experiments. Here too, the parameters are set at their midpoint levels i.e 0 in coded form. In the uncoded form, the peak to peak voltage across the electrodes was 24 $V_{p\text{-}p}$, frequency of square waveform was 525 Hz, duty cycle was 60%, effective IEG was kept at 1250 µm and the polishing time was 95 sec.

A snapshot of the entire system used for carrying out these experiments is shown in Figure 35:

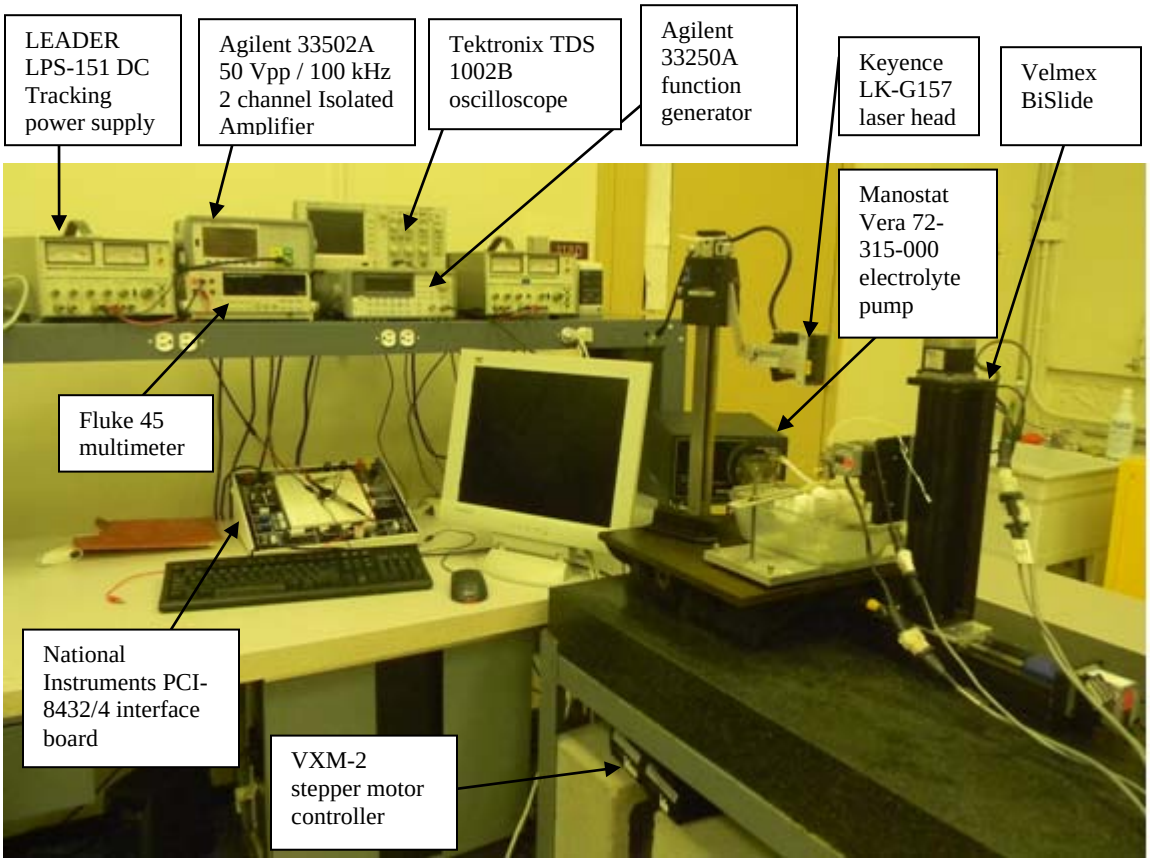

Fig. 35: Snapshot of setup for ECM & ECP

4. RESULTS AND DISCUSSIONS

Images of the workpiece surface were taken on the optical microscope, atomic force microscope (AFM) and Scanning electron microscope (SEM) before being polished. These are shown in Figure 36:

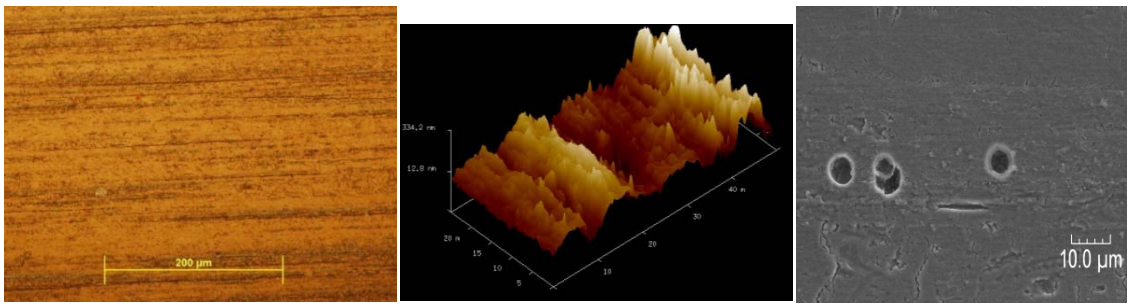

(a) (b) (c)

Fig. 36: (a) Optical image (b) 3D AFM image (c) SEM image of unpolished surface

The surface roughness value depends on the direction along which it is measured. Along the direction of waiviness, the surface roughness measured was lower, whereas across the direction it gave much higher values. Thus, on the interferometer, the roughness values were taken along a circular section to incorporate the directional effect. Also, different surface roughness values were obtained at different locations and hence the measurements were taken at two locations, one close to the center of the scanned spot (radius of circular section = 130 µm) and another away from it (radius of circular section = 380 µm). The average was used as the measured surface roughness.

4.1 Steps in analyzing using DOE technique

A step by step procedure that has to be followed while carrying out DOE analysis is provided as follows:

Step 1: Determine the factors and their levels that are to be studied in the experiment.

Step 2: If there are many factors, carry out a screening experiment using standard fractional factorial design and determine the significant factors at the specified significance (α) level by using linear regression.

Step 3: Using only the significant factors carry out a full factorial experiment at the decided levels to study all the main effects and interaction effects of the factors.

Step 4: Using the factors in the coded form i.e. -1 for the low level of the factor and +1 for its high level, fit a straight line through the data using least squares method. Carry out analysis of variance (ANOVA) to check the significance of the linear regression model at specified α.

Step 5: Check the significance of each factor by using t-test.

Step 6: Determine the prediction equation for the response value from the estimated effects calculated by the linear regression model.

Step 7: Based on the objective function i.e. to minimize or maximize the response value, determine the factor level settings that would achieve the objective. For instance, when the factors are used in the coded form; in order to minimize the response value we have to set those factors whose coefficients are positive in the prediction model at their -1 level and factors with negative coefficients are set at their +1 level. The factors can be uncoded using interpolation.

4.2 Calibration of ZygoNewView 100 Interferometer

The interferometer was calibrated to check for the accuracy of the measurements and repeatability of the instrument. A calibration block in the form of a circular disc with a step of 8.017 μm was used for calibration. The step size was measured at three different locations and five measurements of the step size were taken at each location. The data collected is listed in Table 7:

Table 7: Calibration data for ZygoNewView 100 Interferometer

	Location 1	Location 2	Location 3	Average	% error
Measurement 1 (μm)	7.925	7.988	8.287	8.067	0.624
Measurement 2 (μm)	7.935	7.915	7.965	7.938	-0.985
Measurement 3 (μm)	8.074	8.008	8.287	8.123	1.322
Measurement 4 (μm)	7.952	8.067	8.158	8.059	0.524
Measurement 5 (μm)	7.967	7.925	8.169	8.02	0.037

Thus, an average error of 0.304 % in the measured values is observed.

4.3 Analysis of spots polished using direct current

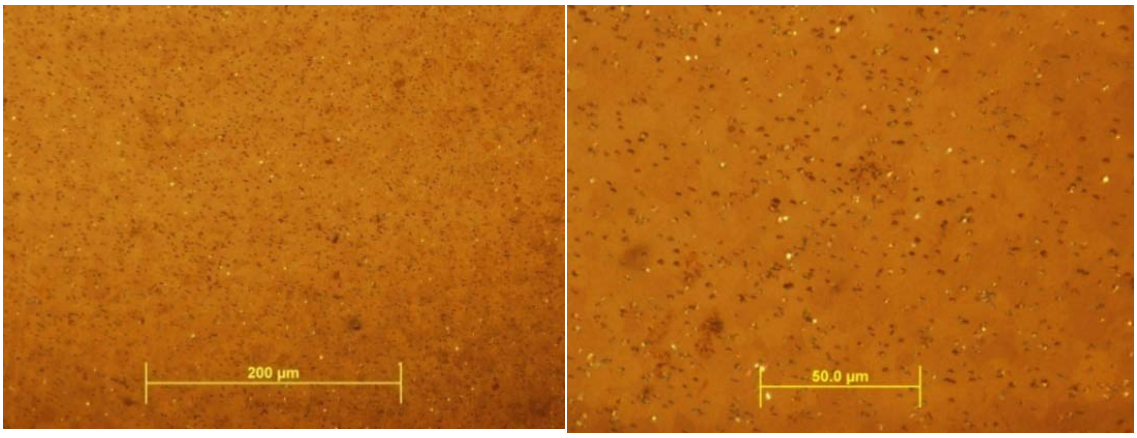

(a) (b)

Fig. 37: (a) Optical image (b) Magnified optical image of polished surface. (Electrolyte flow rate (F) = 190 ml/min, Voltage across terminals (V) = 55 V, effective IEG (g) = 2370 µm and machining time (t) = 45 sec.)

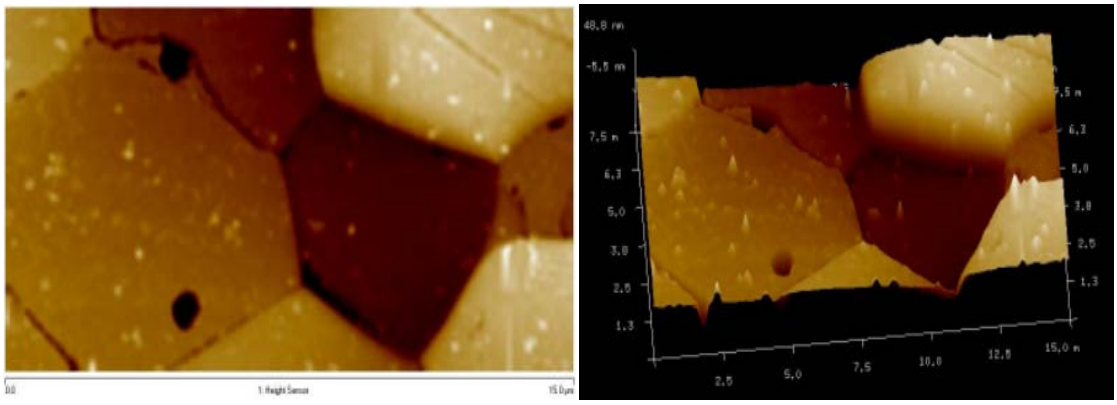

(a) (b)

Fig. 38: AFM (a) 2D surface (b) 3D surface image of polished surface using DC current. (Electrolyte flow rate (F) = 190 ml/min, Voltage across terminals (V) = 55 V, effective IEG (g) = 2370 µm and machining time (t) = 45 sec.)

It can be seen from Figure 37 and Figure 38 that the process gives a polished surface, but it is more aggressive at the grain boundaries. A surface roughness of R_a = 170 nm and R_z = 786 nm was achieved at these conditions.

The current flowing through the circuit as recorded with a multimeter and the surface roughness as measured using interferometry are tabulated below. The sequence is the same as that in the design matrix for this experiment. Surface roughness (R_a and R_z) was measured at two different circular sections of radius 130 µm and 380µm as shown in Figure 39:

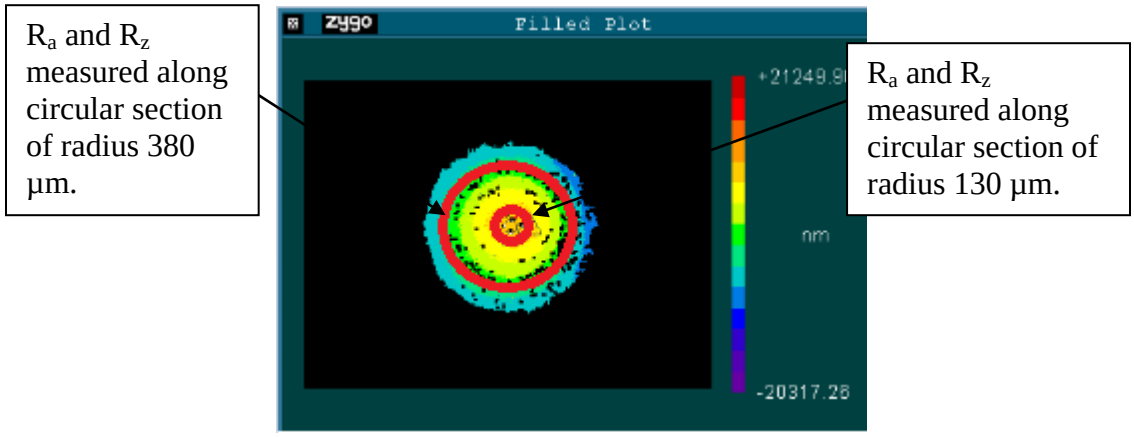

Fig. 39: Snapshot showing circular cross section along which R_a and R_z were measured

The values tabulated in Table 8 are the average of the two values. R1 is the average surface roughness for the respective run while R2 is the average surface roughness of its replication run. A table containing the individual values is provided in Appendix E.

Table 8: Summary of data from DC experiments

Run No.	Current (mA)		Current density (mA/mm^2)		R_a (nm)		R_z (nm)	
	R1	R2	R1	R2	R1	R2	R1	R2
1	148	245	121	201	196	262	786	845
2	65	65	53	53	326	396	2008	2182
3	175	150	143	123	308	330	1465	1504
4	225	105	184	86	309	337	1519	1535
5	30	30	25	25	424	438	1986	1781
6	25	33	20	27	397	245	2527	2516
7	70	45	57	37	257	363	1695	2534
8	35	33	29	27	474	377	2867	3094
9	115	130	94	106	146	193	675	897
10	75	70	61	57	232	286	1302	1126
11	120	150	98	123	294	343	1455	1475
12	125	111	102	91	249	252	1283	1261
13	45	42	37	34	326	310	1306	1597
14	25	25	20	20	238	263	1864	1258
15	77	82	63	67	352	271	1855	1864
16	47	50	39	41	323	252	1685	1158

It was observed that the current in the circuit varied during the entire machining time. The current recorded is the maximum current in the circuit during the entire duration of the machining.

The typical plots generated by the interferometer are shown in Figure 40:

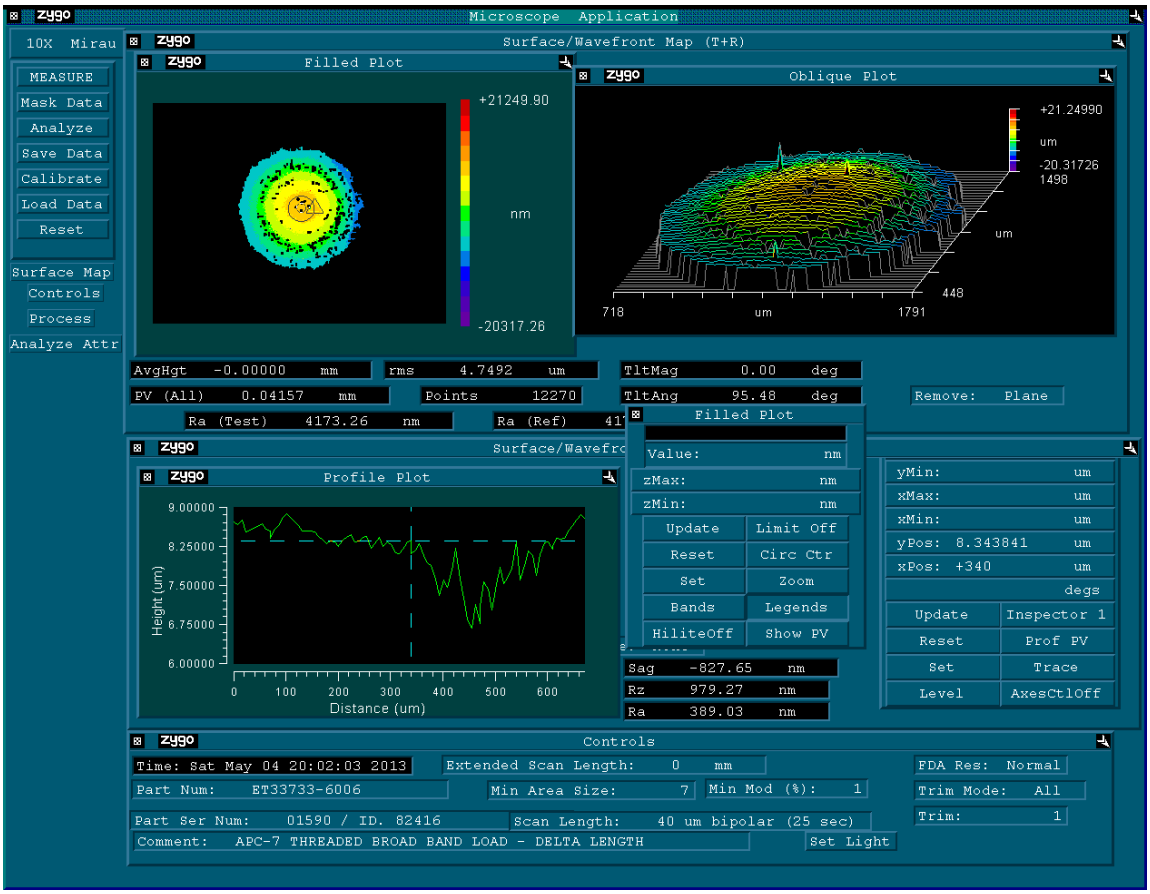

Fig. 40: Snapshot of plots generated of polished surface by the interferometer

The R_z data from the interferometer was used to fit a regression line through it, incorporating all the main effects and interaction effects. JMP Pro 10 statistical software was used to carry out this analysis. The model for a full factorial design can be written as follows:

$$y = \beta_0 + \beta_1 F + \beta_2 V + \beta_3 g + \beta_4 t + \beta_{12} F*V + \beta_{13} F*g + \beta_{14} F*t + \beta_{23} V*g + \beta_{24} V*t + \beta_{34} g*t + \beta_{123} F*V*g + \beta_{124} F*V*t + \beta_{134} F*g*t + \beta_{234} V*g*t + \beta_{1234} F*V*g*t + \varepsilon \quad (12)$$

The estimates for the coefficients in the regression model are obtained by fitting a straight line through the data using the least squares method. The solid line in the following figure is the straight line generated by the software using the least squares method for the above model. The results are shown in Figure 41:

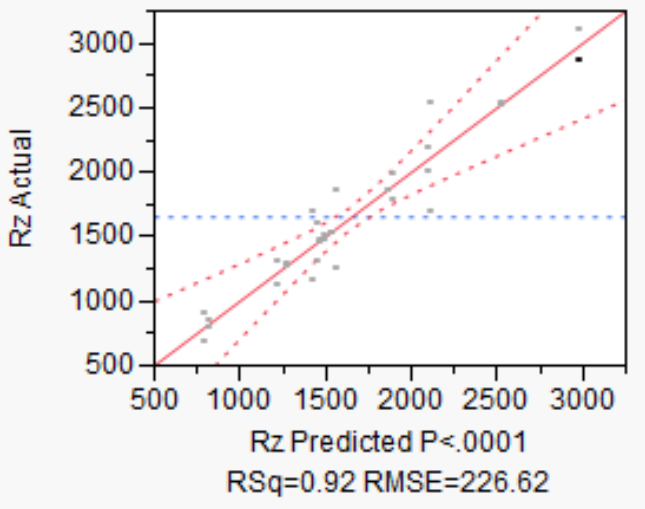

Fig. 41: R_z actual by R_z predicted plot for DC experiments with complete model

R^2 and adjusted R^2 are measures that determine how well the model helps in predicting the response. They represent the amount of variability in the data that is incorporated by the model. Analysis of variance (ANOVA) is used to test the hypothesis for significance of the regression model. For ANOVA,

The null hypothesis is: $H_0: \beta_0 = \beta_1 = \beta_2 = \beta_3 = \ldots\ldots = \beta_{1234} = 0$ (13)

The alternate hypothesis is that atleast one of the factors is useful in predicting the response values: H_a: Atleast one of $\beta_0, \beta_1, \beta_2, \ldots\ldots, \beta_{1234} \neq 0$ (14)

We shall use alpha level (α) = 0.25 to test significance of our model and the estimated parameter values. The results are summarized in Table 9:

Table 9: Summary of fit for complete regression model of DC experiments

Summary of Fit

RSquare	0.923987
RSquare Adj	0.852725
Root Mean Square Error	226.621
Mean of Response	1653.31
Observations (or Sum Wgts)	32

Analysis of Variance

Source	DF	Sum of Squares	Mean Square	F Ratio
Model	15	9988449	665897	12.9660
Error	16	821713	51357	Prob > F
C. Total	31	10810162		<.0001*

Different coefficients have different significance levels towards predicting the response value. The significance level of each effect is found by carrying out a t-test. Here,

The null hypothesis is: $H_0: \beta_i = 0; \quad \beta_i \epsilon$ each coefficient in regression model (15)

The alternate hypothesis is: $H_a: \beta_i \neq 0$ (16)

The results are summarized in Table 10:

Table 10: JMP results for estimates of complete regression model of DC experiments and their significance levels.

Term	Estimate	Std Error	t Ratio	Prob>|t|
V	-320.9061	40.06131	-8.01	<.0001*
F	274.51496	40.06131	6.85	<.0001*
F*t	-182.3797	40.06131	-4.55	0.0003*
t	-170.8576	40.06131	-4.26	0.0006*
g*t	-136.0933	40.06131	-3.40	0.0037*
F*V	-126.3669	40.06131	-3.15	0.0061*
g	-112.2986	40.06131	-2.80	0.0128*
V*g*t	-96.13954	40.06131	-2.40	0.0289*
F*V*g*t	-86.98371	40.06131	-2.17	0.0453*
F*V*g	66.066606	40.06131	1.65	0.1186
F*V*t	46.540269	40.06131	1.16	0.2624
V*t	-23.82264	40.06131	-0.59	0.5604
F*g	13.457231	40.06131	0.34	0.7413
F*g*t	9.9975437	40.06131	0.25	0.8061
V*g	7.4745188	40.06131	0.19	0.8543

The main effect of a factor can be shown graphically by a line connecting the average of the R_z values at the high and low levels of that factor. This is shown in Figure 42:

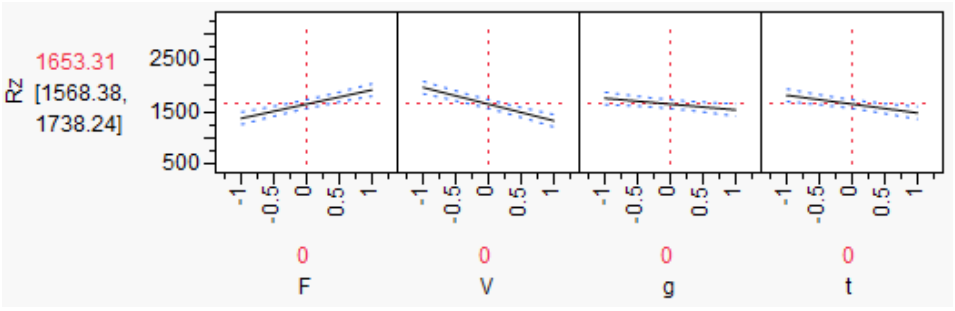

Fig. 42: Plots showing the main effects in complete regression model of DC experiments

The individual factors in the ECM process can interact synergistically or antagonistically and this can be shown graphically by an interaction effect plot. An interaction effect plot displays the average of the response at each level combination i.e. ((+1, +1), (+1, -1),

(-1,+1), (-1,-1)) of the factors. The factors on the horizontal and vertical axis are in the sequence F, V, g, t. The plot displayed within the box represents the interaction between the factors on the two axes that intersect at that location. If the lines drawn on the plot are parallel then it indicates that there is no interaction effect between the factors being represented and vice versa. For example, the interaction between voltage (V) and interelectrode gap (g) is not significant since the lines are parallel whereas that between interelectrode gap (g) and machining time (t) is significant as they intersect. Other results can be interpreted accordingly. The interaction plots are shown in Figure 43:

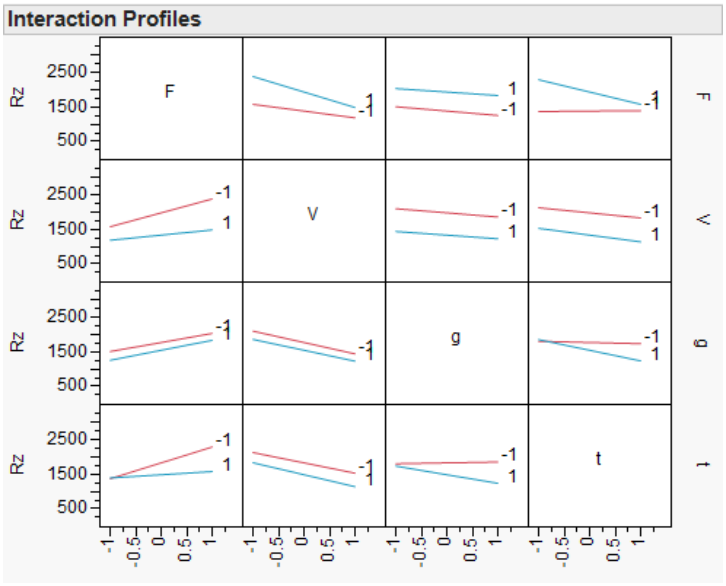

Fig. 43: Two factor interaction effect plots in complete model of DC experiments.

The direction of maximum descent to minimize the R_z value is found by using only the main effects i.e using the model:

$$y(R_z) = \beta_0 + \beta_1 F + \beta_2 V + \beta_3 g + \beta_4 t + \varepsilon \quad (17)$$

The estimates for the coefficients in the regression model and results of the least squares fit for the reduced model are shown in Figure 44:

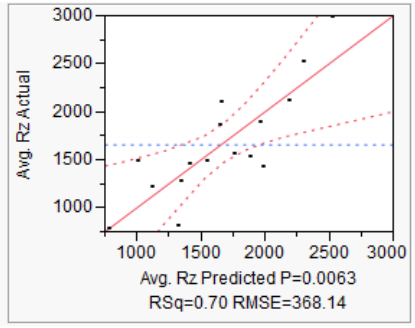

Fig. 44: Avg. R_z actual by Avg. R_z predicted plot for reduced model of DC experiments

ANOVA test was carried out for the reduced model and the goodness of fit was tested. The results are summarized in Table 11:

Table 11: Summary of fit and ANOVA for reduced model of DC experiments

Summary of Fit	
RSquare	0.70106
RSquare Adj	0.592355
Root Mean Square Error	368.1385
Mean of Response	1654.588
Observations (or Sum Wgts)	16

Analysis of Variance

Source	DF	Sum of Squares	Mean Square	F Ratio
Model	4	3496126.7	874032	6.4492
Error	11	1490785.3	135526	Prob > F
C. Total	15	4986912.0		0.0063*

Thus, we can see that this model is also significant in predicting the R_z values at $\alpha = 0.25$

Estimates of the coefficients of reduced model using the least squares fit and their significance levels are tabulated in Table 12:

Table 12: JMP results for estimates of reduced regression model for DC experiments and their significance levels.

Term	Estimate	Std Error	t Ratio	Prob>|t|
Intercept	1654.5882	92.03462	17.98	<.0001*
F	273.29359	92.03462	2.97	0.0128*
V	-319.6274	92.03462	-3.47	0.0052*
g	-113.5772	92.03462	-1.23	0.2429
t	-169.579	92.03462	-1.84	0.0925

Thus, we see that all the factors have a significant effect on the R_z value at specified α

From the above fit we get the prediction equation as follows:

$$y = 1654.59 + 273.294 * F - 319.63 * V - 113.58 * g - 169.58 * t \quad (18)$$

where F, V, g and t are in their coded form and lie between -1 to +1. -1 corresponds to low level of the factor while +1 corresponds to its high level.

The direction of steepest descent from the above location model is given by:

(ρ(-273.29359), ρ(319.6274), ρ(113.5772), ρ(169.579)), where ρ > 0.

A further analysis in the direction of steepest descent can be carried out by selecting a suitable step size for the most significant factor. The direction of steepest descent suggests that we have to reduce the flow rate while increasing the voltage, inter electrode gap and machining time proportionately but due to equipment limitations we were unable to increase the voltage across the electrodes. Thus, a further exploration to find the optimal parameters was not possible. From the available range of values, it was decided to set the parameters at low level for flow rate and high level for voltage, effective IEG and machining time to obtain the minimum surface roughness. A surface roughness R_a = 170 nm and R_z = 786 nm was obtained at these parameters.

Interferometry, although accurate, covers a large area of millimeter range of polished workpiece while AFM covers much smaller scale, in micro or nanometer ranges. AFM was used to measure the surface roughness of a local area and to estimate the capability of the process. The spot polished at the best parameters was analyzed using the AFM. The surface roughness was measured for the entire scanned surface, area within a grain and some area across the grains of the workpiece as shown in Figure 45:

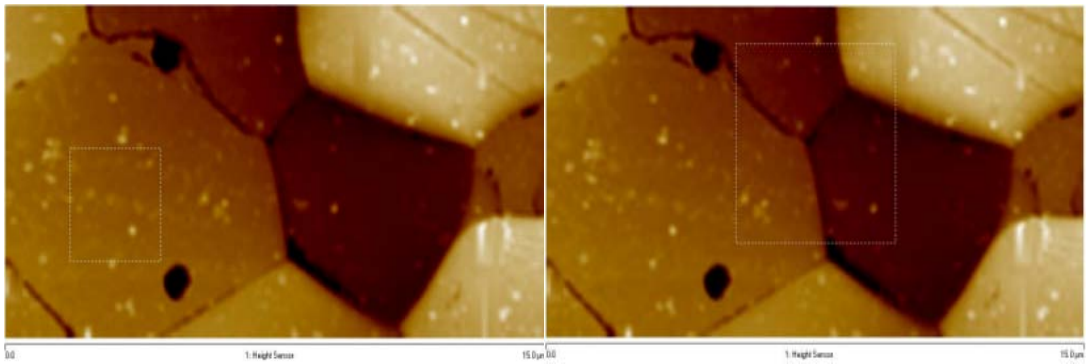

(a) (b)

Fig. 45: Surface finish (a) within a grain (R_a = 1.11 nm) (b) across grains (R_a = 9.86 nm) (Electrolyte flow rate (F) = 190 ml/min, Voltage across terminals (V) = 55 V, effective IEG (g) = 2370 µm and machining time (t) = 45 sec was measured (a) within a grain (b) across grains.)

Within a grain, the roughness was measured inside a box of size 2.5 µm X 2.5 µm and it was found to be R_a = 1.11 nm, R_{max} = 23.6 nm. Across grains, a box of size 5 µm X 5 µm was used and a roughness value of R_a = 9.86 nm, R_{max} = 82.8 nm was obtained. The roughness of the entire surface of the scanned image was R_a = 15.3 nm, R_{max} = 226 nm.

4.4 Analysis of spots polished using alternating current

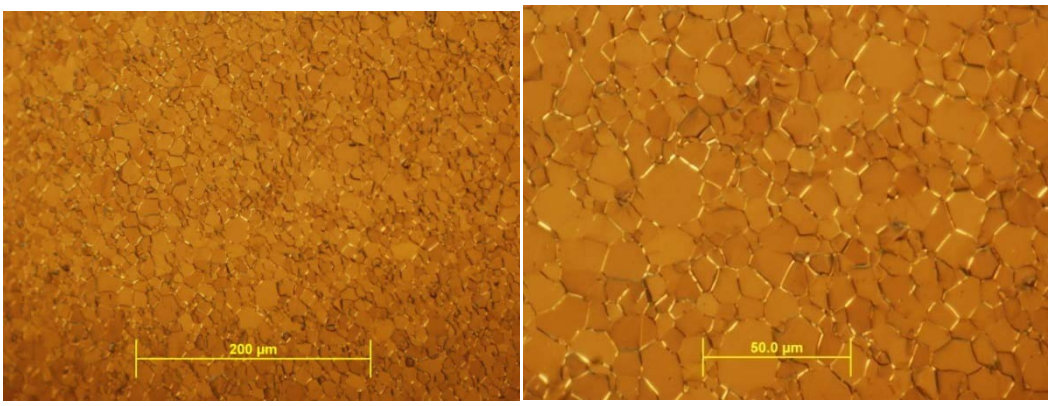

(a) (b)

Fig. 46: (a) Optical image (b) Magnified optical image of polished surface.
(Electrolyte flow rate (F) = 135 ml/min, peak to peak voltage (Vp-p) = 28 V, alternating current waveform frequency (N) = 50 Hz, duty cycle (D) of AC waveform = 80 %, effective IEG (g) = 1180 µm, polishing time (t) = 150 sec.)

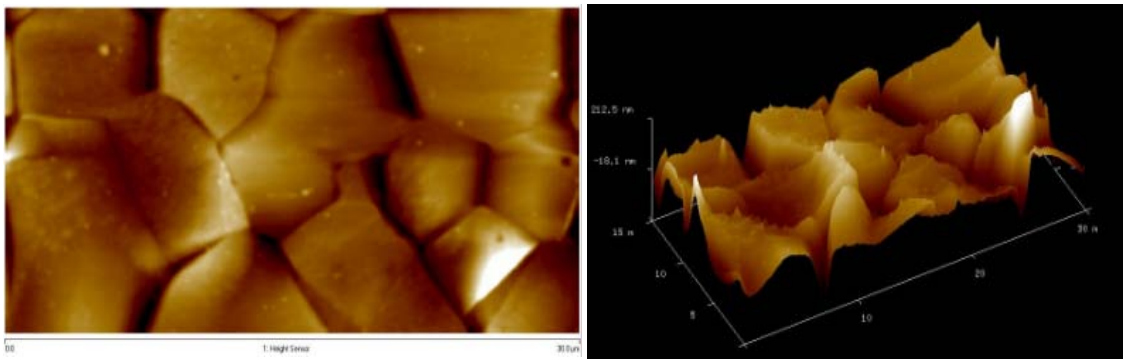

(a) (b)

Fig. 47: (a) 2D AFM image and (b) 3D view of polished surface using AC current.
(Electrolyte flow rate (F) = 135 ml/min, AC peak to peak voltage (Vp-p) = 28 V, alternating current waveform frequency (N) = 1000 Hz, duty cycle (D) of AC waveform = 80 %, effective IEG (g) = 1180 µm and polishing time (t) = 150 sec.)

Figure 46 and Figure 47 show the polishing effect on Ti when an AC current is used. A similar procedure as that followed for experiments with direct current was used with alternating current. The current flowing through the circuit and the surface roughness as measured using interferometry are tabulated below in Table 13. The sequence is the same as that in the design matrix for this experiment.

The current in the circuit was varying during the machining period and hence the minimum and maximum values of the current were recorded. The reported current density is calculated from the maximum current observed in the circuit. Surface roughness values were measured at two different circular sections of radius 130 μm and 380 μm. The values shown in the following table is the average of these two values. R1 is the average surface roughness for the respective run while R2 is the average surface roughness of its replication run. A table containing all the individual values of the data collected at each cross section is provided in Appendix E.

The recorded data is enlisted in the following table:

Table 13: Summary of data collected from AC experiments.

Run No.	Current (mA - AC)		Current density (mA/mm^2)		R_a (nm)		R_z (nm)	
	R1	R2	R1	R2	R1	R2	R1	R2
1	2.4 - 5.5	2.5 - 6.1	2 - 6	3 - 6	310	286	1491	1163
2	2.5 - 2.7	2.5 - 2.7	3 - 3	3 - 3	477	457	4232	2548
3	7.2 - 16.2	7.3 - 16.2	17	17	293	198	736	681
4	7.2 - 12.3	7.3 - 12.1	7 - 13	7 - 12	314	457	1472	1066
5	2.9 - 4.4	3.1 - 4.4	3 - 4	3 - 4	437	763	1732	2703
6	2.9 - 3.2	2.9 - 3.2	3 - 3	3 - 3	586	895	2894	3836
7	12.2 - 20.2	13.2 - 20.3	12 - 21	13 - 21	707	496	1858	1443
8	12.2 - 16.2	12.8 - 16.1	12 - 17	13 - 16	420	480	2014	1852
9	2.4 - 4.9	2.5 - 5.2	2 - 5	3 - 5	377	288	1453	1237
10	2.6 - 2.9	2.6 - 2.9	3 - 3	3 - 3	322	322	1660	1876
11	6.5 - 11.2	7.2 - 12.8	7 - 11	7 - 13	330	298	808	676
12	8 - 10.6	7.2 - 9.4	8 - 11	7 - 10	391	338	1313	1253
13	3.1 - 4.7	3.1 - 4.5	3 - 5	3 - 5	383	402	1866	1637
14	3 - 3.2	2.95 - 3.2	3 - 3	3 - 3	573	541	2812	2486
15	9.6 - 12.2	10.2 - 12.8	10 - 12	10 -13	371	445	1172	1419
16	9.8 - 11.1	9 - 9.8	10 -11	9 - 10	328	346	1370	1922
17	1.8 - 3.5	1.7 - 3.5	2 - 4	2 - 4	372	402	1835	2093
18	1.4 - 1.55	1.5 - 2.1	1 - 2	2 - 2	650	522	4481	2846
19	7.9 - 18	9 - 23	8 - 18	9 - 23	1495	382	1883	936
20	9.9 - 18.2	7.9 - 15.9	10 - 19	8 - 16	387	347	1723	1344
21	1.81 - 1.91	1.8 - 3	2 - 2	2 - 3	729	755	2956	2763
22	1.8 - 1.85	1.85 - 1.95	2 - 2	2 - 2	508	544	2797	3864
23	7.9 - 22	9.5 - 25.2	8 - 22	10 - 26	436	404	1995	1589
24	9.5 - 15.5	10 - 16.5	10 - 16	10 - 17	430	703	2684	2876
25	1.6 - 5	1.65 - 2.65	2 - 5	2 - 3	279	363	1346	1424
26	1.79 - 1.92	1.67 - 1.85	2 - 2	2 - 2	503	475	2516	1939
27	7.2 - 14.7	7.5 - 17.1	7 - 15	8 - 17	523	503	2458	2278
28	7.5 - 13.1	6.3 - 11.7	8 - 13	6 - 12	570	405	1496	1340
29	1.61 - 1.72	1.8 - 2.9	2 - 2	2 - 3	839	444	3164	1868
30	1.8 - 1.9	2 - 2.1	2 - 2	2 - 2	457	359	2385	1819
31	8.1 - 19.3	8.5 - 20.1	8 - 20	9 - 20	910	478	1452	1402
32	8.5 - 14.5	8.5 - 16.5	9 - 15	9 - 17	385	431	2147	2276

The above data was used to fit a regression line through it incorporating all the main effects and interaction effects of the factors. JMP Pro 10 statistical software was used to carry out this analysis. The model for a full factorial design can be stated as follows:

$$y = \beta_0 + \beta_1 V + \beta_2 N + \beta_3 D + \beta_4 g + \beta_5 t + \beta_{12} V*N + \beta_{13} V*D + \beta_{14} V*g + \beta_{15} V*t + \beta_{23} N*D + \beta_{24} N*g + \beta_{25} N*t + \beta_{34} D*g + \beta_{35} D*t + \beta_{45} g*t + \beta_{123} V*N*D + \beta_{124} V*N*g + \beta_{134} V*D*g + \beta_{234} N*D*g + \beta_{125} V*N*t + \beta_{135} V*D*t + \beta_{235} N*D*t + \beta_{145} V*g*t + \beta_{245} N*g*t + \beta_{345} D*g*t + \beta_{1234} V*N*D*g + \beta_{1235} V*N*D*t + \beta_{1245} V*N*g*t + \beta_{1345} V*D*g*t + \beta_{2345} N*D*g*t + \beta_{12345} V*N*D*g*t + \varepsilon \quad (19)$$

The estimates for the coefficients in the regression model are obtained by fitting a straight line through the data using the least squares method. The results are shown in Figure 48:

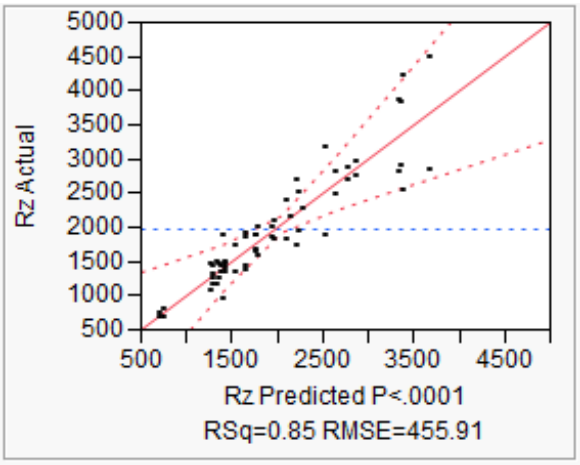

Fig. 48: R_z actual by R_z predicted plot for complete regression model of AC experiments

The solid line in the above figure is the straight line generated by the software using the least squares method for the above model.

R^2 and adjusted R^2 are measures which determine how well the model helps in predicting the response. They represent the amount of variability in the data that is incorporated by the model. Analysis of variance (ANOVA) is used to test the hypothesis for significance of the regression model. For ANOVA,

The null hypothesis is: $H_0: \beta_0 = \beta_1 = \beta_2 = \beta_3 = \ldots\ldots = \beta_{12345} = 0$ (20)

The alternate hypothesis is that atleast one of the factors is useful in predicting the response values; H_a: Atleast one of $\beta_0, \beta_1, \beta_2, \ldots\ldots, \beta_{12345} \neq 0$ (21)

We shall use alpha (α) = 0.25 to test significance of our model and its estimates. The ANOVA results are summarized in Table 14:

Table 14: Summary of fit for complete regression model of AC experiments

Summary of Fit

RSquare	0.845898
RSquare Adj	0.696612
Root Mean Square Error	455.9085
Mean of Response	1974.163
Observations (or Sum Wgts)	64

Analysis of Variance

Source	DF	Sum of Squares	Mean Square	F Ratio
Model	31	36510300	1177752	5.6663
Error	32	6651281	207853	Prob > F
C. Total	63	43161582		<.0001*

Thus, we can see from the ANOVA table for the model that the regression model predicted from above is significant at $\alpha = 0.25$ level and is useful in predicting the response values.

Different coefficients have different significance levels towards predicting the response value. The significance level for the main effect or interaction effect is found by carrying out a t-test. Here,

The null hypothesis is: $H_0: \beta_i = 0; \quad \beta_i \epsilon$ each coefficient in regression model (22)

The alternate hypothesis is: $H_a: \beta_i \neq 0$ (23)

The results are summarized in Table 15:

Table 15: JMP results for estimates of complete regression model of AC experiments and their significance levels.

Term	Estimate	Std Error	t Ratio	Prob>|t|
g	392.15813	56.98856	6.88	<.0001*
t	-307.3691	56.98856	-5.39	<.0001*
D	-242.1444	56.98856	-4.25	0.0002*
N	225.4575	56.98856	3.96	0.0004*
V	-202.8853	56.98856	-3.56	0.0012*
N*g	172.89734	56.98856	3.03	0.0048*
V*D*g*t	154.86016	56.98856	2.72	0.0105*
D*g*t	-153.2391	56.98856	-2.69	0.0113*
N*t	-151.1108	56.98856	-2.65	0.0124*
g*t	-138.2242	56.98856	-2.43	0.0211*
N*D*g	103.31313	56.98856	1.81	0.0792
V*t	-84.20734	56.98856	-1.48	0.1493
N*g*t	-75.88031	56.98856	-1.33	0.1924
N*D*t	-67.63344	56.98856	-1.19	0.2440
V*N*D*g*t	-63.87313	56.98856	-1.12	0.2707
V*g	63.230156	56.98856	1.11	0.2755
V*D	-50.03234	56.98856	-0.88	0.3865
N*D	-49.18953	56.98856	-0.86	0.3945
V*N*g*t	-45.25766	56.98856	-0.79	0.4330
V*g*t	-36.59375	56.98856	-0.64	0.5254
V*N*t	36.043125	56.98856	0.63	0.5316
V*N*g	-35.96531	56.98856	-0.63	0.5325
V*N*D*g	-33.86828	56.98856	-0.59	0.5565
V*N*D	32.507188	56.98856	0.57	0.5724
D*t	-29.72172	56.98856	-0.52	0.6056
V*D*t	-27.09813	56.98856	-0.48	0.6377
V*N*D*t	-24.66953	56.98856	-0.43	0.6680
N*D*g*t	-17.44141	56.98856	-0.31	0.7615
V*N	-14.06641	56.98856	-0.25	0.8066
V*D*g	13.474063	56.98856	0.24	0.8146
D*g	9.6751562	56.98856	0.17	0.8663

The main effect due to a factor can be shown graphically by a line connecting the average of the R_z values at the high and low levels of that factor as shown in Figure 49:

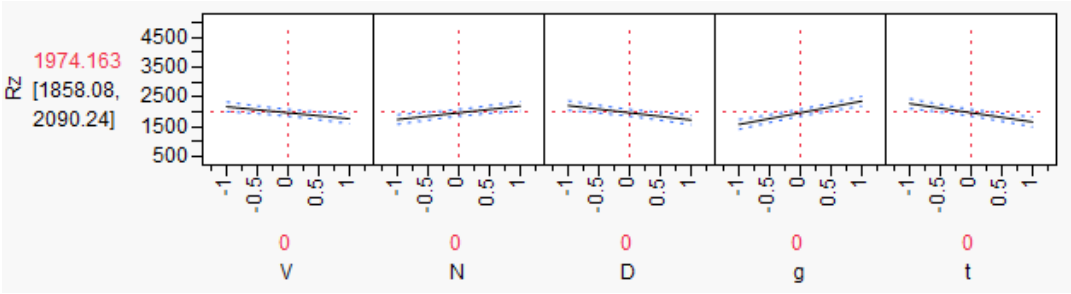

Fig. 49: Plots showing the main effects in complete regression model of AC experiments

The individual factors in the ECM process can interact synergistically or antagonistically and likewise affect the outcome. The interpretation of these plots was explained earlier and the plots are shown in Figure 50:

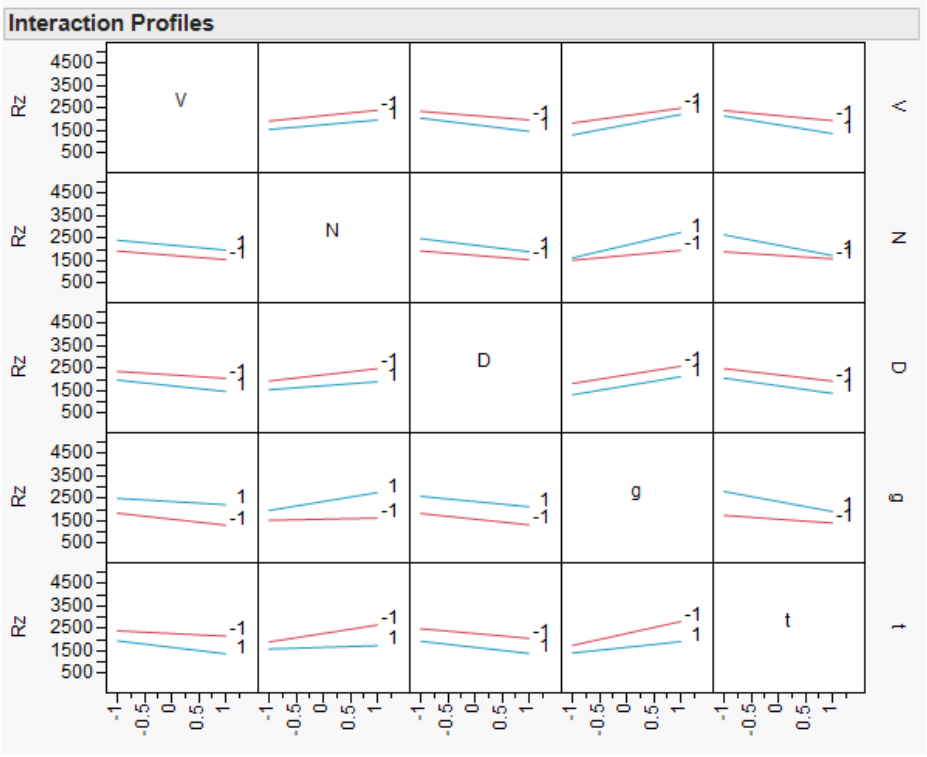

Fig. 50: Two factor interaction effect plots in complete regression model of AC experiments

The direction of maximum descent in order to minimize the R_z value is found from a simplified model incorporating only the main effects of the parameters i.e the model:

$$y(R_z) = \beta_0 + \beta_1 V + \beta_2 N + \beta_3 D + \beta_4 g + \beta_5 t + \varepsilon \quad (24)$$

The estimates for the coefficients in the regression model and results of the least squares fit for the reduced model are shown in Figure 51:

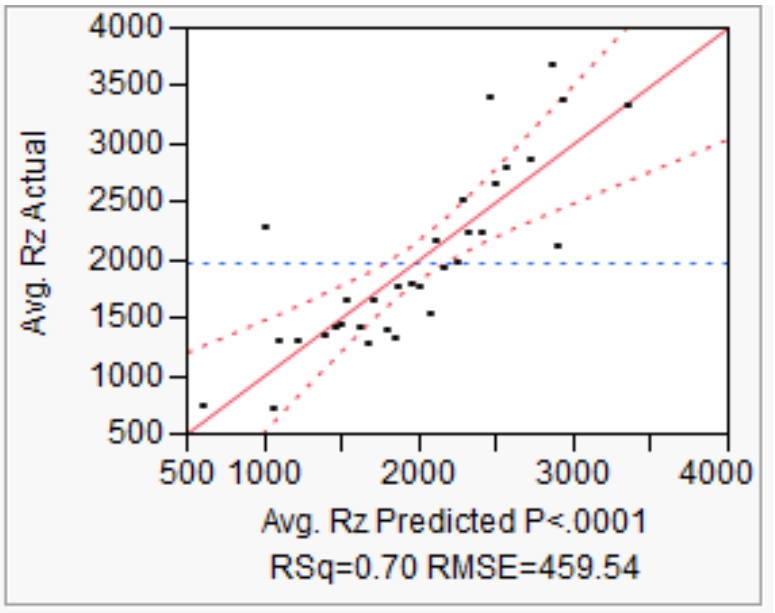

Fig. 51: Avg. R_z actual by Avg. R_z predicted plot for reduced regression model of AC experiments

ANOVA test was carried out for reduced model and the goodness of the fit was tested. The results are summarized in Table 16:

Table 16: Summary of fit and ANOVA of reduced regression model for AC experiments

Summary of Fit

RSquare	0.699228
RSquare Adj	0.641388
Root Mean Square Error	459.5413
Mean of Response	1974.163
Observations (or Sum Wgts)	32

Analysis of Variance

Source	DF	Sum of Squares	Mean Square	F Ratio
Model	5	12764517	2552903	12.0889
Error	26	5490633	211178	Prob > F
C. Total	31	18255150		<.0001*

Thus, we can see that this model is also significant in predicting the R_z values at $\alpha = 0.25$

Estimates of the coefficients of the reduced model using the least squares fit and their significance levels are summarized in Table 17:

Table 17: JMP results for estimates of reduced regression model for AC experiments and their significance levels.

Term	Estimate	Std Error	t Ratio	Prob>|t|
Intercept	1974.1627	81.23619	24.30	<.0001*
V	-202.8853	81.23619	-2.50	0.0192*
N	225.4575	81.23619	2.78	0.0101*
D	-242.1444	81.23619	-2.98	0.0062*
g	392.15813	81.23619	4.83	<.0001*
t	-307.3691	81.23619	-3.78	0.0008*

Thus, we see that all the factors have a significant effect on the R_z value at given α level.

From the above fit we get the prediction equation as follows:

$$y = 1974.16 - 202.88 * V + 225.46 * N - 242.14 * D + 392.16 * g - 307.37 * t \qquad (25)$$

where V, N, D, g and t are in their coded form and lie between -1 to 1. -1 corresponds to the low level of the respective factor while 1 corresponds to their high level.

The direction of steepest descent from the above location model is as follows:

(ρ(202.8853), ρ(-225.4575), ρ(242.1444), ρ(-392.15813), ρ(307.3691)), where $\rho > 0$.

A further analysis in the direction of steepest ascent can be carried out to obtain lower R_z values by initially selecting a suitable step size for the most significant factor. In our case, the direction of steepest descent suggests that in order to get lower R_z values, we have to increase the peak to peak voltage, duty cycle and machining time while decreasing the frequency of alternating current and inter electrode gap proportionately. Due to equipment limitations we are unable to increase the voltage across the electrodes. Also, the high level of the duty factor was set at its maximum level and hence could not be increased further. The low level of the effective IEG is at 970 µm and reducing the gap further was causing instability due to sparking caused by ineffective ion flushing. Increasing the machining time led to machining on the workpiece surface instead of polishing which only caused additional material removal while giving a similar surface finish. Thus, a further exploration to find the optimal parameters was not possible and from the available range of values, it was decided that to obtain the minimum surface roughness value we should set the parameters at the low level for effective IEG and frequency while the peak to peak voltage, duty factor and machining time should be kept at their high level. A surface roughness R_a = 314 nm and R_z = 742 nm was obtained at these parameters.

AFM was used to measure the surface roughness of a local area and to estimate the capability of the process. The surface roughness was measured for the entire scanned surface, area within a portion of a grain and some area across the grains of the workpiece. The locations where these measurements were taken are highlighted by the box shown as in Figure 52:

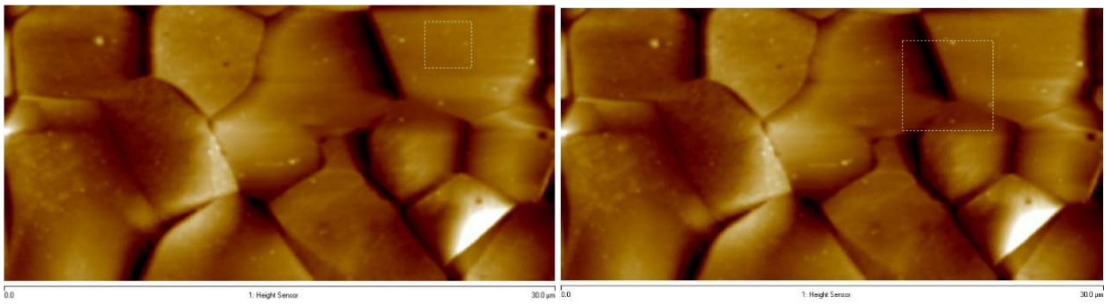

(a) (b)

Fig. 52: (a) Surface finish within a grain (R_a = 2.19 nm) (b) across grains (R_a = 38.7 nm) (Electrolyte flow rate (F) = 135 ml/min, AC peak to peak voltage (V_{p-p}) = 28 V, alternating current waveform frequency (N) = 1000 Hz, duty cycle (D) of AC waveform = 80 %, effective IEG (g) = 1180 µm and polishing time (t) = 150 sec.)

Within a grain, the roughness was measured inside a box of size 2.5 µm X 2.5 µm and it was found to be R_a = 2.19 nm, R_{max} = 27.9 nm. Across grains, a box of size 5 µm X 5 µm was used and a roughness value of R_a = 38.7 nm, R_{max} = 301 nm was obtained. The roughness value of the entire surface of the scanned image was, R_a = 42.8 nm and R_{max} = 621 nm.

4.5 Analysis of comparison experiments

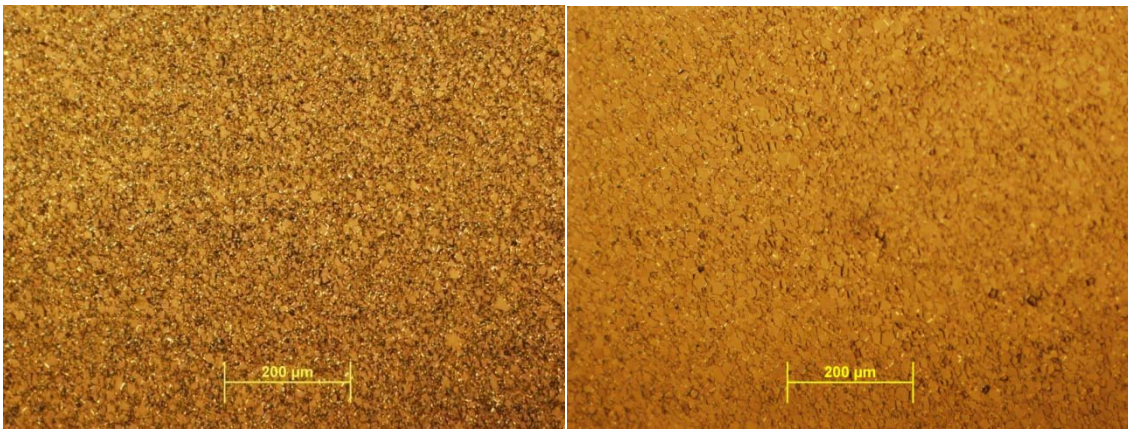

(a) (b)

Fig. 53: Polished spot using comparable (a) DC current and (b) AC current.
((a) Electrolyte flow rate = 135 ml/min, effective IEG = 1235 µm, polishing time = 120 sec and current between 8.3 to 38.1 mA (b) Spot polished with AC current at electrolyte flow rate = 135 ml/min, frequency of square waveform = 50 Hz, duty cycle = 80%, effective IEG = 1235 µm, polishing time = 150 sec and current between 8.3 to 38.1 mA)

Spots polished using DC and AC current are shown in Figure 53. Surface roughness measurements from interferometry were analyzed. As before, the surface finish measurements were taken along circular sections of radius 130 µm and 380 µm and the average of these values was taken as the surface roughness. The data is summarized in Table 18:

Table 18: Summary of data from comparison experiments.

Run no.	AC				DC			
	Current (mA-AC)	R_z (nm)	R_a (nm)	Current density (mA/mm^2)	Current (mA)	R_z (nm)	R_a (nm)	Maximum current density (mA/mm^2)
1	6-39.2	1651	527	6 - 40	8.2-33.4	1750	420	8 - 34
2	6.5-31.1	2360	787	7 - 32	5.3-38.1	2669	624	5 - 39
3	6.3-27.8	1450	434	6 - 28	8.1-34.3	1434	306	8 - 35
4	5.9-23.3	1456	444	6 - 24	6.4-24.3	2160	392	7 - 25
5	6.2-23.9	1318	492	6 - 24	8.2-28.1	2975	729	8 - 29

The results (R_z values) were compared using a paired t-test to check if mean of the surface finish obtained with AC (μ_1) current is less than mean of the surface finish with DC current (μ_2).

Here, the null hypothesis is: $H_0: \mu_1 = \mu_2$ (26)

The alternate hypothesis is: $H_a: \mu_1 < \mu_2$ (27)

The results of the t-test are shown in Table 19:

Table 19: Results of paired t-test

	AC	*DC*
Mean	1646.96	2197.67
Variance	173066.98	402520.99
Observations	5	5
Hypothesized Mean Difference	0	
df	4	
t Stat	-1.82	
P(T<=t) one-tail	0.0714	
t Critical one-tail	2.132	

Since the p-value is less than $\alpha = 0.1$, the level of significance for this experiment, we reject the null hypothesis. Therefore, the mean of the surface roughness obtained using AC current is less than that obtained using DC current under comparable conditions.

4.6 Analysis of verification experiments

4.6.1 Analysis of verification experiments using DC current

The response data and current recorded in the circuit are tabulated in Table 20:

Table 20: Data from verification experiments using DC current

Run no.	R_a (nm)	R_z (nm)	Current (mA - DC)	Current density (mA/mm^2)
1	292	1339	80 - 140	66 - 115
2	255	1205	80 - 165	66 - 135
3	292	1252	150 - 185	123 - 152
4	287	1311	75 - 145	61 - 119
5	288	1203	85 - 150	70 - 123
6	255	1494	80 - 145	66 - 119
7	238	1241	79 - 145	65 - 119
8	376	1498	75 - 145	61 - 119
9	235	1160	80 - 170	66 - 139
10	196	993	75 - 145	61 - 119
Average	271.39	1269.58		
Std. dev.	48.01	151.9		

Substituting 0 for all the parameter setting levels since they are at the midpoint levels, we get the predicted R_z value from regression equation (18) as 1654.59 nm.

The average of the surface roughness obtained from the verification experiments is 1269.58 nm with standard deviation of 151.9 nm. The (%) difference is:

$$\frac{1654.59-1269.58}{1269.58} \text{ X } 100 = 23.27\ \% \qquad (28)$$

4.6.2 Verification experiments for AC current

The response data and current recorded in the circuit are tabulated in Table 21:

Table 21: Data from verification experiments using AC current

Run no.	R_a (nm)	R_z (nm)	Current (mA - AC)	Current density (mA/mm^2)
1	466	1625	7.5 - 37.5	8 - 38
2	256	1398	6.5 - 35.5	7 - 36
3	316	1427	6.5 - 31.5	7 - 32
4	275	1415	5.5 - 34.5	6 - 35
5	559	2646	5.9 - 31.1	6 - 32
6	244	1120	6.5 - 27.5	7 - 28
7	286	1139	5.9 - 28.1	6 - 29
8	266	1314	5.1 - 30.5	5 - 31
9	244	1226	5.4 - 28.1	6 - 29
10	238	1354	5.1 - 34.5	5 - 35
Average	315.21	1466.26		
Std. dev.	108.93	440.5		

Substituting 0 for all the parameter setting levels since they are at the midpoint levels, we get the predicted R_z value from regression equation (25) as 1974.16 nm.

The average of the surface roughness obtained from the verification experiments is 1466.26 nm with a standard deviation of 440.5 nm. The (%) difference from predicted value is:

$$\frac{1974.16-1466.26}{1974.16} \text{ X } 100 = 25.73\ \% \qquad (29)$$

Surface finish of our samples is comparable with those from published literature. A comparison of results obtained in this study with published literature is shown in the following Table 22:

Table 22: Comparison between this study and published literature

Source	Measurement technique	Result
Tajima (7)	Not mentioned	R_a = 30 - 120 nm
Chen (64)	AFM in a scan area of 2 X 2 μm^2	R_z = 1.966 nm
This study	Interferometry along two circular sections of radius 130 µm and 380 µm	With DC current: R_a = 170 nm, R_z = 786 nm; With AC current: R_a = 314 nm and R_z = 742 nm
This study	AFM in a scan area of 2.5 X 2.5 μm^2 within a single grain	With DC current: R_a = 1.11 nm, R_{max} = 23.6 nm; With AC current: R_a = 2.19 nm and R_{max} = 27.9 nm
This study	AFM in a scan area of 5 X 5 μm^2 across grains	With DC current: R_a = 9.86 nm, R_{max} = 82.8 nm; With AC current: R_a = 38.7 nm and R_{max} = 301 nm

A direct comparison between the published literature and this study cannot be made as different methods have been followed and different roughness measures have been reported.

With AC current, high frequency is believed to improve the surface finish and low duty cycle is also expected to give better results due to better flushing during off-times (29), but with CP Ti it was found that the oxide layer does not break easily and low frequency and high duty cycle needs to be used while polishing.

It is also important to note the following observations that have been made during our work:

1. The electrolyte plays a vital role in giving a uniform, polished surface. It was important to keep the electrolyte under controlled atmospheric conditions. If the composition of the electrolyte was altered, it would no longer be effective and did not give consistent results.
2. The machined debris if not filtered from the electrolyte lead to sparking and surface damage.
3. A large area, almost double the area of the electrode, was polished when experimenting with DC current. Thus, good control over the area of polishing cannot be maintained with DC current.
4. Polishing can be carried out at lower interelectrode gap when using pulsed current than with using direct current.
5. With AC current, the polished area was more concentrated due to the relatively smaller area of activation, giving good control over the polished area. More material was removed close to the electrode surface and this decreased as we moved away from the electrode surface. Thus, the surface finish was better in the vicinity of the electrode.

6. Polishing with DC as well as AC current was more aggressive at the grain boundaries of the workpiece material than away from it. By exploring parameters that would give consistent polishing results (i.e. similar machining at the grain and the surrounding surface) over the entire surface, a much consistent surface polishing can be obtained.
7. Although from the comparative experiments it is seen that surface finish with AC current is better than that obtained with DC current under the same conditions, it is seen from the verification experiments that repeatability of results depends upon the parameter levels and under the studied conditions, results with DC current are more consistent with a standard deviation of 48.01 nm for R_a measurements and 151.9 nm for R_z than results with AC current which gave a standard deviation of 108.93 nm for R_a values and 440.5 nm for R_z values.

5. CONCLUSIONS

Electrochemical polishing of titanium using DC and AC current was studied. It was found that:

1. Current density is crucial for obtaining desirable results.
2. AC current produces better surface finish than DC current. Under similar conditions, the surface roughness for AC is R_z = 1647 nm, and that for DC is R_z = 2198 nm when the current density was ~ 31 mA/mm^2
3. The developed process is repeatable. Verification from ten consecutive experiments show the average surface finish for AC current at current density of 33 mA/mm^2 is R_a = 315 nm with a standard deviation of 109 nm, and those for DC current at current density of 126 mA/mm^2 is R_a = 271 nm with a standard deviation of 48 nm.
4. The developed ECP process polished grains at different rate due to different grain orientations. For AC current, surface finish within a grain was R_a = 1.11 nm while across grains it was = 38.7 nm. Also, with DC current, surface finish within a grain was R_a = 1.11 nm while across grains it was R_a = 9.86 nm.

6. RECOMMENDATIONS

1. The technique could be extended to polishing an entire slot by moving the electrode.
2. The current in the circuit varied while the polishing took place. Power sources that are capable of maintaining a constant current through the circuit must be used in order to get a better understanding of the current density required to polish Ti.
3. The electrolyte used for these experiments becomes ineffective after a few days. Other electrolytes that would be more consistent over an extended length of time should be tried. Acid based electrolytes may give better results, though should be used with extreme care.
4. Cleaning the workpiece surface with H_3PO_4 or HCl or H_2SO_4 acid may give a better surface by removing the pitting marks. Extreme care must be taken while handling acids.

REFERENCES

1. W. Eberhardt, T. Gerhäußer, M. Giousouf, H.Kück, R. Mohr, D. Warkentin, "*Innovative concept for the fabrication of micromechanical sensor and actuator devices using selectively metallized polymers"*, Sensors and actuators A (v97-98), pp. 473-477, 2002.

2. P. Choudhury, "*Handbook of microlithography, micromachining, and microfabrication" Vol. 1 and 2*, Bellingham, WA, SPIE optical engineering press, 1997.

3. B. H. Weigl, P. Yager, "*Microfluidics - Microfluidic diffusion-based separation and detection"*, Science (v283, n5400), pp. 346-347, 1999.

4. D. D. Cunningham, "*Fluidics and sample handling in clinical chemical analysis"*, Analytica chimica acta (v429), pp. 1-18, 2001.

5. T. Hwang, J. Kim, D. Yang, Y. Park, W. Ryu, "*Targeted electrohydrodynamic printing for micro-reservoir drug delivery systems"*, Journal of micromechanics and microengineering (v23, n3), pp. 9, 2012.

6. C.N. Elias, J.H.C. Lima, R. Valiev, M.A. Meyers, "*Biomedical applications of titanium and its alloys"*, JOM (v60, n3), pp. 46-49, 2008.

7. K. Tajima, M. Hironaka, K. Chen, Y. Nagamatsu, H. Kakigawa, Y. Kozono, "*Electropolishing of CP titanium and its alloys in an alcoholic solution based electrolyte"*, Dental materials journal (v27, n2), pp. 258-265, 2008.

8. L. K. Gillespie, "*Deburring and edge finishing handbook"*, Dearborn, Michigan, Society of manufacturing engineers, 1999.

9. Y.H. Jeong, B.H. Yoo, H.U. Lee, B. Min, D. Cho, S. J. Lee, "*Deburring microfeatures using micro-EDM"*, Journal of materials processing technology (v209), pp. 5399-5406, 2009

10. F. Benedict, "*Nontraditional manufacturing processes"*, New York, CRC Press, 1987.

11. J. McGeough, *"Electrochemical machining (ECM)"*, [Online] [Accessed: Feb 24, 2013.] URL: http://electrochem.cwru.edu/encycl/art-m03-machining.htm.

12. J. McGeough, "*Principles of electrochemical machining"*, London, Chapman and Hall, 1974.

13. J. A. Kenney, G.S. Hwang, "*Electrochemical machining with ultrashort voltage pulses: Dynamics and feature profile evolution"*, Institute of physics publishing nanotechnology, Nanotechnology (v16, n7), pp. 309-313, 2005.

14. J. A. McGeough, "*Advanced methods of machining"*, London, Chapman & Hall, 1988.

15. M. P. Groover, "*Fundamentals of modern manufacturing"*, New York, John Wiley & Sons, 2000.

16. D. M. Drazic, J. P. Popic, "*Anomalous dissolution of metals and chemical corrosion"*, J. Serb. chem. soc.(v70, n3), pp. 489-511, 2005.

17. M. G. Fontana, R. W. Staehle, "*Advances in corrosion science and technology"*, New York, Plenum Press, 1974.

18. J. A. McGeough, "*Micromachining of engineering materials"*, New York, Marcel Dekker, 2002.

19. G. E. Benedict, "*Nontraditional manufacturing processes"*, New York, Marcel Dekker, 1987.

20. J. Kozak, D. W. Siems, N.A. Chandrana, S. Malicki, P. Salgaocar, *"Electrochemical machining"*, [Online] [Accessed: Feb 20, 2013.] URL - http://www.scribd.com/doc/49986579/Electrochemical-Machining.

21. B. Wei, "*Modeling and analysis of pulse electrochemical machining"*, PhD dissertation, The University of Nebraska, Lincoln, 1994.

22. Y. Zhang, "*Investigation into current efficiency for pulse electrochemical machining of nickel alloy"*, Master of science thesis, The University of Nebraska, Lincoln, 2010.

23. L. Yong, Z. Yunfei and Y. Guang, P. Liangqiang, *"Localized electrochemical micromachining with gap control"*, Sensors and actuators A (v108, n1-3), pp. 144-148, 2003.

24. B. Wei, J. Kozak, K.P. Rajurkar, *"Pulse electrochemical machining of Ti-6Al-4V Alloy"*, Transaction of NAMRI/SME (v22), pp. 141-147, 1994.

25. B. Karasev, *"Pulse influence on electrochemical technological performance"*, Proceedings of ISEM-9, pp. 159-162, 1989.

26. C. Y. Yu, *"Pulse ECM",*Proceedings of symposium of electromachining, Poland, pp. 74-99, 1988.

27. C. Regt, *"ECM for the production of high precision components"*, Proceedings of ISEM-8, pp. 120-128, 1986.

28. G. Gevorkian, *"Trends in the development of electrochemical machining"*, Proceedings of ISEM-9, pp. 170-174, 1988.

29. K. P. Rajurkar, D. Zhu, J. A. McGeough, J. Kozak, A. DeSilva, *"New developments in electrochemical machining"*, Annals of the CIRP - Manufacturing technology (v48, n2), pp. 567-579, 1999.

30. A. Bhuyan, B. Gregory, H. Lei, S. Yee, Y. Gianchandani, *"Pulse and DC electropolishing of stainless steel for stents and other devices"*, Sensors, 2005 IEEE, pp.314-317, Irvine, CA, 2005.

31. G. A. Alekseev, *"Improvements of electrochemical copy-piercing machines"*, Proceedings of ISEM-7, pp. 383-392, 1983.

32. M. Datta, L. T. Romankiw, *"Application of chemical and electrochemical micromachining in the electronics industry"*, Journal of the electrochemical society (v136, n6), pp. 285-292, 1989.

33. B. Bhattacharyya, M. Malapati, J. Munda, *"Experimental study on electrochemical micromachining"*, Journal of materials processing technology (v169, n3), pp. 485-492,2005.

34. S. S. Sundarram, *"Development of electrochemical micro machining"*, Master of science thesis, Texas A&M University, College Station, 2008.

35. F. M. Ozkeskin, *"Feedback controlled high frequency electrochemical micromachining"*, Master of sciencethesis, Texas A&M University, College Station, 2008.

36. L. Cagnon, V. Kirchner, M. Kock, R. Schuster, G. Ertl, W.T. Gmelin, H. Kück, *"Electrochemical micromachining of stainless steel by ultrashort voltage pulses"*, Zeitschrift für physikalische chemie (v217), pp. 299-313, 2003.

37. M.A. El-Dardiry, M.A. Asfoor, H.M. Osman, *"Experimental investigation into the performance of electrochemical machining processes - Part-II: Parameters affecting the surface quality"*, Proceedings of the fifth international conference on production engineering, pp. 382–388, Tokyo, 1984.

38. M. Sen, H.S. Shan, *"A review of electrochemical macro- to micro-hole drilling processes"*, International journal of machine tools & manufacture (v45, n2), pp. 137–152, 2005.

39. M. Sen, H.S. Shan, *"Comparative study of small hole drilling in nimonic C-263"*, Proceedings of the 13th ISME conference, Roorkee, 2003.

40. F. Krieth and D. Y. Goswami, *"CRC Handbook of mechanical engineering"*, CRC Press, Boca Raton, 1998.

41. C. H. Jo, B. H. Kim, C. N. Chu, *"Micro electrochemical machining for complex internal micro features"*, CIRP annals - Manufacturing technology (v58, n1), pp. 181-184, 2009.

42. B. H. Kim, S. H. Ryu, D. K. Choi, C. N. Chu, *"Micro electrochemical milling"*, Journal of micromechanics and microengineering (v15), pp. 124-129, 2005.

43. D. B. Stofesky, *"Manufacturing with microECM"*, Proceedings of ASME, Intl.Conf. on manufacturing science and engineering, pp. 1025-1031, 2006.

44. H. El-Hofy, *"Fundamentals of machining processes: Conventional and nonconventional processes"*, CRC Press, Boca Raton, 2007.

45. M. J. Donachie, Jr., *"Titanium: A technical guide"*, ASM international, The materials information society, Ohio,2000.

46. E. Lee, T. Shin, B. Kim, S. Baek, *"Investigation of short pulse electrochemical machining for groove process on Ni-Ti shape memory alloy"*, International journal of precision engineering and manufacturing (v11, n1), pp. 113-118, 2010.

47. R. Schuster, V. Kirchner, P. Allongue, G. Ertl, *"Electrochemical micromachining"*, Science (v289, n5476), pp. 98-101, 2000.

48. M. S. Amalnik, J. A. McGeough, *"Intelligent concurrent manufacturability evaluation of design for electrochemical machining"*, Journal of material processing technology (v61, n1), pp. 130-139, 1996.

49. B. Bhattacharyya, J. Munda, *"Experimental investigation on the influence of electrochemical machining parameters on machining rate and accuracy in micromachining domain"*, International journal of machine tools and manufacture (v43, n13), pp. 1301-1310, 2003.

50. R. Maeda, K. Chikamori, H. Yamamoto, *"Feed rate of wire electrochemical machining using pulsed current"*, Precision engineering (v6, n4), pp. 193-199, 1984.

51. A. D. Davydov, V. M. Volgin, V. V. Lyubimov, *"Electrochemical machining of metals: fundamentals of electrochemical shaping"*, Russian journal of electrochemistry (v40, n12), pp. 1230-1265, 2004.

52. K.P. Rajurkar, D. Zhu, B. Wei, *"Minimization of machining allowance in electrochemical machining"*, Annals of CIRP (v47, n1), pp. 165-168, 1998.

53. L. Cagnon, V. Kirchner, M. Kock, R. Schuster, G. Ertl, W. T. Gmelin, H. Kück, *"Electrochemical micromachining of stainless steel by ultrashort voltage pulses"*, Z. Phys. Chem. (v217), pp. 299–313, 2003.

54. J. Kozak, K. P. Rajurkar, B. Wei, *"Modeling and analysis of pulse electrochemical machining (PECM)"*, Transactions of the ASME (v116, n3), pp. 316-323, 1994.

55. B. Bhattacharyya, J. Munda, M. Malapati, *"Advancement in electrochemical micro-machining"*, International journal of machine tools & manufacture, (v44, n15), pp. 1577-1589,2004.

56. C. D. Zhou, E. J. Taylor, J. J. Sun, L. Gebralt, E. C. Stortz, R. P. Renz, *"Electrochemical machining of hard passive alloys with pulse reverse current"*, Transactions of NAMRI/SME (v25), pp. 147-152, 1997.

57. E. Uhlmann, U. Doll, R. Forster, R. Schikofsky, *"High precision manufacturing using PECM"*, Proceedings of the international symposium for electromachining (ISEM-8), pp. 261-268,Bilbao, Spain.2001.

58. M. Valenti, *"Making the Cut"*, Mechanical engineering-CIME, American society of mechanical engineers, 2001.

59. *"Delstar: A user's guide to applications, Quality standards and specifications"*, [Online] [Accessed: May 24, 2013.] URL - www.delstar.com.

60. J. Kozaka, K. E. Oczos, "*Selected problems of abrasive hybrid machining"*, Journal of materials processing technology (v109, n3), pp. 360-366, 2001.

61. *"ABLE electropolishing, Inc., Electropolishing: Advanced metal improvement technologies"*, [Online] [Accessed: May 24, 2013.] URL - http://ableelectropolishing.com/electropolishing_workbook.pdf.

62. J. Maurer, J. Hudson, S. Fick, T. Moffat, G. Shaw, *"Electrochemical micromachining of NiTi shape memory alloys with ultrashort voltage pulses"*, Electrochemical and solid state letters (v15, n2), pp. 8-10, 2011.

63. D. Bilgi, P. Jadhav, *"Enhancement of surface finish of pulse electrochemically machined surface using rotating electrode"*, International journal of computer communication and information system (v2, n1), pp. 49-54, 2010.

64. C. Chen, J. Chen, C. Chao, W. Say, *"Electrochemical characteristics of surface of titanium formed by electrolytic polishing and anodizing"*, Journal of material science (v40), pp. 4053-4059, 2005.

65. *"Motorized bislide and xslide"*, [Online] [Accessed: Jan 21, 2013.] URL - http://www.velmex.com/pdf/bislide-pdf/motorized_bislide.pdf.

66. *"VXM-2 Users manual extended"*- Velmex unislide, [Online] [Accessed: Jan 20, 2013.] URL - http://www.velmex.com/pdf/controllers/vxm_user_manl.pdf.

67. *"High-speed, high-accuracy CCD laser displacement sensor"*, [Online] [Accessed: Dec 21, 2012.] URL - http://www.keyence.com/products/measure/index.jsp.

68. *"Agilent 33250A function/arbitrary waveform generator data sheet"*, [Online] [Accessed: Dec 20, 2012.] URL - http://cp.literature.agilent.com/litweb/pdf/5968-8807EN.pdf.

69. *"Leader LPS - 151/152 dc tracking power supply instruction manual"*, [Online] [Accessed: Dec 20, 2012.] URL - http://elektrotanya.com.

70. *"Tektronix TDS1002B digital storage oscilloscope"*, [Online] [Accessed: Jan 21, 2013.] URL - http://www.testequity.com/products/1916/.

71. *"Fluke45 dual display digital multimeter"*, [Online] [Accessed: Jan 13, 2013.] URL - http://www.testequipmentconnection.net/Test-Equipment-Detail.asp?model=45.

72. Texas A&M University - Materials characterization facility, *"Dimension icon AFM"*, [Online] [Accessed: Jun 02, 2013.] URL - http://mcf.tamu.edu/instruments/new-afm.

APPENDIX A

Design of various components

Tool holder design

The tool holder used, is a modular component built up of five main parts. The following Figure A-1 shows the various components of the tool holder and the entire setup.

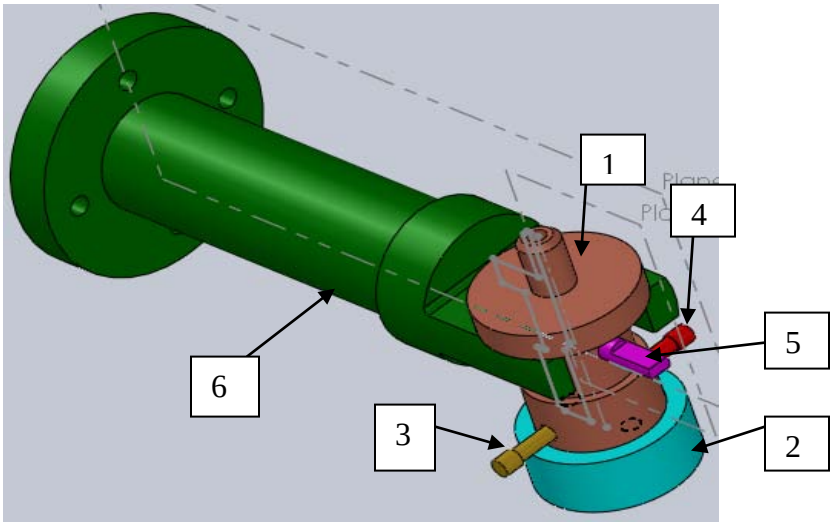

Fig. A-1: View of electrode holder assembly mounted on arm

(1) is the integral component of the tool holder. The silicone tube outlet from the pump is fixed on the top of (1) at the small cylindrical portion. An internal bore (A) as shown in Figure A-2 is drilled through (1) which provides the opening for the electrode to be held. If a solid electrode is used then the electrolyte flows through this internal bore, surrounding the electrode, whereas if a hollow electrode is used, the electrolyte flows through the internal of the electrode.

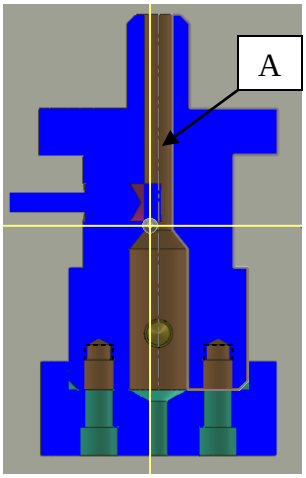

Fig. A-2: Cross sectional view of electrode holder showing internal bore.

An adapter as shown in Figure A-3 is required if a hollow electrode is used. It streamlines the flow of the electrolyte. Details of this adapter coupling are given in Appendix B. This adapter sits on top of the cylindrical portion of the electrode holder (1). It is held firmly in position by clamping the electrode which is press fit into the adapter. The streamlining is done by component (2) if a solid electrode is used. Cross section of component (2) is shown in Figure A-4.

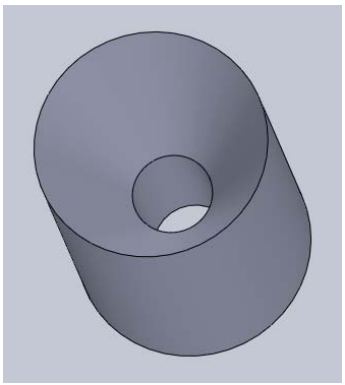

Fig. A-3: Adapter coupling for internal flow

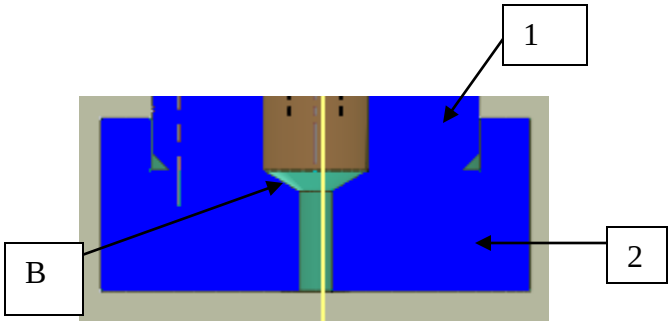

Fig. A-4: Cross section of component 2 showing design for streamlining the flow

The primary function of (2) is to streamline the flow of the electrolyte when a solid electrode is used. The conical section “B” helps in achieving this purpose helping the electrolyte flow uniformly all around the solid electrode. (2) is available in three different sizes and the hole size bigger than electrode diameter but closest to it is the one that is best suited for use. It is fastened to (1) at the lower end by means of shoulder screws “C” and aligned so that it holds in place securely. This is shown in Figure A-5:

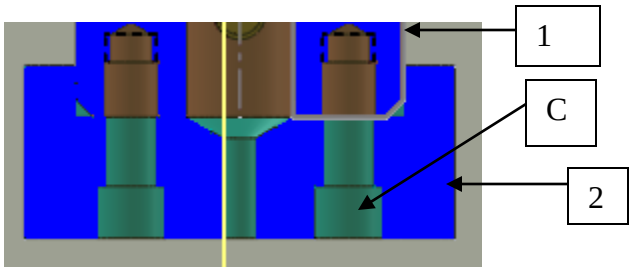

Fig. A-5: Square shoulder screws for screwing component 2 and 1 together

(3) and (4) are screws used to align and hold the electrode in position. These are screwed through the holes drilled on the sides in (1). (3) is made up of plastic and its end is machined to make a cone. The sharp point on the end of the cone helps in holding the

electrode securely in position especially in case of the solid electrode since it fits directly into a groove machined on the electrode. (4) has a groove machined on its end. The electrode is supported from the sides by this groove and it keeps the electrode in position. The groove in (4) also helps in aligning the electrode exactly at the center of the bore. Once the electrode has been aligned at the center, it is securely held in place by tightening the plastic screw from the other end. The screws are shown in Figure A-6:

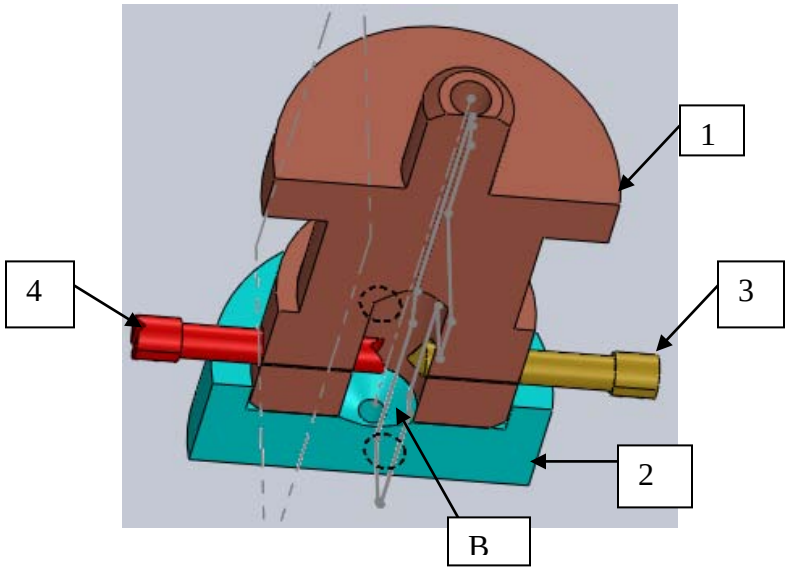

Fig. A-6: Cross section showing electrode holding arrangement

(5) is a dowel pin and its top surface is machined flat to aid in positioning the electrode relative to the workpiece. The entire assembly consisting of components (1), (2), (3), (4) and (5) with the electrode clamped in position is mounted on the arm of the bi-slide (6) and is fastened by a screw to stay in position as shown in Figure A-7.

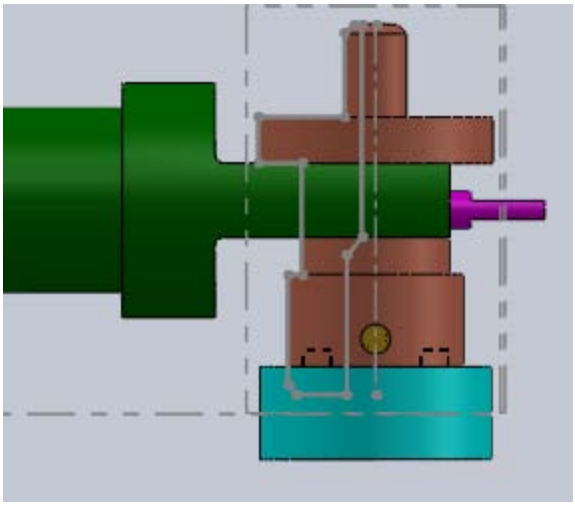

Fig. A-7: Electrode holder mounted on arm for bi-slide

As discussed earlier, the material used must be highly corrosion resistant to prevent system degradation and it should be light weight at the same time. Keeping these in mind, the materials shown in Table A-1 have been selected for the different components:

Table A-1: Materials used for the various components in ECM.

Component number / name	Material
Tool holder (1)	Stainless steel 316
Tool holder (2)	Stainless steel 316
Tool holder (3)	Plastic (nylon)
Tool holder (4)	Stainless steel 316
Tool holder (5)	Stainless steel 316
Tool holder (6)	Stainless steel 316
Tubing for electrolyte flow	Silicone
Adapter for hollow electrode	Teflon
Workpiece holding fixture	Teflon
Workpiece clamping fixture	Teflon
Electrolyte bath	Glass
Ice-water bath	Glass
Flat plate	Aluminium

Workpiece clamping and electrolyte bath design

The design of the electrolyte bath must be such that the workpiece is easily accessible by the tool for machining, provide a good means for collecting and re-circulating the electrolyte. We should be able to secure the workpiece with the fixture and the fixture should not react with the electrolyte while machining is being carried out. The workpiece surface also has to be leveled in order to maintain the inter electrode gap constant while the tool is moving laterally.

The proposed design to fulfill this purpose is shown in Figure A-8:

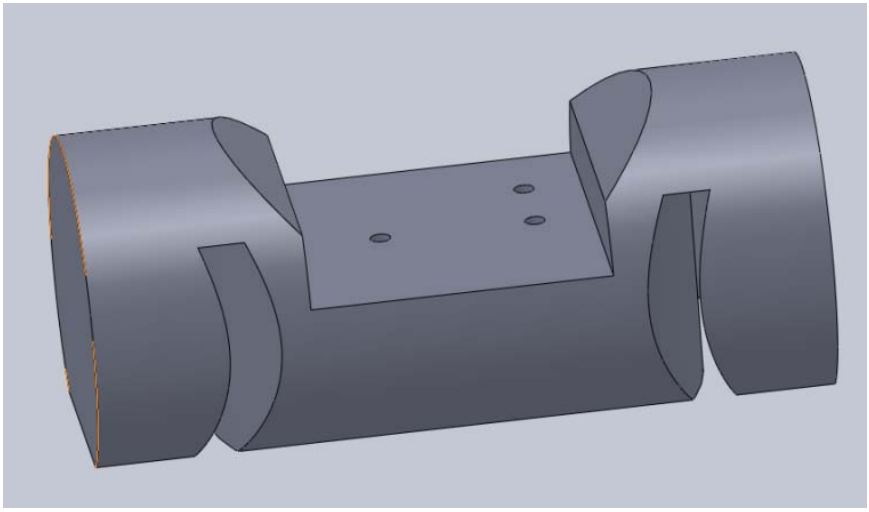

Fig. A-8: Workpiece clamping fixture (D)

The details of this workpiece clamping fixture are given in Appendix B. The flat plate "A" is shown in Figure A-11, and the machining setup is mounted on it. The flat plate has leveling screws which can be used to level the surface of the workpiece after it has been secured in place. "B" as shown in Figure A-10 is the tank (ice-water bath) used for

holding the ice bath for cooling the electrolyte while machining and maintaining its temperature. “C” is the glass container (electrolyte bath) used for holding the electrolyte. The electrolyte, filled in the glass at the start of the machining, is pumped through the system and it collects in the glass again after flowing through the electrode. “D” as shown in Figure A-8, is a Teflon fixture on which the workpiece can be clamped. “D” is secured on the glass tank i.e the electrolyte bath shown in Figure A-9 by means of aluminium plates screwed into the flat plate “A”. This setup helps maintain close dimensional control and stability while machining. The various components designed for this purpose are as follows:

The electrolyte bath for containing the electrolyte is shown in Figure A-9:

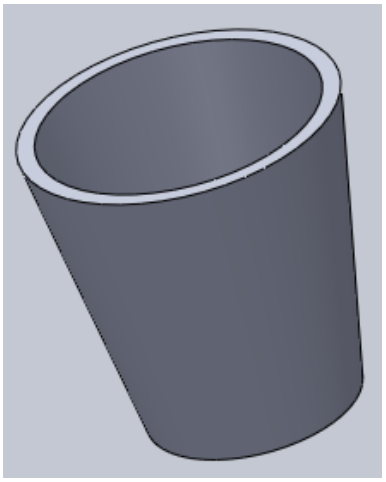

Fig. A-9: Electrolyte bath (C)

The ice-water bath for this setup is shown in Figure A-10:

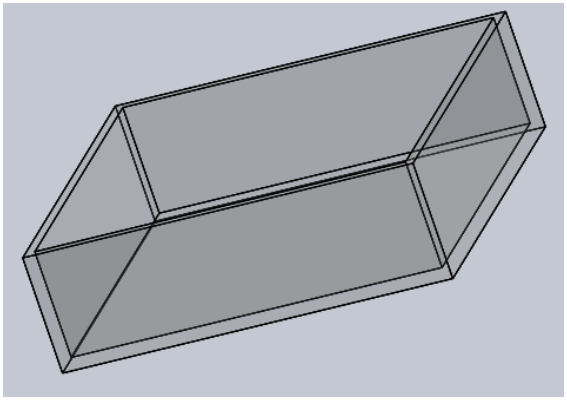

Fig. A-10: Ice-water bath (B)

The flat plate used for the set up is shown in Figure A-11:

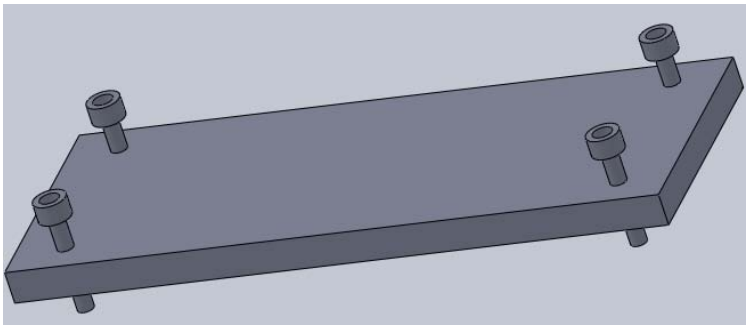

Fig. A-11: Flat plate (A)

The entire setup is shown in Figure 31. Detailed drawings of the components not shown here are available in the study carried out by S. Sundarram (34).

APPENDIX B

Detailed drawings

Detailed drawing of workpiece fixture is shown in Figure B-1 as follows:

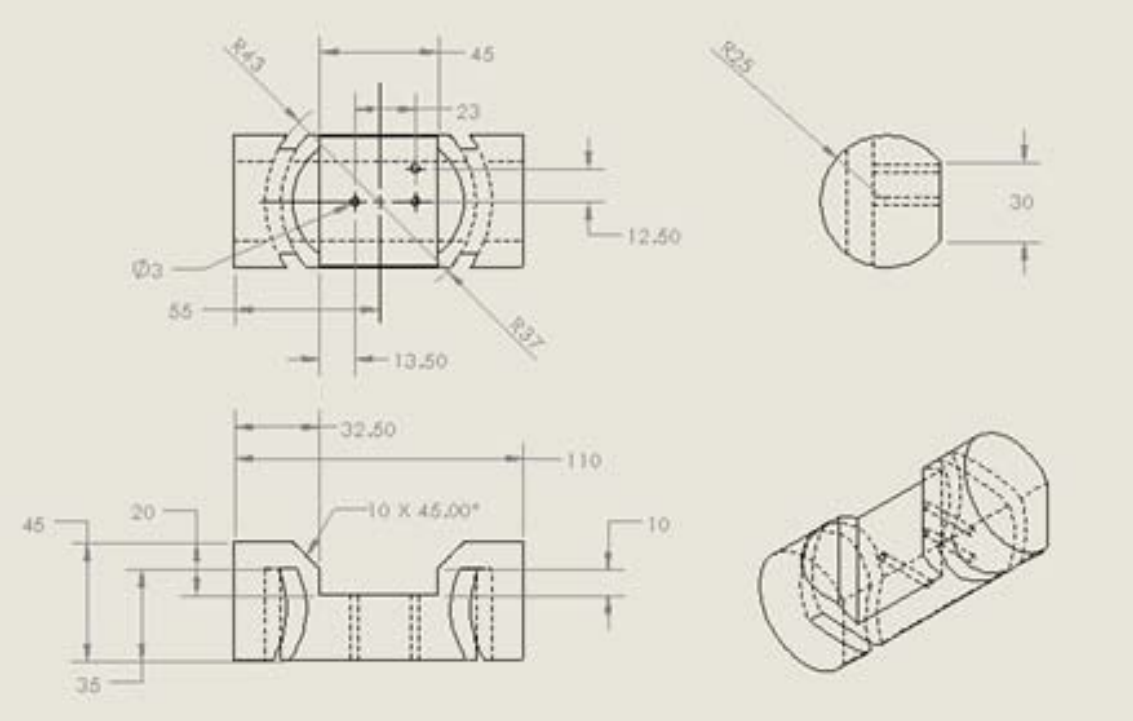

Note: All dimensions are in mm.

Fig. B-1: Detailed drawing of workpiece fixture

Detailed drawing of the adapter coupling is shown in Figure B-2 as follows:

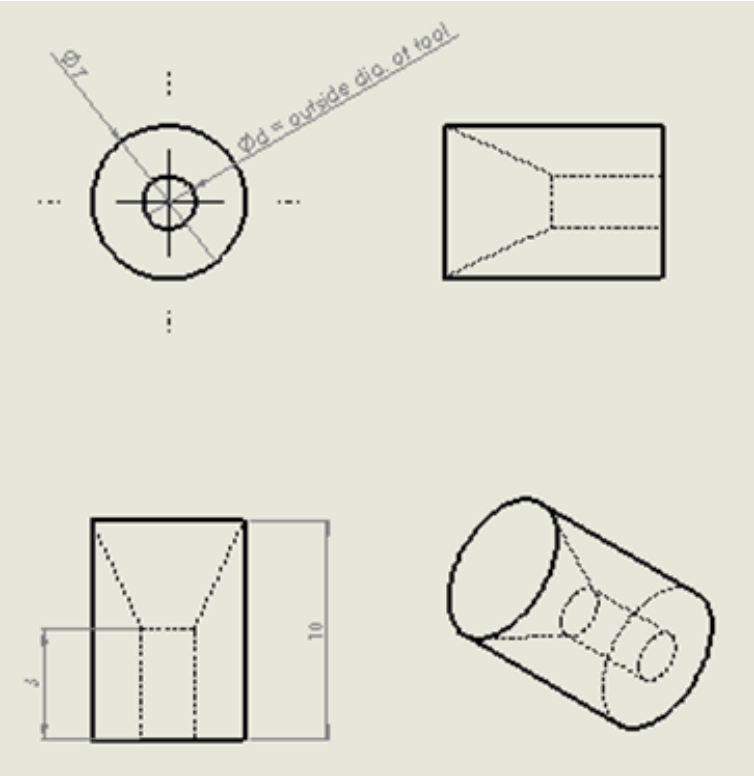

Note: All dimensions are in mm.

Fig. B-2: Detailed drawing of adapter coupling

APPENDIX C

Equipment description

Velmex Bi-Slide and VXM-1 Controller

These were used to accurately position the electrode with the workpiece. The bi-slide is a modular system which can be assembled as needed for multi-axes movements. The lead screw on the bi-slide has a resolution of 0.00025” with a repeatability of 0.00015” making it possible to accurately position the system. The bi-slide and stepper motor controller are shown in Figure C-1. Important features of this bi-slide are as follows:

1. Low cost and high precision positioning possible
2. PTFE linear bearings and long life anodized aluminum ways.
3. Operates without lubricants
4. High load carrying capacity of 300 lb (normal centered and static or dynamic)
5. Cleat system for mounting
6. High rigidity in all directions

The bislide used for these experiments was configured for movements in the X and Z axes. The tool was mounted on this bi-slide using the cleat system for mounting and was securely held in place. This bislide is compatible with NEMA size 23 and NEMA size 34 motors and can be controlled by a computer using a suitable interface. This makes precise positioning of the workpiece possible for critical applications. Important features of this controller are as follows:

1. Compact size and low cost.
2. Manual as well as programmable.
3. Graphical interface with computer using COSMOS software.
4. Easy to program using the command instruction set.
5. Simultaneous as well as individual motor movement is possible.
6. Variable speeds can be obtained.

During the experiments the stepper motors were controlled by using the COSMOS software. The number of pulses received by the motor controls the amount of rotation of the motor which in turn controls the movement of the bi-slide in the forward or backward direction, thus helping us position the tool precisely.

Fig. C-1: (a) Velmex bi-slide for X-Y-Z axes movements (65) & (b) Velmex VXM2 stepping motor controller (66)

Keyence LK-G157 Laser Head and LK-GD500V Controller

The laser sensor was used in combination with the bi-slides to position the tool and the workpiece precisely. The laser was mainly used to measure and record the interelectrode gap. It was also used to level the workpiece so as to maintain a constant interelectrode gap. The salient features of this instrument are as follows:

1. Very high speed sampling (50 kHz).
2. High accuracy (0.05%).
3. Excellent repeatability (0.5 µm)
4. High measuring range of 110 – 190 mm
5. Capable of measuring different materials like plastic, transparent or translucent and metal targets effectively.

Settings of sensor head for data gathering can be adjusted for optimal values depending on the type of surface by making use of the software available.

Fig. C-2: Keyence laser head and controller (67)

Figure C-2 shows the laser head and controller. Once the electrode gap is set by using the laser we do not need the laser and the system can function without the laser head.

Agilent 33250A Function Generator

The function generator shown in Figure C-3 provided the power supply for the pulsed ECM experiments. Its main features are as follows:-

1. Capable of generating 10 standard waveforms.
2. Frequency can be set as high as 80 MHz.
3. Parameters can be adjusted using a keypad or knob provided on the front panel.
4. AM, FM, PM, FSK, PWM internal modulating options help in modulating the waveform independently.

Fig. C-3: Function generator (68)

LEADER LPS-151 DC Tracking power supply

This power supply shown in Figure C-4 supplied the power for the DC experiments.

Fig. C-4: DC power supply (69)

Tektronix TDS 1002B Oscilloscope

The oscilloscope shown in Figure C-5 was used to measure and analyze the dynamic machining parameters for the system. It was also used to see the deviation from the input waveform conditions caused by the noise in the circuit. The bandwidth of the instrument is 60 MHz while it can sample at 1 GS/s.

Fig. C-5: Oscilloscope (70)

Fluke 45 Multimeter

This multimeter shown in Figure C-6 was used in the system to measure the current in the circuit. It has a measuring range upto 10A with a resolution of 0.1 µA.

Fig. C-6: Multimeter (71)

Monostat Vera 72-315-000 electrolyte pump

The electrolyte needs to be pumped through the entire system in order to carry out the machining and it also helps flush out the debris. The above pump was used to pump the electrolyte through the system. It provided variable speed control giving different flow rates.

Agilent 33502A 50 Vpp / 100 kHz 2 channel Isolated Amplifier

The amplifier was used to amplify the signal (i.e voltage) from the function generator for the AC experiments since the function generator was not able to establish sufficient current in the circuit independently.

National Instruments PCI-8432/4 interface board

The PCI interface board was used to communicate with the control computer. It has four 128 B data transmitting and receiving ports. The baud rate for this board ranges between 57 b/s to 1Mb/s and is within 0.01% accurate.

Olympus STM 6 Optical Microscope

The machined surfaces on the workpieces were observed on the Olympus STM 6 Optical Microscope to determine their quality. The workpiece surface was positioned under the objective lens and brought in focus by moving the table of the optical microscope and the lens along the three axes (X, Y, and Z) in coarse or fine modes. Pictures of the surface could be taken using the DP 70, 12.5 megapixel camera, installed to support the

optical microscope. The resolution of the optical microscope was 0.1µm and different objective lenses1.25X-50X were used for measurements as per the requirements.

ZygoNewView 100 Interferometer

The Zygo interferometer that works on the principles of interferometry was used to measure surface roughness of the polished surface on the workpiece. Ti being reflective, this instrument could be used to measure the surface roughness of the polished area. The resolution of the interferometer was 0.1 nm and thus, it was capable of giving highly accurate data in a short time. Also, it being a non-contact type method, was preferred since it would not damage the polished surface.

The software to operate the ZygoNewView 100 microscope was installed on a computer. The workpiece was positioned and brought in focus by using Zygo joystick box that controlled direction and motion speed along X, Y, and Z axes during measurements. ZygoMetroPro software was used to analyze the measured three dimensional surface profiles generated on filled plot, oblique plot, and profile plot. R_a and R_z can be measured using this software. Three objective lens (2.5x, 5x, and 10x) can be used on the Zygo microscope and the bipolar scanning depth (length) can be adjusted in the range 10 µm -100 µm, depending on the measured profile.

JEOL6400 Scanning Electron Microscope

Scanning Electron Microscope (SEM) was utilized to observe the surface characteristics of polished spots. Higher magnification images than optical microscope could be

generated with this instrument. Samples were cleaned ultrasonically in 70% Isopropyl alcohol and dried with pressurized air. Secondary electron (SE) and back scatter electron (BSE) images were formed by placing the workpiece in a vacuum chamber generated by a pump.

Bruker Dimension Icon Atomic Force Microscope (AFM)

The surface topography of an extremely small area was measured with an atomic force microscope. In AFM, a sharp probe scans the surface of the workpiece in a raster pattern to collect information on the surface topography in three dimensions. Other information on magnetic properties, chemical properties and forces between the tip and sample can also be measured using the AFM.

The resolution of AFM is not limited by the diffraction of light and hence it can be used to achieve a high resolution (Z < 0.1 nm, XY < 1 nm). The AFM used for our purpose is shown in Figure C-7:

Fig. C-7: Bruker dimension icon atomic force microscope (72)

APPENDIX D

Electrolyte solution preparation

A suitable alcohol-based electrolyte for Ti polishing was developed in another project. The procedure to prepare this electrolyte solution of ~115 mL is as follows:

Step 1: Prepare an alcohol rinse of 300 mL of a 3:7 mixture of isopropyl alcohol and ethyl alcohol i.e take 90 mL of isopropyl alcohol and 210 mL of ethanol and mix them thoroughly by stirring mechanically or by using a stir bar for ~5 min. Maintain the temperature of the alcohol rinse around 10^0C by keeping it in an ice bath.

Step 2: Rinse a 500 mL capped container with acetone to dissolve contamination followed by washing with deionized water to remove the acetone. Then rinse it three times with the alcohol rinse.

Step 3: Prepare a 100 mL 3:7 mixture of isopropyl alcohol and ethanol by mixing 30 mL isopropyl alcohol and 70 mL ethyl alcohol. Mix the solution thoroughly using a magnetic stirrer while maintaining the temperature ~10^0C.

Step 4: Chill the mixture in an ice-water bath for 10 minutes and place the mixture underneath a vent hood.

Step 5:- Add 30 g of $ZnCl_2$ from the container kept in a dessicator. Cap the container immediately and place it back in the dessicator.

Step 6: Place the container in the ice-water bath and chill it. Simultaneously stir the contents using a magnetic stirrer to facilitate the dissociation of the salt into the solution.

Step 7: Once most of the $ZnCl_2$ is dissolved in the solution, remove the $AlCl_3$ salt container from the dessicator and add 6 g of $AlCl_3$ to the solution.

Step 8: Cap the bottle and place it in the ice-water bath again. Stir it until all the salt has dissociated into the solution. The dissociation is exothermic and hence the stirring needs to be done when the container is immersed in the ice-water bath.

The complete dissociation of the salt takes approximately 90 min to complete. It is extremely important to cap the $ZnCl_2$ and $AlCl_3$ containers and keep them in the dessicator as soon as possible to prevent it from absorbing atmospheric moisture.

APPENDIX E

Raw data of DC and AC experiments

The following Table E-1 shows the raw data collected from the DC current experiments.

Table E-1: Raw data for surface roughness of spots polished using DC current

Run no.	R_a (nm)				R_z (nm)			
	r1	r1'	r2	r2'	r1	r1'	r2	r2'
1	179	214	172	351	511	1061	494	1196
2	139	513	470	322	448	3569	2511	1853
3	284	332	312	348	674	2256	796	2212
4	245	372	356	318	1116	1922	943	1640
5	381	466	475	402	1326	2647	1409	2153
6	364	429	205	285	1674	3380	1585	3448
7	299	416	179	336	2802	2266	942	2449
8	505	443	348	406	2524	3209	1459	4729
9	125	168	178	208	405	945	647	1147
10	219	246	316	257	1124	1480	937	1315
11	276	362	253	385	1155	1815	1387	1583
12	287	211	227	278	1234	1332	853	1670
13	287	364	253	368	1168	1443	1238	1955
14	218	259	280	246	1419	2310	1008	1509
15	334	370	218	324	1105	2605	1307	2420
16	213	434	256	249	885	2486	904	1412

r1 = R_a/R_z value of polished spot along circular section of 130 µm radius for given run.

r1'= R_a/R_z value of polished spot along circular section of 380 µm radius for given run.

r2 = R_a/R_z value of polished spot measured circular section of 130 µm radius for its corresponding replication run.

r2'= R_a/R_z value of polished spot measured along a circular cross section of 380 µm radius for its corresponding replication run.

The following Table E-2 shows the raw data collected from the AC current experiments.

Table E-2: Raw data for surface roughness of spots polished using AC current

Run no.	R_a (nm)				R_z (nm)			
	r1	r1'	r2	r2'	r1	r1'	r2	r2'
1	306	314	255	317	1093	1890	797	1530
2	437	517	506	409	3096	5368	2724	2373
3	231	354	136	261	632	840	448	914
4	265	363	403	511	1310	1634	900	1231
5	385	490	733	793	1463	2001	2499	2907
6	578	593	1106	684	2889	2899	4240	3432
7	491	923	231	761	1328	2387	692	2195
8	378	461	299	660	1350	2677	1450	2254
9	390	364	258	318	1292	1614	1021	1452
10	281	363	314	330	1140	2180	1312	2441
11	313	347	224	373	722	894	617	735
12	338	445	242	435	864	1761	848	1657
13	382	384	496	308	1720	2012	1700	1575
14	536	610	462	621	1939	3684	1680	3292
15	415	327	461	430	887	1457	1110	1727
16	358	299	348	344	1066	1674	1798	2046
17	301	442	401	403	1178	2492	1386	2800
18	589	712	606	439	3046	5917	3011	2681
19	1201	1789	354	411	0	3767	896	976
20	374	400	290	405	1555	1892	969	1718
21	677	781	558	952	2105	3806	2162	3365
22	500	517	535	553	1419	4174	3628	4099
23	362	510	271	538	1618	2372	868	2310
24	462	398	769	638	1901	3468	2531	3221
25	257	301	430	296	1166	1526	1126	1722
26	453	553	334	617	1931	3100	1369	2510
27	427	619	350	657	2127	2789	1115	3440
28	394	745	382	429	1076	1917	861	1819
29	676	1002	401	487	2363	3966	1584	2152
30	302	611	329	389	1083	3687	1220	2417
31	586	1234	268	688	942	1961	1033	1771
32	397	373	368	494	1622	2672	1654	2898

In the above table,

r1 = R_a/R_z value of polished spot along circular section of 130 µm radius for given run.

r1'= R_a/R_z value of polished spot along circular section of 380 µm radius for given run.

r2 = R_a/R_z value of polished spot measured circular section of 130 µm radius for its corresponding replication run.

r2'= R_a/R_z value of polished spot measured along a circular cross section of 380 µm radius for its corresponding replication run.

APPENDIX F

Programming with COSMOS

The stepper motor control can be automated for precise movement by sending commands to the stepper motors through the COSMOS software. A complete description of the commands and their purpose is provided in Table F-1:

Table F-1: Codes for programming with COSMOS

Code	Purpose
F"+" space	Starting command
C"+" space	Cancel all previous commands
1M	Call the 1st motor which moves the electrode in X-direction
2M	Call the 2nd motor which moves the electrode in Z-direction
S"+" motor number"+" xxx	Controls speed of mentioned motor and moves it at xxx steps/sec
I"+" motor number"+" xxx	Incremental motion command that directs the motor to increment by xxx steps
LM"+" x	Loop starting mark with loop name x
P xxx	Pauses the motors by xxx milliseconds
Lxxx	Repeats commands within the loop xxx times
R	Ends the program

Note: 1 step = 2.5 µm

A sample program is provided below which will help explain the use of above codes.

The code moves the electrode down by 150 steps at 500 steps per second. Then it moves back and forth 20 times, for a distance of 1000 steps, along the horizontal direction (X axis) at 200 steps per second. The tool then raises back to its original position i.e it raises 150 steps at a speed of 500 steps per second. The program for this is as follows:

F C S2M500, I2M150, S1M200, LM0, I1M1000, I1M-1000, L20, S2M500, I2M-150, R